

# Hydrogen plasma-based treatments of polycrystalline diamond materials

Matthew Billing  
School of Chemistry  
University of Bristol

2012

Supervisor: Dr N. A. Fox  
Second Assessor: Professor P. W. May



A thesis submitted in partial fulfilment of the requirements for the award of the Honours degree of Master of Science in Chemistry.

# Abstract

---

This project forms part of the work in the direction of preparing diamond materials with smooth surfaces suitable for use in cold cathode devices. In this project, hydrogen plasma treatments were the main focus.

Polycrystalline diamond materials produced using CVD by Element6 were exposed to a range of hydrogen plasmas using different combinations of parameters. SEM, AFM and Raman spectroscopy were used to analyse the samples following the treatments. It was shown that hydrogen plasmas predominantly etch the non-diamond material located at grain boundaries causing the grain boundaries to become deeper and, in some cases, led to the release dislocations and relief of strain within the diamond material which resulted from the growth process. These all increased the surface roughness of the diamond material.

Despite roughening the surface significantly by hydrogen plasma treatment, it was also noted that the sharp edges of the diamond crystallites become more rounded during the treatment. This smoothing appeared to occur at a higher rate as the temperature of the treatment was increased, however, other processes also become prominent.

High power hydrogen plasma treatments were shown to produce significant etching of the diamond crystals on the surface in addition to the etching of non-diamond material. This was attributed to the increase in the abundance of species with sufficient energy to interact with the diamond lattice and break the strong C-C bonds. In contrast to this, high temperature treatments were shown to graphitise the surface greatly, as confirmed by Raman spectroscopy. It has also been shown that prolonged exposure to the plasma causes increased roughness and in the case of long duration treatments can cause graphitisation.

Despite not producing a flat diamond surface, the findings of the initial investigation have been shown to be useful. A brief period of graphitisation of the diamond surface under hydrogen plasma conditions was shown to greatly increase the rate at which material could be removed from the sample using a manual polishing technique with a diamond file.

An experiment using SCD showed that hydrogen plasma etches the surface at defects edges to produce pyramidal etch pits. These pits were thought to form due to etching of under-coordinated atoms at step edges or the edges of defects in the surface. This experiment corresponded well with previous literature reports.

In addition to standard hydrogen plasma treatments, LPSSS-style treatments were also performed. LPSSS is a widely unstudied technique which makes use of hydrogen plasmas, so the project began a short investigation into the technique. These treatments used hydrogen plasma to treat diamond samples coated with thin layers of Ag, Cu, Fe or Ti. The presence of the metal did not seem to have any enhancing effect on the hydrogen plasma treatment. In all cases, the metals were noted to melt at temperatures hundreds of degrees below their standard melting point. This was attributed to hydrogen embrittlement processes causing cracking in the metal film in combination with etching by the hydrogen plasma at grain boundaries and cracks to

produce metal nanoparticles. These metal nanoparticles experienced a phenomenon known as melting point depression as a result of this etching. It has also been suggested that the formation of hydride compounds by the interaction of hydrogen species with the metal may have caused further reductions in the melting points of the metal particles. Once molten, these metal globules are thought to be able to move across the surface and coalesce to form larger globules and snake-like structures. Since the metals were not in contact with the diamond crystals, the crystals appear very similar to those which have been treated in the standard way using hydrogen plasma (i.e. the crystals show high brightness under SEM due to the NEA of the hydrogen terminated surface).

Experiments using thicker metal coatings on microcrystalline diamond showed that the metals can have a thermochemical reaction with the diamond surface and that this effect increases with an increasing number of unpaired d-electrons.

# Acknowledgements

---

I would like to thank my supervisor Dr Neil Fox for offering me this project and allowing me work in this fascinating and exciting field. It has been a fantastic experience and I am extremely grateful for the support he has given me this year. I would like to thank Neil for all of the useful discussions which we have had and suggestions that he has made.

I would also like to thank Dr Oliver Fox for teaching me how to use the MWCVD reactor, his expertise and patience has been very gratefully received this year. Thanks also goes to Dr James Smith for helping me get started this year with the laser cutting and preparation of my samples, as well as showing me how to use the Raman spectrometer and other equipment in the diamond lab. These two people have been extremely useful on countless occasions, answering any questions which I have had. I would like to thank them again for this.

A huge thank you also goes to the Electron Microscopy unit for teaching me how to use the microscopes and assisting me with technical issues which were encountered during this project.

I have learnt so much this year and there are many other people who deserve my thanks. I would like to thank all of the Bristol University Diamond Group (BUDGies) for making this year so enjoyable. It has been a pleasure. I wish everyone all the best in the future.

# Contents

---

<b>Chapter 1: An introduction to the field of diamond materials</b>	7
1.1 Diamond	7
1.2 Graphite	8
1.3 Diamond formation	9
1.3.1 Natural diamond formation	10
1.3.2 Early work in diamond synthesis	12
1.3.3 HPHT diamond formation	13
1.3.4 Chemical Vapour deposition	14
1.4 Defects in the diamond lattice	19
1.5 Doping of the diamond lattice	21
1.6 Negative electron affinity	23
1.7 Potential applications of the NEA of diamond	25
References	26
<b>Chapter 2: Current issues in the realisation of commercial cold cathode devices</b>	32
2.1 The production of SCD	32
2.2 Alternative diamond materials	36
2.3 Polishing of diamond materials	39
References	40
<b>Chapter 3: Diamond from a low pressure solid state source</b>	44
References	48
<b>Chapter 4: Experimental techniques and apparatus</b>	49
4.1 The reactor	49
4.2 Optical emission spectroscopy	50
4.3 Raman spectroscopy	52
4.4 Scanning electron microscopy	55
4.5 Atomic-force microscopy	56
4.6 Diamond samples	57
4.7 Manual abrasion	59
References	60
<b>Chapter 5: Results and discussion</b>	62
5.1 Hydrogen plasma treatments of PCD	62
5.2 Hydrogen plasma treatments of SCD	87
5.3 The smoothing mechanism of hydrogen plasma treatment on SCD	91
5.4 Hydrogen plasma treatment of PCD and manual abrasion	97
5.5 LPSSS-style treatments	102
References	119

<b>Chapter 6: Conclusions</b>	123
<b>Chapter 7: Suggestions for future work</b>	126

# Chapter 1

## An introduction to the field of diamond materials

---

As the fourth most abundant element in the universe and the foundation of all life on Earth, carbon is a remarkable element. Add to this the fact that carbon is found in almost 10 million different compounds and a number of pure allotropic forms, it is clear to see that carbon is certainly one of the most important elements in the periodic table from a chemist's point of view.

This work forms part of current research into the use of carbons allotropic forms, in particular diamond, as materials for future high performance technological applications.

### 1.1 Diamond

Diamond is a material made up of  $sp^3$  hybridised carbon atoms which are bonded together by covalent  $\sigma$ -bonds. When a large number of carbon atoms bond together in this tetrahedral fashion, a giant covalent lattice structure forms known as the diamond lattice [1]. This structure can be seen in **Figure 1.1**.

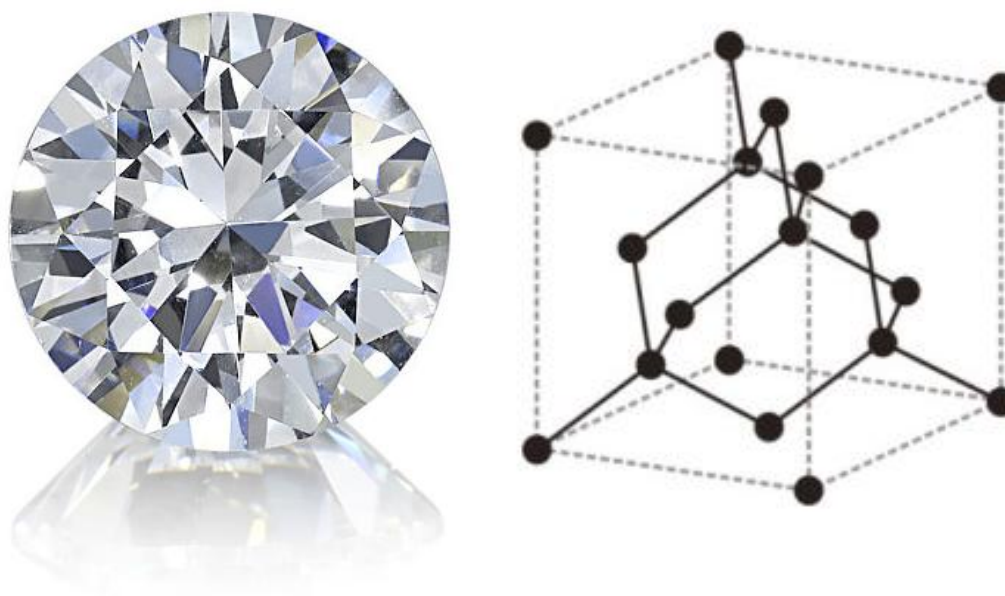


**Figure 1.1:** A diamond gemstone (left) and the unit cell of the diamond lattice (right) showing carbon atoms bonded together in a tetrahedral fashion. *Figures are from [2] and [3] respectively.*

The extreme strength and highly symmetric nature of the diamond structure leads to a number of distinctive properties [4] which can be seen in **Table 1.1**. This makes diamond an extremely attractive material for engineering and scientific applications in a wide range of fields.

**Table 1.1:** A selection of diamonds extraordinary properties [3,5,6]

Physical	Extreme mechanical hardness (90 GPa) and wear resistance Low compressibility ( $8.3 \times 10^{-13} \text{ m}^2 \text{ N}^{-1}$ ) High bulk modulus ( $1.2 \times 10^{12} \text{ N m}^{-2}$ ) High thermal conductivity at 298 K ( $2 \times 10^3 \text{ W m}^{-1} \text{ K}^{-1}$ ) High speed of sound ( $18000 \text{ m s}^{-1}$ )
Electronic	Wide band gap (5.45 eV or lower for doped material) High electrical resistivity ( $10^{13}$ - $10^{16} \Omega \text{ m}^{-2}$ ) High electron mobility ( $2200 \text{ cm}^2 \text{ V}^{-1} \text{ s}^{-1}$ ) High hole mobility ( $1600 \text{ cm}^2 \text{ V}^{-1} \text{ s}^{-1}$ ) High electrical breakdown field ( $10000 \text{ kV cm}^{-1}$ ) Some surfaces exhibit low or negative electron affinity
Chemical	Chemically inert to all solvents Biologically compatible
Optical	Transparent from deep-UV to far-IR High refractive index at 591 nm (2.41)

## 1.2 Graphite

Graphite is a material made of  $sp^2$  hybridised carbon atoms which covalently bond together to form a planar hexagonal structure. The  $\sigma$ -bonds in graphite are shorter than those found in carbon due to the increased s-orbital character in the  $sp^2$  hybrid orbitals. The sheets of hexagonally arranged carbon atoms are then stacked on top of each other to form a layered structure, shown in **Figure 1.2**, which is held together by weak Van der Waals forces [1].

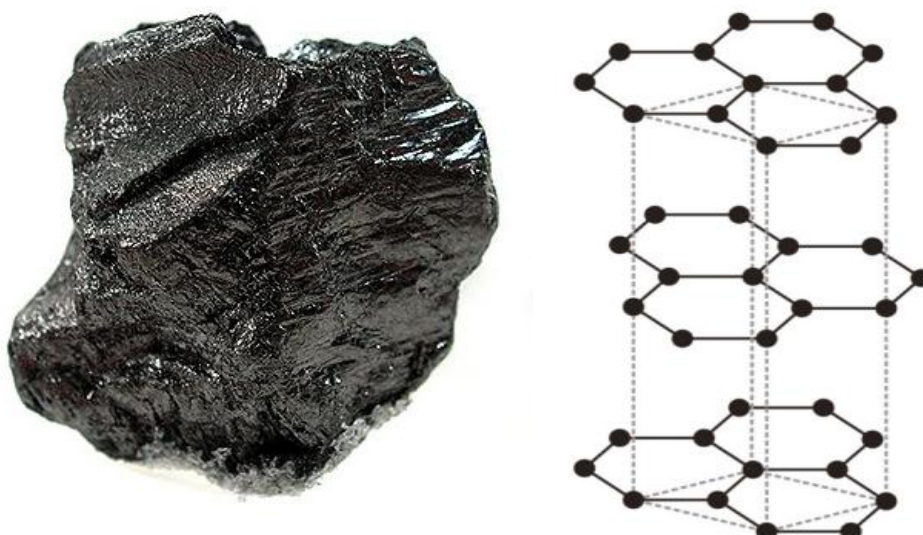


**Figure 1.2:** A piece of graphite (left) and a portion of the graphite structure (right) showing stacked layers of hexagonally arranged  $sp^2$  hybridised carbon atoms. *Figures are from [7] and [3] respectively.*

The hybridisation of the carbon in graphite means that there is a free p-orbital on each of the atoms which lies perpendicular to the planes of hexagonally arranged atoms. These p-orbitals can overlap to form delocalised  $\pi$ -systems between the hexagonal layers, thus making graphite an electrically conducting non-metal [8]. This electrical conductivity is one of many properties where diamond and graphite show behaviour at opposite ends of the scale; for example, graphite is opaque and soft whilst diamond is transparent and very hard.

### 1.3 Diamond formation

Even with such different structures and properties, diamond and graphite are not very different from a thermodynamic viewpoint. The difference in free energy between the two materials is only  $2.9 \text{ kJ mol}^{-1}$  [9] and at standard conditions (1 atm and 298 K) graphite is the most thermodynamically stable phase [10]. In addition to this, there is a massive energy barrier which makes conversion between the two materials extremely difficult [6]. These energetic factors are depicted in **Figure 1.3**.

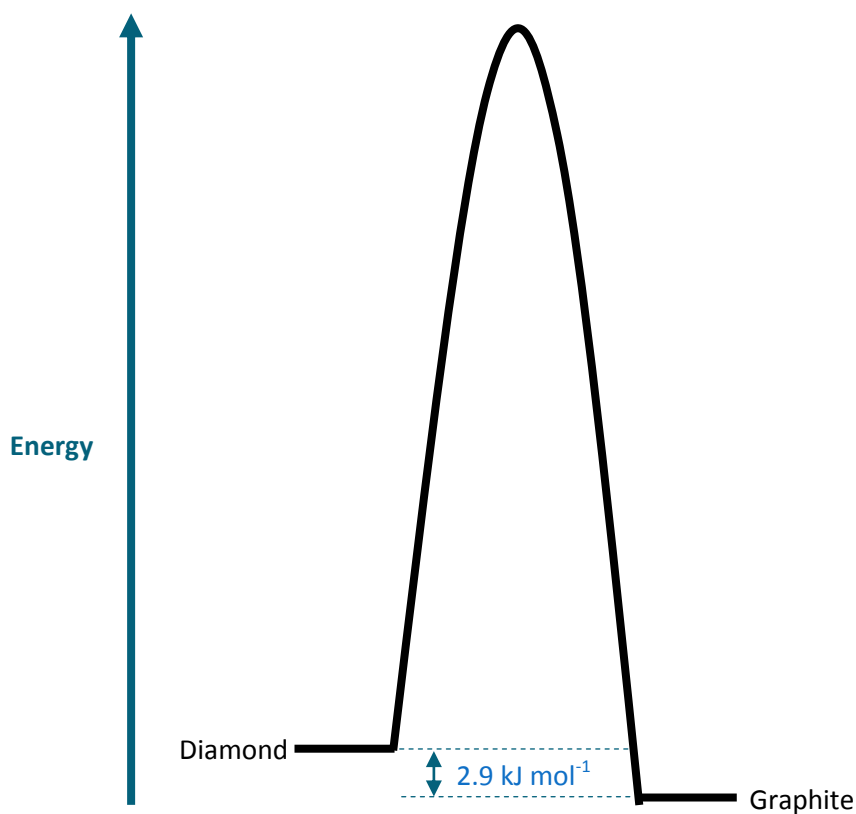


**Figure 1.3:** A representation of the free energies of graphite and diamond separated by a large energy barrier. *This figure was designed by the author and is not to scale.*

These energetic factors mean that the conditions required for diamond formation are very extreme, as can be seen in **Figure 1.4**. However, once diamond is formed the massive energy barrier prevents conversion back to graphite under standard conditions and so “diamonds are forever...” [11].

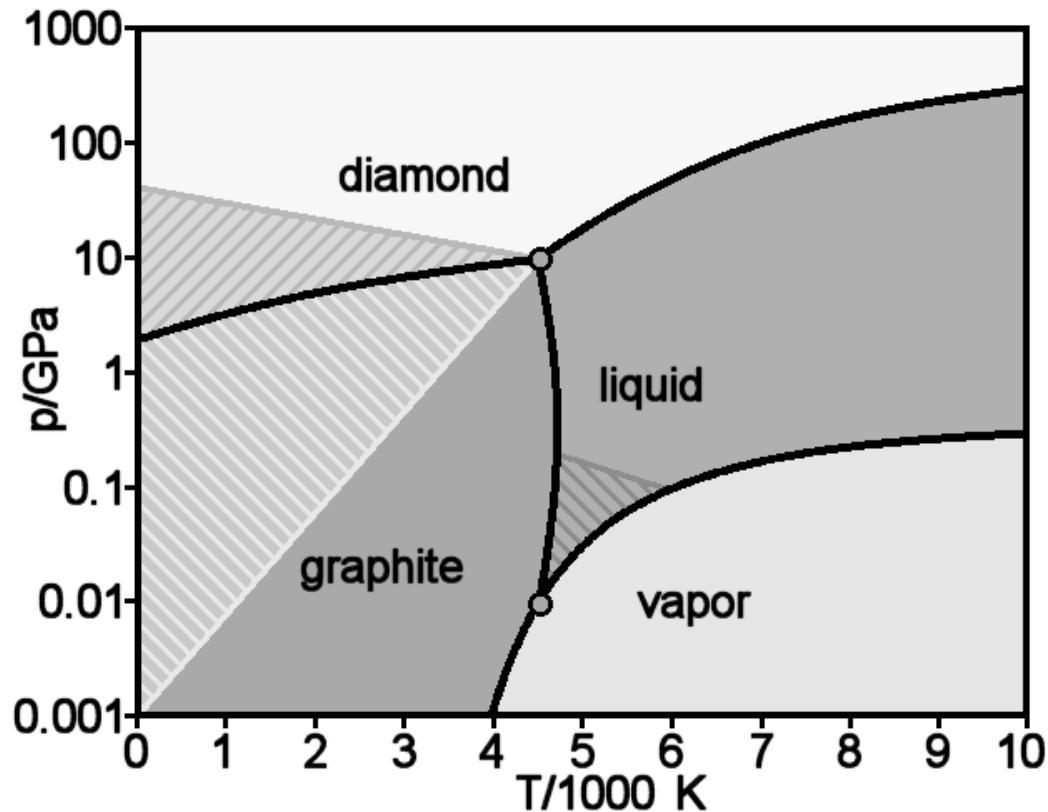


**Figure 1.4:** A simplified phase diagram of pure carbon indicating the conditions at which the allotropic solids, liquid and vapour phases of carbon exist. *Figure is adapted from [12].*

### 1.3.1 Natural diamond formation

The extreme conditions required for diamond formation can be met naturally in a few different circumstances, as depicted in **Figure 1.5**. The most well-known conditions for diamond formations are found deep beneath the surface of the Earth in the lithospheric mantle, where carbon containing minerals slowly transform into diamond over billions of years [13]. The diamonds which form in this region of the mantle simply remain deep within the Earth's crust unless they are brought to the surface by volcanic eruptions, a process which destroys a significant proportion of the diamond. The diamonds which survive the eruption become spread over vast areas by the eruption and as the magma cools these diamonds become encased in igneous rock. The erosion of these rocks cause diamonds to be spread over vast areas, as found in central and southern Africa [14].

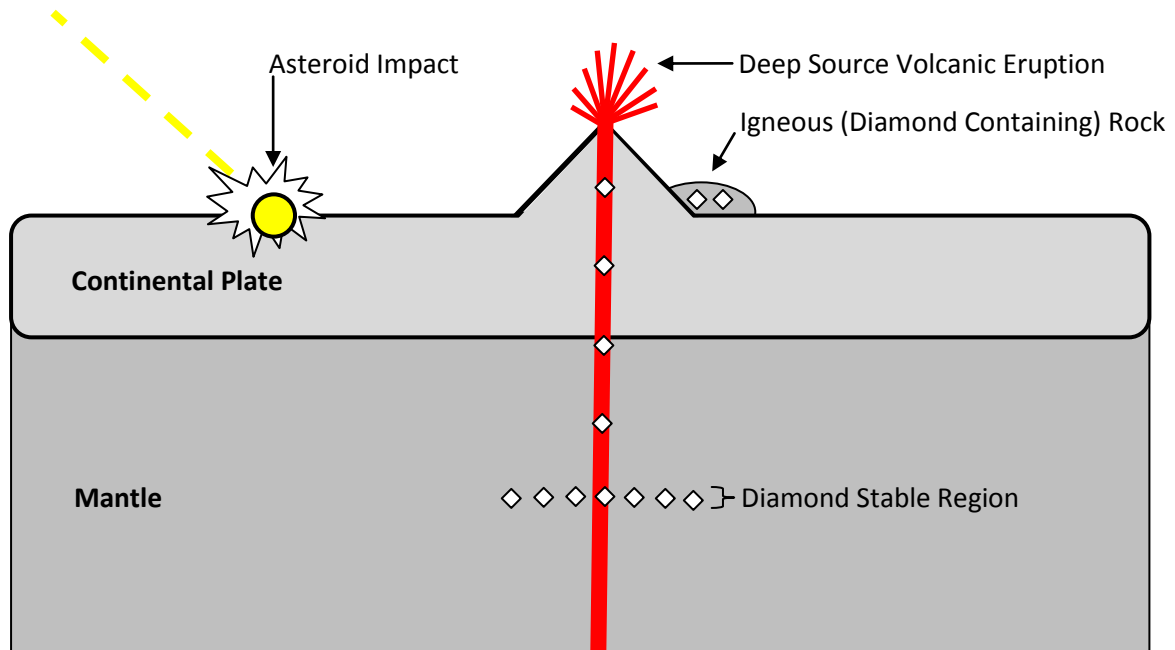


**Figure 1.5:** A diagram of natural diamond formation showing the diamond formation region found deep within the Earth's crust. These diamonds are then brought to the surface by deep source volcanic eruptions. The magma then cools to form diamond containing igneous rocks. Additionally, a meteor impact with the Earth is shown. At these impact sites diamond formation can also occur. *This figure was designed by the author.*

Beyond this geological process, diamonds can also be formed when meteorites strike the surface of the Earth [15]. The huge impacts created at such sites produce short-lived high pressure and high temperature environments in which diamond formation can occur. Since these conditions are extremely brief, very small, micron scale diamonds are formed. These diamonds are commonly used as an indication of an ancient impact site [15].

In addition to microdiamonds formed during a meteor strike, some of the diamond found at impact sites may have come from extraterrestrial origins [16]. An example of a strange, black, porous 'carbonado' diamond is shown in **Figure 1.6** and such diamonds have been shown to be polycrystalline with high hydrogen content, comparable with that of a star-like environment [17]. For this reason, 'carbonado' diamonds are thought to have been formed in supernovae and brought to Earth by meteorites. Since these materials have only been found on the east coast of South America and the west coast of Africa [18], these diamonds are thought to have been brought to Earth when a large asteroid collided with the supercontinent Pangaea over 2 billion years ago.



**Figure 1.6:** A carbonado diamond found at a meteorite impact site on the east coast of Brazil. Figure is from [19].

The concept of diamond being found in space has a great deal of support and many think that diamond may in fact be the most abundant solid in the universe [20]. Recently, there has been some exciting evidence for this: the largest white dwarf found in the universe so far (BPM 37093) was shown to have a core described as a 2500 mile-wide diamond [21,22].

Entertainingly, the scientists at the Harvard-Smithsonian Centre for Astrophysics, who made the discovery, named this diamond 'Lucy' in tribute to the famous Beatles song 'Lucy in the sky with diamonds' [23].

Despite potentially being the most abundant solid in the universe, diamond is incredibly rare on Earth, which is reflected in the material having a high price. For this reason, there has been a lot of interest in producing diamond synthetically. This would make the attractive properties of diamond more accessible.

### 1.3.2 Early work in diamond synthesis

In the 18<sup>th</sup> century, combustion experiments famously showed that diamond was carbon, and only carbon [24,25]; and ever since attempts have been made to produce diamond from many carbon containing starting materials. Following this important discovery, there were many reports of diamond growth using a variety of methods, many of which attempted to replicate natural diamond formation at high pressures and high temperatures. Perhaps the most famous of these reports were experiments in which molten mixtures of iron and charcoal were dropped into a bath of water [26,27]. Supposedly, the rapid contraction produced during this procedure produced a high pressure environment sufficient for diamond growth. Many attempts were made to replicate these diamond synthesis experiments, but many well renowned scientists could not produce any diamond [28]. In 1928 it was concluded that no synthetic diamond had been produced to that date [29].

### 1.3.3 HPHT diamond formation

The breakthrough in diamond synthesis came during the 1950s, when research at AESA showed that a mixture of graphite and an iron carbide compound could be transformed into small diamond crystals under high pressures and high temperatures [30]. At the same time, General Electric in America also reported diamond formation at high pressure and high temperature using graphite in a solvent metal [31]. The presence of a metal solvent-catalyst was shown to be the key component for the graphite to diamond transformation, and due to the conditions required for the technique, the process became known as the high-pressure high-temperature (HPHT) diamond synthesis. HPHT is still widely used in industry today and a typical schematic of HPHT is shown in **Figure 1.7**.

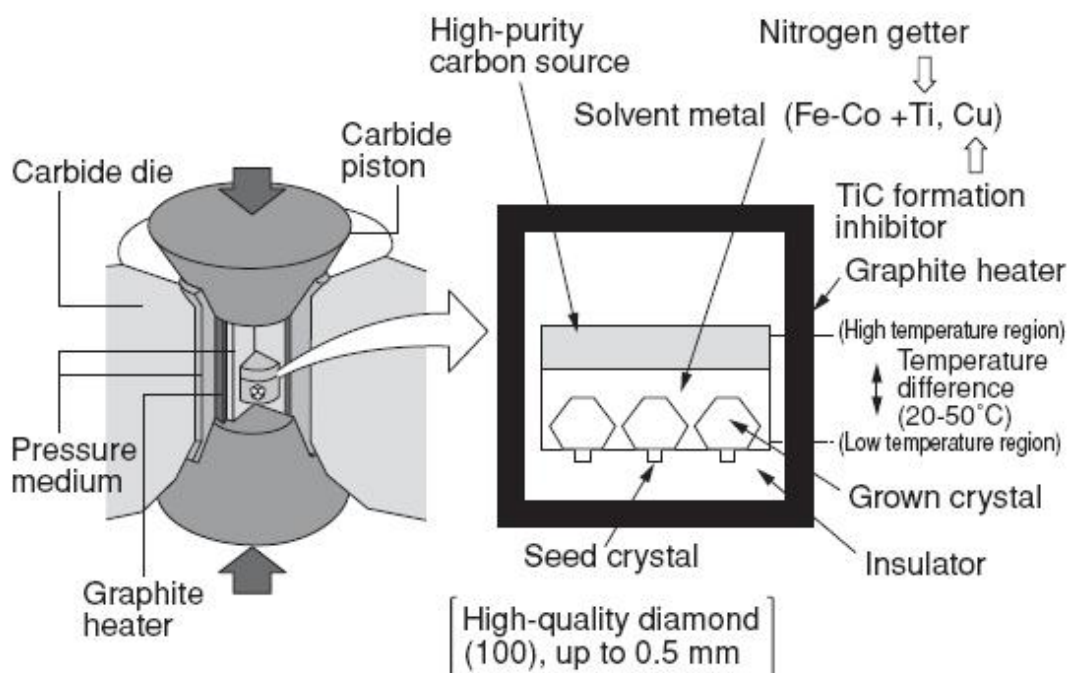


**Figure 1.7:** Schematic of a belt press used for HPHT. Metals such as titanium (Ti) are added to remove nitrogen from the environment, whilst copper (Cu) prevents the titanium from being used in carbide formation. The iron (Fe) solvent metal transports carbon from a high purity carbon source to the diamond seeds for growth. *Figure is from [32].*

The exact mechanism of HPHT is widely debated in the literature due to the HPHT environment being very difficult to analyse during the growth process. This has led to a great deal of indirect evidence being accumulated for the mechanism of HPHT, but at present, numerous theories are supported by the evidence collected [33].

Despite the mechanism being unknown, HPHT is still a very successful method of diamond production and is a key method of producing materials for the abrasives industry. There is however one issue with HPHT, the crystals produced are generally small and non-uniform and so cannot be find use in many applications other than use in the abrasives market [6].

As already demonstrated earlier in this chapter, diamond has fantastic potential for use in many different applications. This has led to a large research effort being put into the development of other diamond syntheses which produce diamond in a form other than small crystals.

### 1.3.4 Chemical vapour deposition

Since diamond can only be produced in a thermodynamically stable regime at extreme conditions, considerable research has targeted the development of diamond syntheses within a metastable regime. This is where diamond, the less thermodynamically stable phase at low pressures, is formed by kinetic preferences rather than thermodynamics.

At the time of HPHT's development, the concept of using gas-phase chemistry to deposit highly pure materials onto solid substrates was becoming popular, and a wide range of pure elements and compound materials were produced using such chemical vapour deposition (CVD) techniques. The breakthroughs in diamond synthesis did not come until the 1980s [34,35] when two groups showed that resistively heated filaments could be used to thermally 'activate' hydrocarbon gases mixed with hydrogen ( $H_2$ ) under low pressure conditions to deposit diamond material onto solid substrate materials. Excess hydrogen was used in these experiments so that the thermal activation would yield atomic hydrogen (H), which had been shown to etch  $sp^2$  carbon at much faster rates than  $sp^3$  carbon [36] and so the diamond would be the kinetically preferred phase.

Hot filament activated CVD (HFCVD) is still widely used today in diamond CVD, however there is one major issue with the technique: the filaments degrade in the CVD environment and this corrosion can lead to contamination of the diamond product [3,4,6]. To prevent this contamination, a number of other activation methods have been developed such as arc jet [37] and combustion CVD [38,39]. The CVD system which is most widely used in the field of diamond CVD research is microwave-assisted CVD (MWCVD), which uses a microwave discharge to activate the gaseous reagents [40]. A schematic of a MWCVD reactor can be seen in **Figure 1.8** along with a HFCVD system, but from this point on, this work will focus on the use of MWCVD systems.

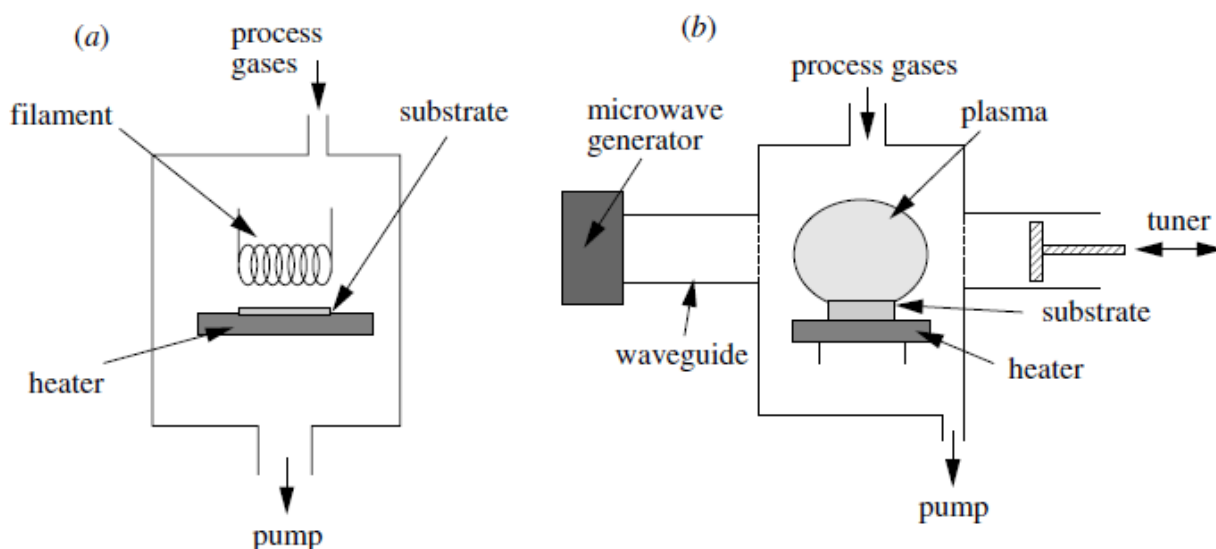


**Figure 1.8:** Schematics of a HFCVD system (left) and MWCVD reactor (right) used to deposit diamond materials. *These diagrams are from [6].*

CVD diamond growth is ultimately comprised of three stages which lead to the gaseous reagents becoming solid diamond materials. These stages can be defined as activation of the gaseous reagents, gas-phase reactions and diffusion to the growing material where surface-reactions occur. Despite the wide range of reactor designs and the use of different feed gases reported [41], the chemistry of diamond CVD is thought to be very similar in all cases [42].

In a MWCVD system, energy is first transferred to lightest components of the system, the free electrons, in the form of heat due to coupling with the electric component of the microwave field. These electrons continue to gain energy and transfer this energy to the gaseous  $H_2$  molecules in the process gas by gas-phase collisions. The energy transferred to the hydrogen molecule can cause vibrational excitation, ionisation or molecular dissociation. This creates a highly reactive state of matter known as plasma.

Since the plasma contains charged species, it can be influenced by electric and magnetic fields. For this reason, MWCVD systems focus the electric field maximum in the centre of the reaction chamber above the substrate [43]. Within the plasma, roughly one third of the hydrogen in the reactor will be dissociated into H [3], and this H is critical for further gas-phase reactions [44].

In the presence of such a high proportion of H in the reactor the carbon containing gas (usually  $CH_4$ ) is rapidly converted to other carbon containing species through hydrogen abstraction and addition reactions. Computational modelling of the CVD plasmas has shown that the distribution of these various carbon species is highly dependent on the local temperature and concentration of H [45]. **Figure 1.9** shows the H-shifting and third-body mediated reactions which cause the thermodynamic distribution of different species between hot and cold regions of the reactor.

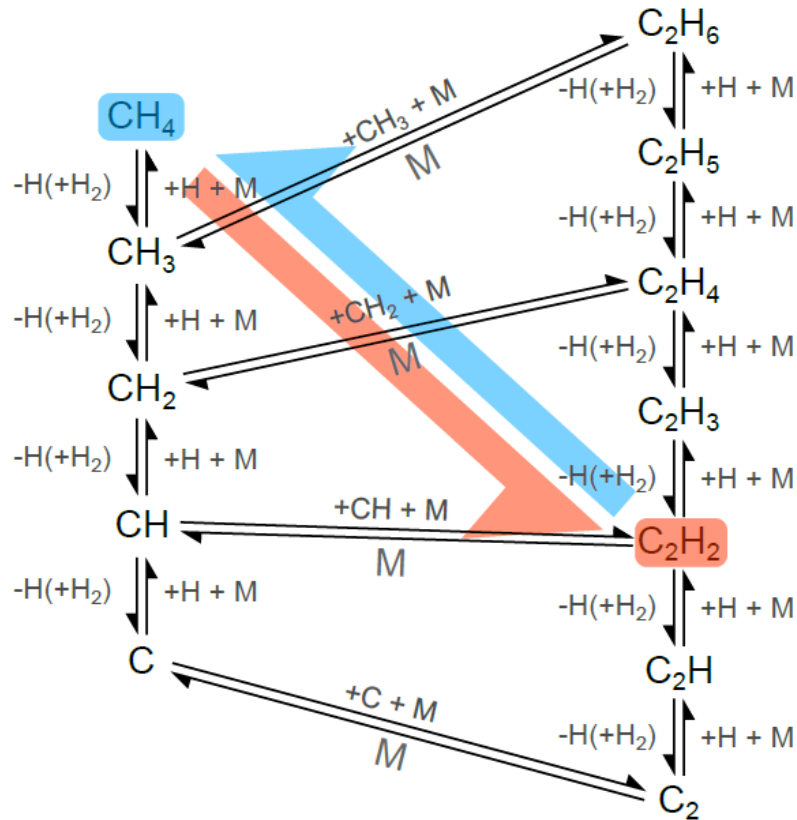


**Figure 1.9:** The various H-shifting and third-body mediated reactions occurring in CVD plasmas which lead to the thermodynamic distribution of  $\text{CH}_4$  at cool regions of the reactor, whilst  $\text{C}_2\text{H}_2$  is most abundant at the centre of the plasma. *This figure is from [4].* The red and blue arrows indicate the trend in conversions within from hot and cold regions of the reactor respectively.

Since the substrate is situated at a cooler region in the reactor,  $\text{C}_1$  species are highly abundant at the growing diamond surface [46] and it is generally believed that the  $\text{CH}_3$  radical is the main growth species [47]. H plays a key role in the surface chemistry of standard model of diamond growth, abstracting H from the diamond surface to produce activate sites on the lattice.  $\text{CH}_3$  radicals can then add to these sites to form new C-C bonds. The pendant methyl groups formed by this reaction can then become incorporated into the diamond lattice by further  $\text{CH}_3$  radical additions and H abstractions, as shown in **figure 1.10**. The idea that  $\text{CH}_3$  is the main growth species during CVD is supported by experiments which show that molecular beams containing  $\text{CH}_3$  can be used to deposit diamond quite rapidly [48,49].

Despite showing how diamond can grow under CVD conditions, the standard model does not account for other processes which have been shown to also occur at the diamond surface. These reactions will be described in a later section of this work. In addition to the surface reactions, which are not accounted for by the standard model, it has been shown that carbon species other than  $\text{CH}_3$  can also add to the lattice and lead to diamond growth [50].

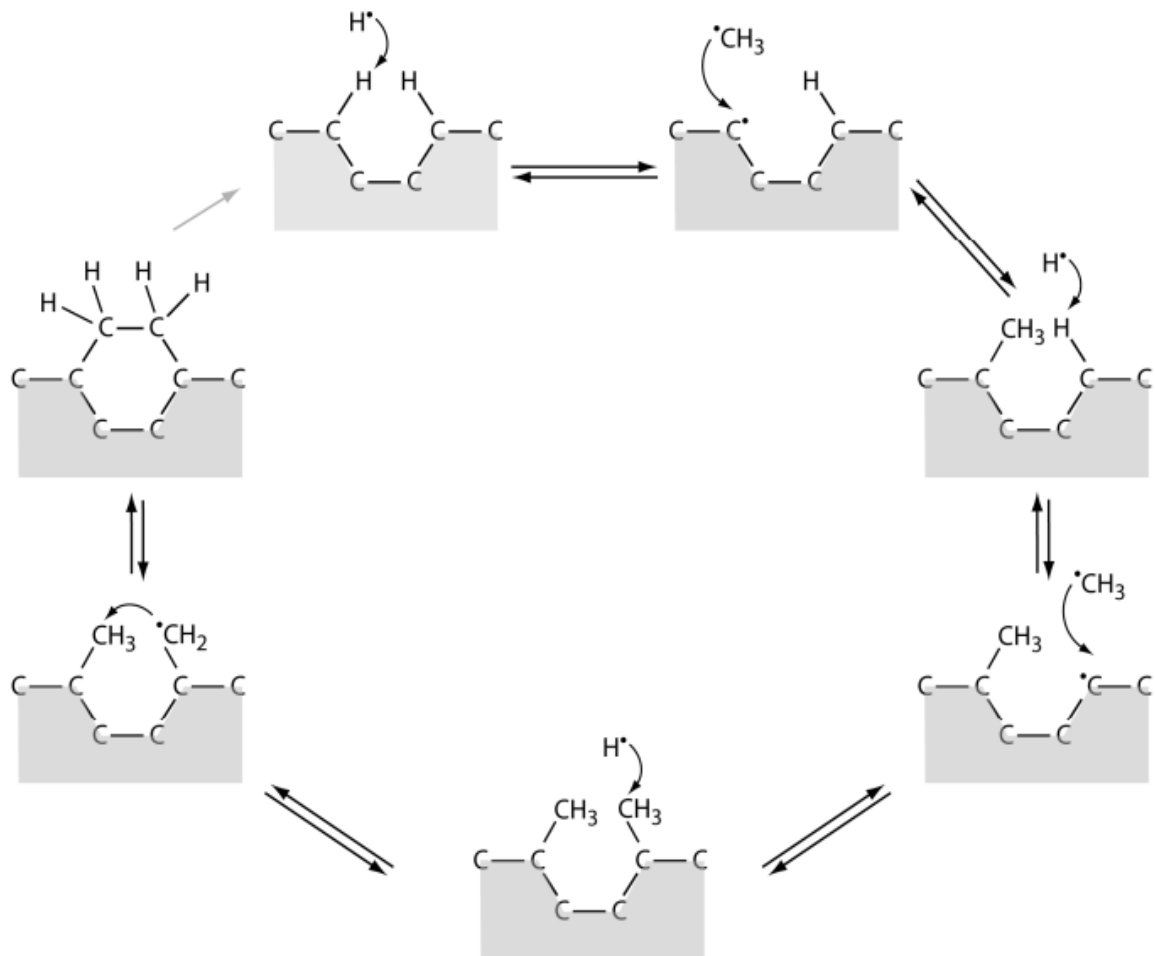


**Figure 1.10:** An illustration of the standard CVD diamond growth model. *This figure is from [3].*

Now that the mechanism by which diamond grows by CVD has been presented, the structure of the diamond produced can be described. In contrast to HPHT which produces numerous small single crystal diamonds (SCD's), CVD usually produces a film composed of small diamond crystallites, which grow together in a columnar structure [51,52]. This material is known as polycrystalline diamond (PCD). In addition to being composed of many diamond crystals, PCD also contains a significant proportion of non-diamond carbon at boundaries between the grains [6]. This leads to slight deterioration in the mechanical and electronic properties of the material in comparison to SCD.

It has been shown that varying the ratio of C:H in the process gas has a significant effect on the morphology of PCD films [50] with grain sizes reducing from micrometre to nanometre scales as the concentration of  $\text{CH}_4$  is increased. Typical CVD conditions of  $\sim 1\%$   $[\text{CH}_4]/[\text{H}_2]$  produce PCD with a grain size of 1-1000  $\mu\text{m}$  and this leads to the material being known as microcrystalline diamond (MCD)[53]. As a matter of fact, most of this project is based on MCD material.

As with all crystalline materials, the diamond unit cell can be divided by a number of different planes which repeat throughout the structure. These planes are described using an  $x,y,z$  coordinate system known as Miller indices. In general, the growth of one particular plane is favoured during CVD growth due to slight nuances in the growth mechanisms of different

planes. This leads to PCD films exhibiting different crystal morphologies characteristic of the deposition conditions. In diamond, there are three dominant crystal planes are described by the {100}, {110} and {111} Miller indices. The {110} surface is the fastest growing diamond surface under standard CVD conditions, but is not often seen due to the surface growing out [3], the different morphologies of {100}- and {111}-oriented crystals in PCD can be seen in **Figure 1.11**.

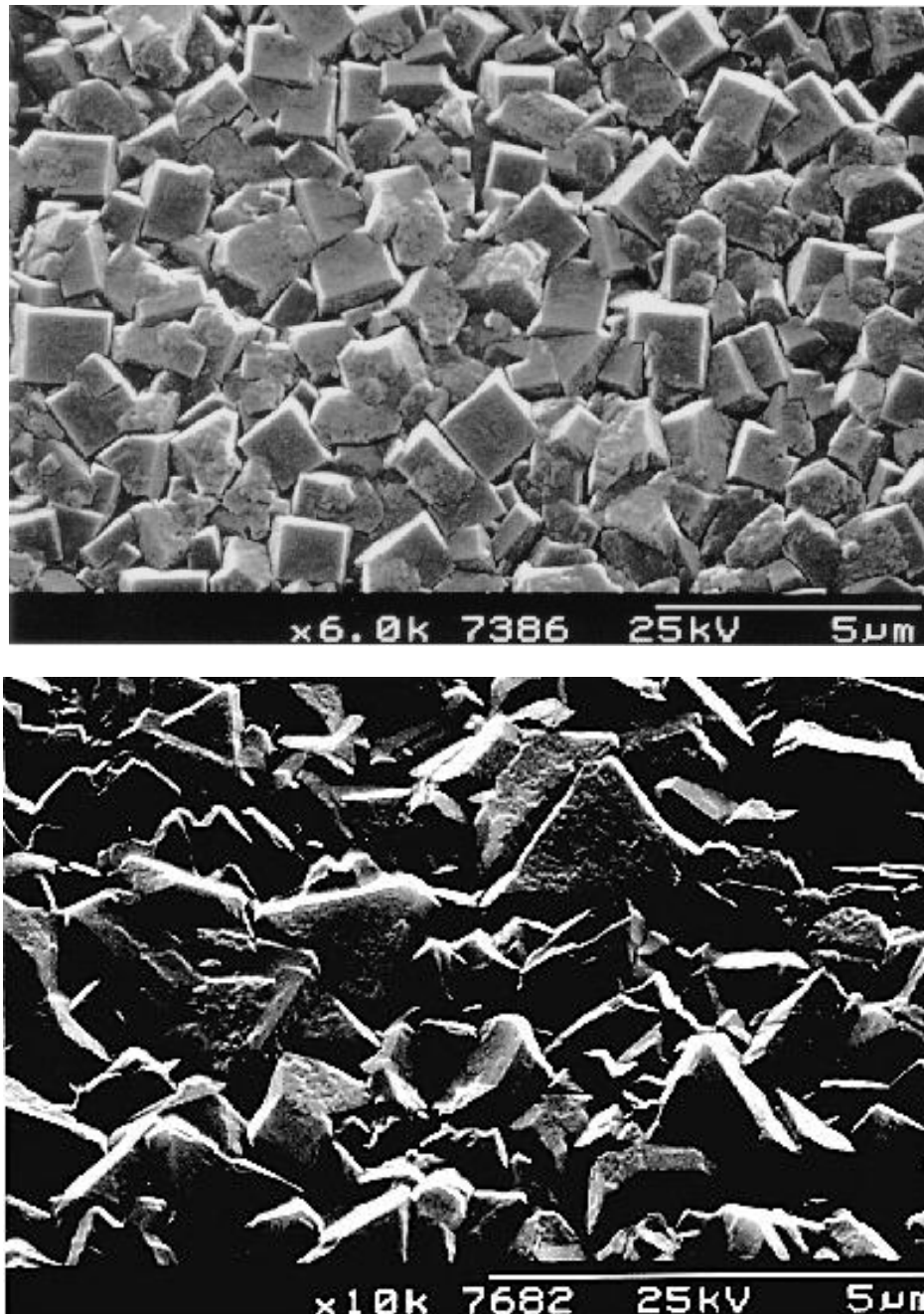


**Figure 1.11:** SEM images of two PCD films deposited by CVD exhibiting different crystal morphologies, one showing surfaces with predominantly square {100} faceting (top) and triangular {111} facets (bottom). *These figures are presented courtesy of Professor Paul May.*

Since these different surfaces grow by slight variations on the standard mechanism, and the rate at which each surface grows depends greatly on the gas composition and the substrate temperature, it is possible to control the crystal morphology observed at the end of CVD. This

has given rise to the  $\alpha$ -parameter which uses the ratio of the {100} and {111} growth rates ( $v_{100}$  and  $v_{111}$  respectively) under certain CVD conditions to predict the major crystal morphology seen on a PCD film at the end of deposition [54]. The  $\alpha$ -parameter is defined as

$$\alpha = \sqrt{3} \left( \frac{v_{100}}{v_{111}} \right)$$

where  $v_{100}$  is the growth rate of the {100} diamond surface and  $v_{111}$  is the growth rate of {111} diamond surface. The value of  $\alpha$  gives an indication as to the shapes of the diamond crystals, as shown in **Figure 1.12**.

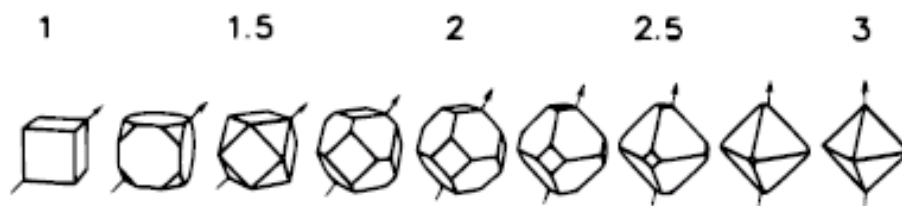


**Figure 1.12:** Crystal morphologies for different growth parameter ( $\alpha$ ) values. The arrows highlight the direction of fastest growth. From [55].

## 1.4 Defects in the diamond lattice

Now that the way in which PCD grows by CVD has been described, imperfections and defects within the crystal structure can be considered. A perfect diamond crystal would be made up of  $sp^3$  hybridised carbon, and nothing but, at every point in the lattice. Unfortunately, perfect crystals are only hypothetical (due to the second law of thermodynamics) and diamond is often found with a number of defects in the structure.

As mentioned previously, the major deviation of PCD from SCD is the presence of grain boundaries between the crystallites. These regions have been shown to contain large amounts of disordered  $sp^3$  bonded carbon,  $sp^2$  carbon and a high proportion of hydrogen [56,57,58], which lead to PCD films having slightly inferior properties in comparison to SCD.

After grain boundaries, the next most significant type of defect is the result of errors made during the diamond growth known as twinning and dislocations [59]. Diamond normally has an ABCBA stacking pattern and is a structure with high symmetry. However, carbon atoms can occasionally be trapped in an eclipsing configuration due to rotation around the C-C bond, as shown in **Figure 1.13**. This leads to a mirror plane being formed, which in turn causes the diamond to adopt an ABCBA stacking structure; this leads to a boat conformation of cyclohexane forming rather than the chair conformer [60]. This is known as twinning and leads to the formation of two crystals with a shared point.

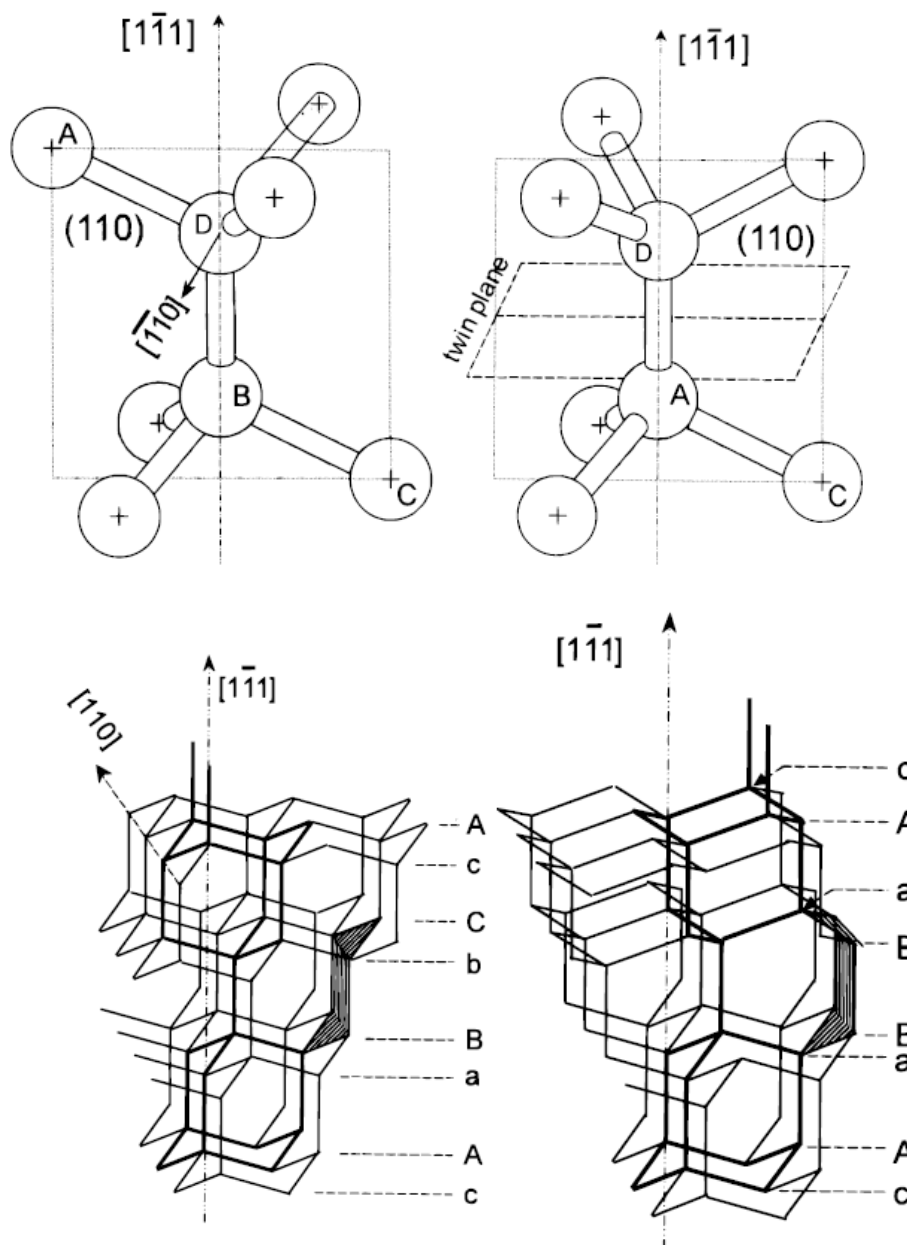


**Figure 1.13:** Twinning at the atomic level is the result of the regular stacking pattern of the diamond lattice (top left) becoming eclipsed (top right). This causes a boat conformation in the structure (bottom right) instead of a chair (bottom left). The conformers of the cyclohexane rings are highlighted in the diamond structure. From [60]

In addition to twinning, completely independent diamond growth can also occur at a site in close proximity to the growing lattice [61]. This is known as a dislocation. These are extremely rare in single crystals, but can be common in PCD films. As a matter of fact, independent crystal nucleation such as this gives rise to nanocrystalline diamond (NCD) films produced using increased C:H ratios during CVD [50].

In addition to these fairly large defects in the diamond structure, small scale errors can also occur within the crystal lattice. In some cases, a carbon atom can be completely missing from its place in the lattice: this is known as a vacancy and leaves a number of non-bonded electrons free on the neighbouring carbon atoms. Since the diamond lattice is highly symmetrical, these high energy electronic states become trapped in the crystal and this allows them to be identified

using absorption spectroscopy [4]. Furthermore, a number of carbon atoms can be absent from the lattice at certain positions, this is called a vacancy cluster.

In addition to vacancies, carbon atoms can be found at sites other than their usual positions within the lattice and are known as interstitials. In general the presence of interstitial atoms is prevented by the rigidity and high atomic density of the diamond structure; however interstitials can sometimes occur, leading to a huge change in the geometry of the lattice. The most common interstitial found in diamond forms when a carbon atom in a normal lattice site is replaced with two carbon atoms, which then symmetrically arrange themselves around the vacant site [61]. The other most common interstitials found in diamond are shown in **Figure 1.14**.

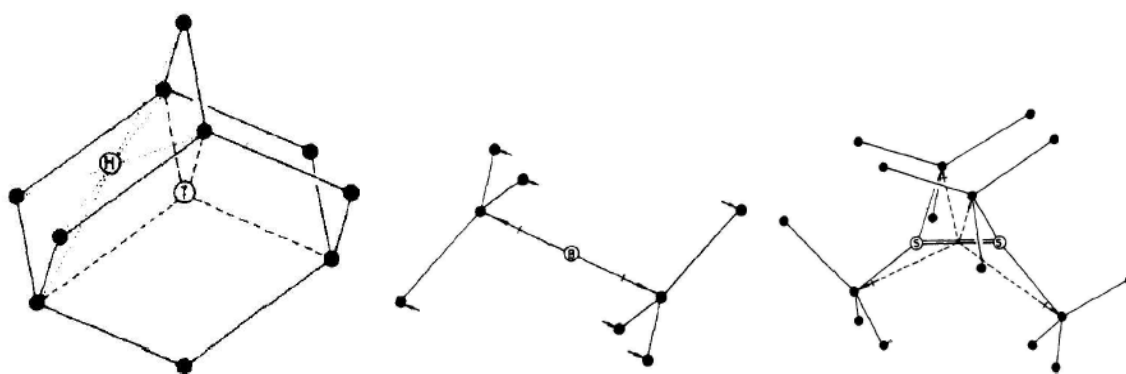


**Figure 1.14:** The three most common interstitial geometries found in diamond where atoms do not occupy their normal positions instead filling hexagonal (left) and tetrahedral holes (middle), as well as the {100} split interstitial showing the change in geometry. From [62].

In addition to carbon atoms being found at interstitial sites, other elements from the environment in which the diamond was grown can be trapped in the lattice as interstitial atoms or, more interestingly, they can displace carbon from points in the lattice. These are known as point defects and will be discussed in more detail with regards to the electronic properties that they impart to diamond.

## 1.5 Doping of the diamond lattice

At the start of this work, diamond was shown to have a very large band gap and is thus an electrically insulating material. This band structure is depicted in **Figure 1.15**. As mentioned in the previous section, atoms other than carbon can sometimes be found at points in the diamond lattice and all of the naturally occurring point defects of this kind found in diamonds are caused by atoms smaller than carbon. This means that the foreign atoms can easily fit into the densely packed lattice without causing too much disturbance to the structure. This project will focus on the introduction of boron into the diamond structure.

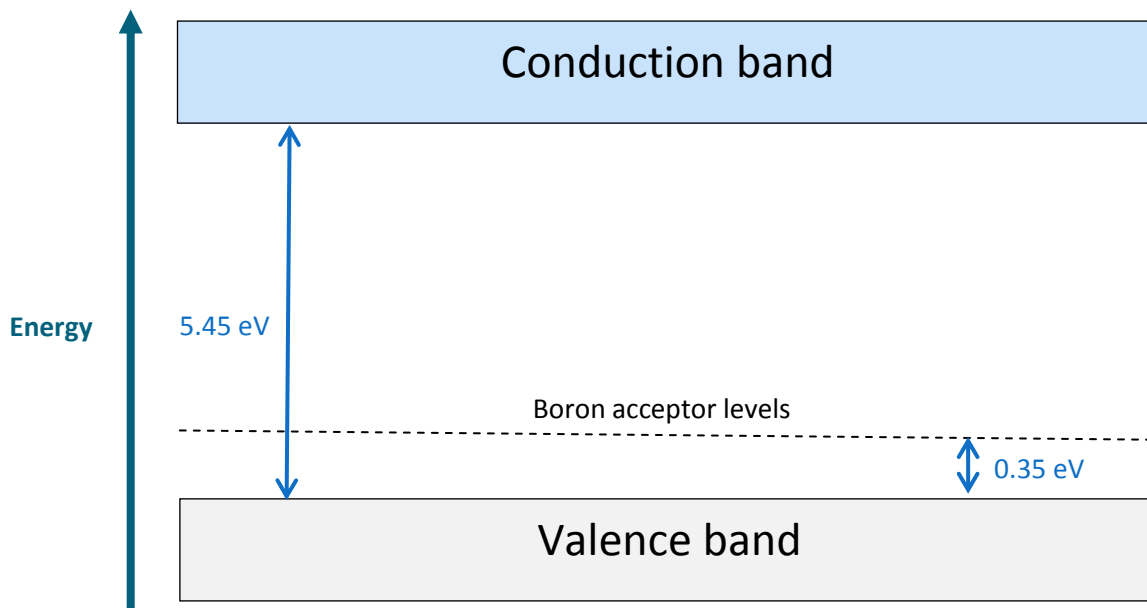


**Figure 1.15:** A band diagram of diamond showing the large band gap of 5.45 eV of undoped diamond and an acceptor level due to boron doping 0.35 eV above the maximum of the valence band. *This figure was designed by the author and is not to scale.*

Boron is a natural dopant of the diamond lattice and gives the crystals a blue colour when present at concentrations of a few ppm [3]. These boron atoms form an acceptor band 0.35 eV above the valence band maximum [63] and electrons from the valence band can fill these acceptor levels. This created holes in the valence band and since these can move through the material, boron-doped diamond is conductive. This form of conductivity is known as p-type semiconductivity. If the concentration of boron is increased further in the diamond crystal, an impurity band forms and the diamonds become semi-metallic [63]. These diamonds are black in colour, as depicted in figure 1.1.6.

Natural boron doped diamonds are incredibly rare and fetch a high price, however with the dawn of CVD boron doped diamond can be produced by the simple addition of a boron containing gas to the standard  $\text{CH}_4/\text{H}_2$  mixture [35]. The most common reagent used for boron doping of CVD diamond is  $\text{B}_2\text{H}_4$  [64,65], and it is possible to control the concentration and position of the boron within the diamond by altering the boron concentration of the feed gas and other reactor parameters. For this reason, boron doping accounts for the majority of p-type diamond produced and the material is beginning to be used in electronic applications as a component of Schottky diodes [66], various switches [67,68], electrodes [69] and microelectromechanical systems (MEMS) [70].



**Figure 1.16:** a representation of the variation in colour with increasing boron concentration from pure diamond (left) through p-type semi-conductive diamond (middle) to semi-metallic diamond (right). *This figure was designed by the author.*

At present there is a lot of interest in producing n-type diamond, which if achieved could lead to diamond completely replacing silicon in some technologies. However, this is an extremely difficult problem to solve since many dopants commonly used for n-type doping are simply too big to fit into the diamond lattice without causing significant disruption to the structure [71]. Many different elements have been added to the process gas in attempts to produce n-type diamond, but attempts to use methods similar to those for p-type doping with boron have not yet produced any breakthroughs [72]. The most effective techniques used so far in the quest for n-type diamond have been co-doping techniques which use nitrogen to disrupt the diamond lattice and thus allow larger atoms to find suitable doping sites [73,74].

Despite these difficulties in producing true n-type diamond, a number of publications have reported p-n junctions made from diamond materials [53]. In these studies, boron doped MCD was used as the p-type material and nitrogen doped ultrananocrystalline diamond (UNCD) was used as the n-type material. UNCD is a material is deposited using Ar dominated plasmas to produce films with crystals sizes < 5 nm [50]. The conductivity seen in the UNCD material is not true n-type conductivity, since the dopant atoms are not incorporated into the diamond lattice itself. UNCD shows n-type conductivity due to the large nitrogen atoms preventing the small diamond crystals from packing closely together, which in turn, causes increased amounts of graphitic material to form between the grains leading an enhancement in the electrical conductivity of the material [75].

## 1.6 Negative electron affinity

In addition to showing increased conductivity, hydrogen terminated boron-doped diamond has been shown to emit electrons from its surface when negatively biased in vacuum [76]. At the time of this discovery it was thought that the energy barrier for this electron emission incredibly small, maybe even negative which has led to it being said that diamond has a negative electron affinity (NEA).

True negative electron affinity arises when the vacuum energy is below the energy of the surface conduction band minimum [77], as shown in **Figure 1.17**. In diamond, this property is thought to arise due to the effects of a dipole at the surface of the material which is induced by the differences in electronegativity between the carbon atoms and the species which terminate the dangling surface bonds [78]. In the case of the H terminated surface, the dipole created is positive at the H and negative at the C. This increased electron density on the C leads to a slight increase in the energy of the surface conduction band minimum relative to the vacuum level. When the diamond surface is fully terminated with hydrogen, the vacuum level actually becomes lower in energy than the surface conduction band minimum and so the surface has NEA.

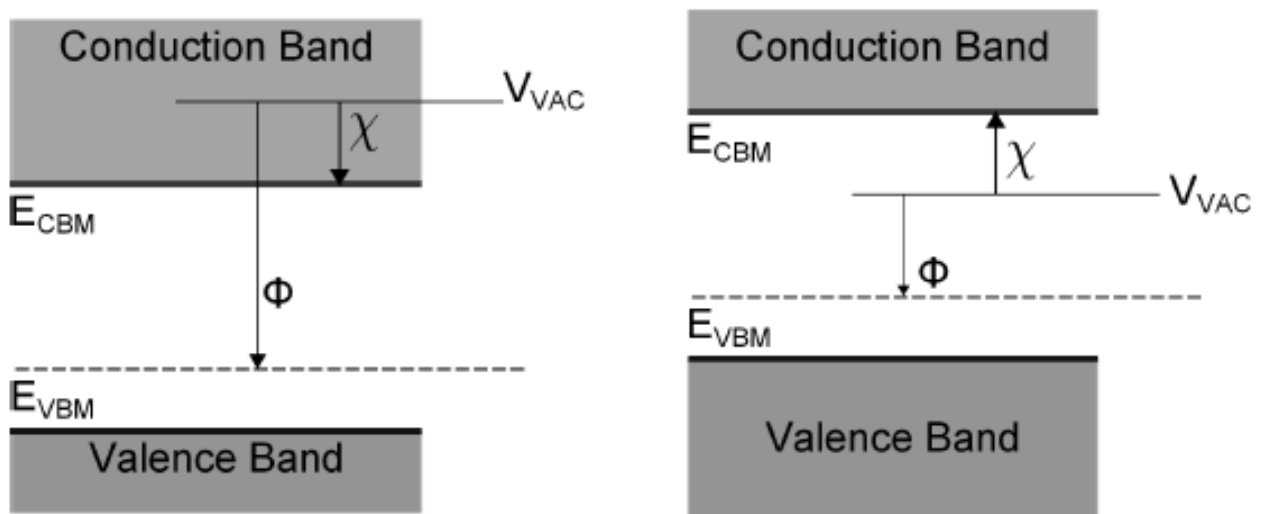


**Figure 1.17:** A band diagram showing the position of the vacuum level relative to the surface conduction band minimum in diamond with a positive electron affinity (left) and a negative electron affinity (right).  $E_{VBM}$  is the valence band maximum,  $E_{CBM}$  is the conduction band minimum,  $V_{VAC}$  is the vacuum level,  $\chi$  is the electron affinity,  $\phi$  is the work function (shown from the boron acceptor levels above  $E_{VBM}$ ). *Figure was adapted from [79].*

Many studies have shown that changing the terminating species to a more electronegative atom than carbon causes the NEA of the surface to be removed [80,81]. This is due to these terminating species inducing a positive electron affinity at the surface and can be explained using the opposite argument to that described above. Many different surface terminations can be induced on diamond using simple procedures and so the emission properties of the diamond can be easily controlled [82]. In these studies, it was shown that highly electronegative atoms such as the alkali metals reduced the work function of the surface most significantly.

In addition to species at the surface being important for NEA, dopants in the bulk can also induce an effective NEA in diamond. An effective NEA is different from true NEA in that the vacuum energy is not lower than the surface conduction band minimum and it is the conduction band minimum of the bulk material which sits above the vacuum level [78]. This is depicted in **Figure 1.18**. In the case of boron-doped diamond, the electron deficient boron atoms accept electrons from the surface states due to a transfer of charge through the material. This movement of the

charge carriers induces an electric field in the material which is positive at the surface and negative in the bulk. This means that the conduction band of the bulk increases in energy relative to the vacuum level whilst the surface states seem to be bent downwards in comparison to the bulk states. If enough boron atoms are present, this band bending effect can result in the bulk conduction band minimum to be lower in energy than the vacuum level [78]. This means that any electrons from the bulk which are transported rapidly to the surface and do not thermalize to the conduction band minimum at the surface will have sufficient energy to escape from the surface of the material. The NEA induced by metal coating of the diamond surface also only induces an effective NEA, because it traps the surface electrons at the interface between the diamond and the metal leading to a band bending effect similar to boron doing.

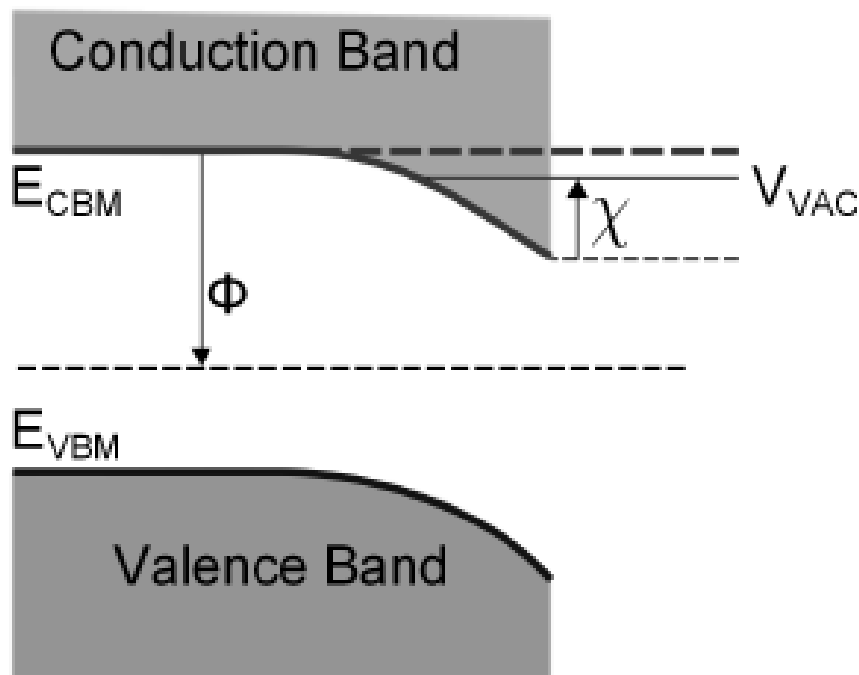


**Figure 1.18:** A band diagram showing the variation in the energy from the bulk to the surface in the case of boron-doped diamond which shows an effective NEA. *Figure was adapted from [79].*

## 1.7 Potential applications of the NEA of diamond

At present there is a lot of interest in using the NEA properties of diamond for a wide range of device applications [79]. Diamond holds a number of advantages over other NEA materials due to its high and stable electron yield, chemical inertness, wide band gap, thermal conductivity, electrical conductivity and the fact that the NEA properties can easily be reactivated by hydrogen treatments in the CVD systems used to create the material [83]. The combination of these factors means that technologies based on diamond are expected to outperform devices based on other materials in the future. However, at the present time, these technologies are still a dream.

A current goal of the diamond group at the University of Bristol, in collaboration with E.ON, is to develop diamond materials for use in thermionic energy converters. These devices will use

lenses to focus solar energy onto a diamond cold cathode material with NEA, thereby causing electrons to be emitted from the material by thermal excitation of the electrons. This is known as thermionic emission [79]. Once emitted from the diamond surface, these electrons can then be collected at an electrode, thereby completing a circuit and producing electricity. An illustration of a thermionic solar converter is shown in **Figure 1.19**.

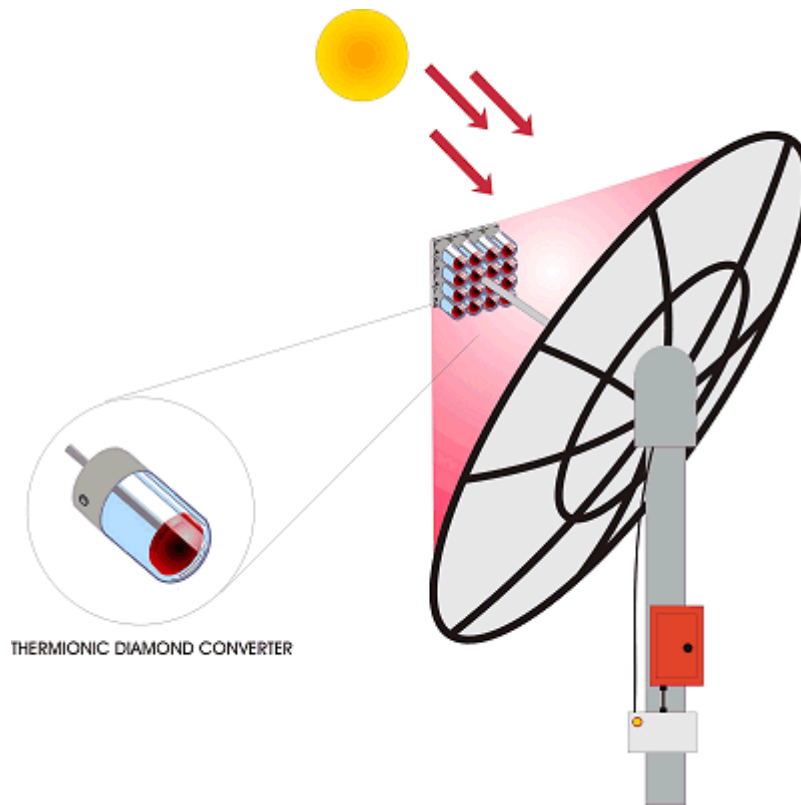


**Figure 1.19:** An illustration of a thermionic energy converters fitted to a parabolic dish which focuses solar energy onto the diamond cold cathode leading to the emission of electrons across a vacuum gap to a collector electrode, thereby transforming solar energy to electricity. *Figure is from [84].*

In the future it is hoped that this technology will become an economically competitive source of renewable energy in its own right, as well as finding use in combination with other suitable technologies to produce increasingly efficient ways of producing electricity. This project forms part of the work in the direction of developing commercially viable diamond-based devices such as thermionic energy converters.

## References

- [1] H. O. Pierson (1993), Handbook of Carbon, Graphite, Diamond and Fullerenes: Properties, Processing and Applications, *Noyes Publications*.
- [2] <http://www.mazaldiamond.com/blog-en/round-brilliant-cut-diamond/>

- [3] O. J. L. Fox (2011), Deposition of nanocrystalline diamond films by MW plasma CVD & Gas-Phase diagnostics using *in-situ* molecular-beam mass spectrometry and emission spectroscopy, PhD Thesis, Department of Chemistry, University of Bristol.
- [4] A. Cheesman (2006), Investigations into the fundamentals of gas-phase and gas-surface chemistry prevalent in the growth of chemical vapour deposited diamond, PhD Thesis, Department of Chemistry, University of Bristol.
- [5] J. E. Field (1992), The properties of natural and synthetic diamond, *Academic Press London*.
- [6] P. W. May (2000), Diamond thin films: a 21<sup>st</sup> century material, *Philosophical Transactions of the Royal Society of London A* **358**(1766), 473.
- [7] <http://en.wikipedia.org/wiki/File:Diamond-and-graphite-with-scale.jpg> Attribution: Rob Lavinsky, [iRocks.com](http://iRocks.com) – CC-BY-SA-3.0
- [8] N. C. Norman (1997), Periodicity and the s- and p-Block Elements, *Oxford University Press*.
- [9] F. P. Bundy (1980), The P, T Phase and Reaction Diagram for Elemental Carbon, *Journal of Geophysical Research* **85**(B12), 6930.
- [10] J. C. Richley (2011), Fundamental Studies of Diamond Chemical Vapour Deposition: Plasma Diagnostics and Computer Modelling, PhD thesis, Department of Chemistry, University of Bristol.
- [11] F. Gerety (1947), De Beers advertising slogan.
- [12] [http://en.wikipedia.org/wiki/File:Carbon\\_basic\\_phase\\_diagram.png](http://en.wikipedia.org/wiki/File:Carbon_basic_phase_diagram.png)
- [13] E. I. Erlic & W. Dan Hausel (2002), Diamond Deposits, *Society for Mining, Metallurgy and Exploration*, 74-94.
- [14] R. M. Hazen (1999), The Diamond Makers, *Cambridge University Press*.
- [15] R. W. Carlson (2005), The Mantle and Core, *Elsevier*.
- [16] Diamond from Outer Space: Geologists Discover Origin of Earth's Mysterious Black Diamonds (2007), *Natural Science Foundation*.  
[http://www.nsf.gov/news/news\\_summ.jsp?cntn\\_id=108270&org=NSF](http://www.nsf.gov/news/news_summ.jsp?cntn_id=108270&org=NSF)
- [17] J. Garai, S. E. Haggerty, S. Rekhi & M. Chance (2006), Infrared Absorption Investigations Confirm the Extraterrestrial Origin of Carbonado Diamonds, *Astrophysical Journal* **653**(2), L153-L156.
- [18] Mystery Diamonds. Geoscientists Investigate Rare Carbon Formation (2007), *American Institute of Physics*. <http://www.aip.org/dbis/APS/stories/17061.html>
- [19] <http://www.liveauctioneers.com/item/7969185>
- [20] J. C-M. Sung & J. Lin (2009), Diamond nanotechnology: Synthesis and Applications, *Pan Stanford Publishing Pte. Ltd*.
- [21] This Valentine's Day, Give The Woman Who Has Everything The Galaxy's Largest Diamond (2004), *Harvard-Smithsonian Centre for Astrophysics*.  
<http://www.cfa.harvard.edu/news/archive/pr0407.html>
- [22] U. Boser (2008), Diamond on Demand, *Smithsonian* **39**(3), 52-59.  
<http://www.smithsonianmag.com/science-nature/diamonds-on-demand.html?c=y&page=2>
- [23] S. Cauchi (2004), Biggest diamond out of this world.  
<http://www.theage.com.au/articles/2004/02/17/1076779973101.html>

- [24] A. Lavoisier (1772), Sur la destruction du diamant par le feu, *Mémoires de l'Académie des sciences*, partie 2e, 564.
- [25] S. Tennant (1797), On the nature of the diamond, *Philosophical Transactions of the Royal Society of London* **87**, 123.
- [26] J. B Hannay (1879), On the Artificial Formation of the Diamond, *Proceedings of the Royal Society of London* **30**(200), 450.
- [27] H. Moissan (1894), Nouvelles expériences sur la reproduction du diamant, *Comptes Rendus* **118**, 320.
- [28] C. A. Parsons (1907), Notes on carbon at high temperatures and high pressures, *Proceedings of the Royal Society* **79**, 532
- [29] C. H. Desch (1928), The Problem of Artificial Production of Diamonds, *Nature* **121**(3055), 799.
- [30] H. Liander & E. Lundblad (1955), Artificial Diamond, *ASEA Journal* **28**, 97.
- [31] F. P. Bundy, H. T. Hall, H. M. Strong & R. H. Wentworf (1955), Man-made diamonds, *Nature* **176**(4471), 51.
- [32] [http://www.diamondlab.org/80-hpht\\_synthesis.htm](http://www.diamondlab.org/80-hpht_synthesis.htm)
- [33] K. Mallika, R. C. DeVries & R. Komanduri (1999), On the low pressure transformation of graphite to diamond in the presence of a 'catalysts solvent', *Thin Solid Films* **339**, 19-33.
- [34] S. Matsumoto, Y. Sato, M. Kamo & N. Setaka (1982), Vapour-deposition of diamond particles from methane, *Japanese Journal of Applied Physics* **29**(8), 1552.
- [35] B. V. Spitsyn, L. L. Bouilov & B. V. Derjaguin (1981), Vapour growth of diamond on diamond and other surfaces, *Journal of Crystal Growth* **52**, 219.
- [36] J. C. Angus, H. A. Will & W. S. Stanko (1968), Growth of diamond seed crystals by vapour deposition, *Journal of Applied Physics* **39**(6), 2915.
- [37] N. Ohtake & M. Yoshikawa (1990), Diamond Film Preparation by Arc discharge Plasma Jet Chemical Vapour Deposition in the Methane Atmosphere, *Journal of The Electrochemical Society* **137**, 717.
- [38] L. M. Hanssen, W. A. Carrington, J. E. Butler & K. A. Snail (1988), Diamond synthesis using an oxy-acetylene torch, *Materials Letters* **7**, 289.
- [39] P. W. Morission Jr & J. T. Glass (1994), Properties and growth of diamond (ed. G. Davies), *London: INSPEC*, 380.
- [40] M. Kamo, Y. Sato, S. Matsumoto & N. Setaka (1983), Diamond synthesis from gas-phase in microwave plasma, *Journal of Crystal Growth* **62**(3), 642.
- [41] P. W. May, N. M. Everitt, C. G. Trevor, M. N. R. Ashfold & K. N. Rosser (1993), Diamond deposition in a hot-filament reactor using different hydrocarbon precursor gases, *Applied Surface Science* **68**, 299-305.
- [42] M. N. R. Ashfold, P. W. May, C. Rego & N. M. Everitt (1994), Thin Film Diamond by Chemical Vapour Deposition Methods, *Chemical Society Reviews* **23**, 21-30.
- [43] M. Fünér, C. Wild and P. Koidl (1998), Novel microwave plasma reactor for diamond synthesis, *Applied Physics Letters* **72**, 1149.
- [44] K. Hassouni, O. Leroy, S. Farhat & A. Gicquel (1998), Modelling of H<sub>2</sub> and H<sub>2</sub>/CH<sub>4</sub> Moderate-Pressure Microwave Plasma Used for Diamond Deposition, *Plasma Chemistry And Plasma Processing* **18**(3), 325-362.

- [45] W. L. Zhu (1992), Gas-phase kinetics during microwave plasma-assisted diamond deposition: Is the hydrocarbon product distribution dictated by neutral-neutral interactions? *Journal of Applied Physics* **72**, 3102.
- [46] Y. A. Mankelevich, N. V. Suetin, M. N. R. Ashfold, J. A. Smith, and E. Cameron (2001), Experimental data vs. 3-D model calculations of HFCVD processes: correlations and discrepancies, *Diamond and Related Materials* **10**(3-7), 364.
- [47] S. J. Harris (1990), Mechanism of diamond growth from methyl radicals, *Applied Physics Letters* **56**(23), 2998.
- [48] S. S. Lee, D. W. Minsek, D. J. Vestyck & P. Chen (1994), Growth of diamond from atomic-hydrogen and a supersonic free jet of methyl radicals, *Science* **263**(5153), 1596.
- [49] K. P. Loh, J. S. Foord, R. B. Jackman & N. K. Singh (1996), Growth studies of thin film diamond using molecular beam techniques, *Diamond and Related Materials* **5**(3-5), 231.
- [50] P. W. May and Y. A. Makelevich (2008), From ultrananocrystalline diamond to single crystal diamond growth in hot filament and microwave plasma-enhanced CVD reactors: a unified model for growth rates and grain sizes, *Journal of Physical Chemistry C* **112**(32), 12432.
- [51] I. Sungawa (1990), Growth and morphology of diamond crystals under stable and metastable conditions, *Journal of Crystal Growth* **99**(1-4, part 2), 1156-1161.
- [52] P.W. May, N.L. Allan, M.N.R. Ashfold, J.C. Richley & Yu.A. Mankelevich (2010), Simulations of Polycrystalline CVD Diamond Film Growth Using a Simplified Monte Carlo Model, *Diamond and Related Materials* **19**, 389-396.
- [53] P. W. May (2010), Chemical vapour deposition – a route to microcrystalline, nanocrystalline, ultrananocrystalline and single crystal diamond films, *Chapter 6 in Carbon Based Nanomaterials, Materials Science Foundations (monograph series)* (N. Ali, A. Öchsner & W. Ahmed Eds., Trans Tech Publications Inc, Switzerland) **65-66**, 145-176. Ed.
- [54] C. Wild, R. Kohl, N. Herres, W. Muller-Sebert, & P Koidl (1994), Oriented CVD diamond films: twin formation, structure and morphology, *Diamond and Related Materials* **3**, 373.
- [55] C. Wild, P. Koidl, W. Müller-Sebert, H. Walcher, R. Kohl, N. Herres, R. Locher, R. Samlenski, and R. Brenn (1993), Chemical vapour deposition and characterization of smooth {100}-faceted diamond films, *Diamond and Related Materials* **3**, 158.
- [56] J. Wagner , C. Wild & P. Koidl (1991), Resonance effects in Raman scattering from polycrystalline diamond films, *Applied Physics Letters* **59**(7), 779-781.
- [57] P. Reichart, G. Datzmann, A. Hauptner, R. Hertenberger, C. Wild & G. Dollinger (2004), Three-Dimensional Hydrogen Microscopy in Diamond, *Science* **306**, 1537.
- [58] S. Praver and R. J. Nemanich (2004), Raman spectroscopy of diamond and doped diamond, *Philosophical Transactions of the Royal Society of London A* **362**(1824), 2537.
- [59] L. S. Hounsoume, R. Jones, P. M. Martineau, D. Fisher, M. J. Shaw, P. R. Briddon & S. Öberg (2006), Origin of brown colouration in diamond, *Physics Reviews B* **73**, 125203.
- [60] E. Blank (2003), Structural Imperfections in CVD Diamond Films in "Semiconductor & Semimetals" (C. E. Nebel & J. Ristein, Eds.) **76**, 49-145.
- [61] C. Weigel, D. Peak, J. W. Corbett, G. D. Watkins & R. P. Messmer (1973), Carbon Interstitial in the Diamond Lattice, *Physical Reviews B* **8**(6), 2906.

- [62] A. Mainwood, F. P. Larkins & A. M. Stoneham (1978), The structure and motion of the self-interstitial in diamond, *Solid-State Electronics* **21**(11-12), 1431-1433.
- [63] P. W. May, W. J. Ludlow, M. Hannaway, J. A. Smith, K. N. Rosser & P. J. Heard (2008), Boron doping of Microcrystalline and Nanocrystalline Diamond Films: Where is the Boron Going?, *Proceedings of Material Research Society Symposium* **1039**, 17
- [64] H. Shiomi, K. Tanabe, Y. Nishibayashi & N. Fujimori (1990), Epitaxial-growth of high quality diamond film by the microwave plasma-assisted chemical-vapour-deposition method, *Japanese Journal of Applied Physics* **29**(1), 34.
- [65] D. W. Comerford, A. Cheesman, T. P. F. Carpenter, D. M. E. Davies, N. A. Fox, R. S. Sage, J. A. Smith, M. N. R. Ashfold & Y. A. Mankelevich (2006), Experimental and modelling studies of B atom number density distributions in hot filament activated B<sub>2</sub>H<sub>6</sub>/H<sub>2</sub> and B<sub>2</sub>H<sub>6</sub>/CH<sub>4</sub>/H<sub>2</sub> gas mixtures, *Journal of Physical Chemistry A* **110**(9), 2868.
- [66] A. Vescan, I. Daumiller, P. Gluche, W. Ebert & E. Kohn (1998), High temperature, high voltage operation of diamond Schottky diode, *Diamond and Related Materials* **7**(2-5), 581-584.
- [67] S. H. Lin, L. H. Sverdrup, K. M. Garner, E. J. Korevaar, C. Cason & C. C Phillips (1993), Electron Beam Activated Diamond Switch Experiments, *Proceedings of the International Society for Optical Engineering Optically Activated Switching Conference III* **1873**, 97-109.
- [68] M. Krishnan, J. R. Thompson, D. Parks, A. N. Gerhan, E. H. Baksht, M. I. Lomaev, D. V. Rybka & V. F. Tarasenko (2006), UV flashlamp source for high-voltage high-current diamond switches, *Proceedings of the International society for Optical Engineering Atomic and Molecular Pulsed Lasers Conference VI* **6263**, 626310.
- [69] H. B. Martin, A. Argoitia, U. Landau. A. B, Anderson & J. C. Angus (1996), Hydrogen and Oxygen Evolution on Boron Doped Diamond Electrodes, *Journal of the Electrochemical Society* **143**(6), L133-L136.
- [70] E. Kohn, P. Gluche & M. Adamschik (1999), Diamond MEMS – a new emerging technology, *Diamond and Related Materials* **8**(2-5), 934-940.
- [71] S. A. Kajihara, A. Antonelli, J. Bernholc & R. Car (1991), Nitrogen and potential normal type dopants in diamond, *Physical Review Letters* **66**(15), 2010.
- [72] P. W. May, M. Davey, K. N. Rosser & P. J. Heard (2008), Arsenic and Antimony Doping: An Attempt to Deposit n-type CVD diamond, *Proceedings of the Materials Research Society Symposium* **1039**, 15.
- [73] G. Z. Cao, W. J. P. van Enckevort, L. J. Giling & R. C. M. de Kruij (1995a), Enhancement of phosphorus incorporation and growth-rate of epitaxial diamond films by the addition of nitrogen, *Applied Physics Letters* **66**(6), 688.
- [74] G. Z. Cao, L. J. Giling & P. F. A. Alkemade (1995b), Growth of phosphorus and nitrogen co-doped diamond films, *Diamond and Related Materials* **4**(5-6), 775.
- [75] O. A. Williams (2006), Ultrananocrystalline diamond for electronic applications, *Semiconductor Science and Technology* **21**, R49-R56.
- [76] F. J. Himpsel, J. A. Knapp, J. A. van Vechten & D. E. Eastman (1979), Quantum photoyield of diamond(111) – A stable negative-affinity emitter, *Physical Review B* **20**(2), 624-627.
- [77] C. I. Wu, A. Kahn, E. S. Hellman & D. N. E. Buchanan (1998), Electron affinity at aluminium nitride surfaces, *Applied Physics Letters* **73**(10), 1346-1348
- [78] J. Robertson (1996), Electron affinity of carbon systems, *diamond and Related Materials* **5**(6-8), 797-801.

- [79] T. L. Martin (2011), Lithium oxygen termination as a negative electron affinity surface on diamond a computational and photoemission study, PhD Thesis, H. H. Wills Physics Laboratory, University of Bristol.
- [80] D. Takeuchi (2005), Total Photoyield Spectroscopy experiments on Hydrogen- and Oxygen-Terminated Diamond Films, *New Diamond and Frontier Carbon Technology* **15**(5), 297-310.
- [81] F. Maier, J. Ristein & L. Ley (2001), Electron affinity of plasma-hydrogenate and chemically oxidised diamond (100) surfaces, *Physical Reviews B* **64**, 165411.
- [82] P. W. May, J. C. Stone, M. N. R. Ashfold, K. R. Hallam, W. N. Wang & N. A. Fox (1998), The effect of diamond surface termination species upon field emission properties, *Diamond and Related Materials* **7**(2-5), 671-676.
- [83] J. S. Lapington, D. P. Thompson, P. W. May, N. A. Fox, J. Howorth, J. Milnes & V. Taillandier (2009), Investigation of the secondary emission characteristics of CVD diamond films for electron amplification, *Nuclear Instruments and Methods in Physics Research A* **610**, 253-257.
- [84] <http://www.chm.bris.ac.uk/pt/diamond/thermionic.htm>

# Chapter 2

## Current issues in the realisation of commercial cold cathode devices

---

For optimal performance, SCD would be the ideal material for use in cold cathode devices [1]. The development of single crystal materials in the field of materials science has received considerable attention and investment over the past few decades, and the reasons are not far to seek. For any given property, a single crystal material will exhibit that property to the best possible extent. An example of this is the use of single crystal silicon in semiconductor fabrication. Since single crystal silicon does not possess any defects or impurities which might affect the local electronic environment in the material [2], the material behaves predictably, reliably and above all exhibits excellent electronic properties. Without single crystal silicon, almost all of the modern electronic technologies which billions of people use in everyday life simply would not exist. Try to imagine daily life without personal computers or mobile phones and it becomes immediately clear how much of an impact single crystal materials have on technology and society.

At the molecular level, silicon and diamond have very similar structures and form tetrahedral giant covalent structures [3]. It is this diamond lattice structure which gives silicon its wonderful properties, but diamond exhibits more extreme and useful properties, making diamond ‘the ultimate engineering material’ [4]. In the future, diamond-based technologies are expected to go far beyond the current capabilities of silicon-based technology and so diamond will become the material of choice for many applications. When this happens, ‘the diamond age’ will have truly begun [5].

### 2.1 The production of SCD

As already described briefly in section 1.3.4, HPHT is capable of producing single crystal diamonds, but due to the slow growth rate and expense of producing large crystals in general, only small, low quality HPHT products are available commercially. This is an unsuitable material for use in diamond electronics. As a matter of fact the majority of commercially available is not even gem grade [6] with a high proportion of imperfections and impurities (such as nitrogen). For this reason, there has been a lot of interest over the past decade in depositing highly pure, high quality SCD over large areas using CVD techniques [7,8,9,10,11].

Over the past decade, two methods of producing SCD have emerged. The use of a low methane concentration in the process gas (<1% CH<sub>4</sub> in H<sub>2</sub>) has been shown to produce high quality, device grade diamond layers on small SCD substrates (4-25 mm<sup>2</sup>) [12] with growth rates of up to 2 μm h<sup>-1</sup> [13]. This method works by limiting the concentration of carbon radical species above the surface, allowing growth of the surface to only occur in a step-flow manner [14]. This is where carbon atoms can only become locked into the lattice at the edges of steps and nowhere else on the surface [15]. Unfortunately, due to the low growth rate of this method, commercial SCD cannot be produced in this way.

Through awareness of the  $\alpha$ -parameter, and how it is affected by the deposition conditions, it has been shown that SCD can be produced by CVD at growth rates up to  $150 \mu\text{m h}^{-1}$  using high  $\text{CH}_4$  concentrations in the feed gas (10%  $\text{CH}_4$  in  $\text{H}_2$ ) [16]. Under normal CVD conditions this C:H ratio is known to produce NCD [14], but this growth mechanism is prevented by the use of high pressures and high microwave powers to generate a high plasma density and a high gas temperature [12]. Under these conditions, there is a high rate of dissociation of  $\text{H}_2$  and so a high concentration of atomic H is present at the surface [12]. This means that the C:H ratio is low at the surface and so the diamond growth is thought to be dominated by  $\text{CH}_3$  radicals adding to the surface in a uniform manner [17]. This allows for “defect-free” diamond deposition [12]. The only major issue with this technique is that the high gas temperature produced under these conditions heats the substrate so strongly that efficient cooling is required to prevent overheating [12].

This second method has shown that device grade SCD can be produced on a practical timescale, but only over small areas due to the use of small SCD substrates. Since CVD growth is limited to the area of substrate, large area SCD substrates up to 100 mm in diameter will need to be produced. At present, it is the production of these large substrates which poses a major hurdle for the development and commercial production of cold cathode devices.

The most obvious way of making such a substrate would be to cut one from natural diamond. However, natural diamonds large enough to be able to produce such substrates are extremely rare and very expensive. The largest diamond crystal found so far, the Cullinan diamond, weighed just over 600g [18]. If this diamond was a spherical crystal, the Cullinan diamond would be the approximately the size of a tennis ball (with a diameter of 6.8 cm). However, large crystals of diamond can fracture easily and the Cullinan diamond has been cut into 9 diamond gemstones, some of which can be seen in the British Crown Jewels [19]. This shows that finding a natural diamond from which a large area SCD substrate could be cut is highly unlikely. Add to this the fact that the substrate needs to be of exceptional quality and it is clear to see that such a crystal will probably never be found. Furthermore, if such a diamond were to be found, it would have a price tag in the region of many \$billions. For these reasons, there is currently a lot of interest in increasing the size of commercially available SCD substrates from HPHT sources and in some cases, substrates cut from small natural diamonds.

Interestingly, when a silicon crystal is grown homoepitaxially on a single crystal substrate using CVD techniques, the area at the top of the film increases with the thickness of the grown layer [20]. In diamond, however, the area at the top of the diamond shrinks as the film grows thicker (especially when nitrogen is present in the system) [21]. The growth of Si and SCD can be seen in **figure 2.1**. Nitrogen is a common additive to the CVD gas mixture used for SCD growth [22,23] because it enhances growth in the {100} direction whilst suppressing the growth of other crystallographic planes. This makes the growth of the diamond more reproducible and enhances the rate of deposition [21]. In addition to nitrogen in the process gas, the growth of diamond can be controlled by careful manipulation of the growth conditions to alter the  $\alpha$ -parameter. The only issue with this technique is it is very difficult to maintain the sensitive parameter throughout a long growth procedure [21].

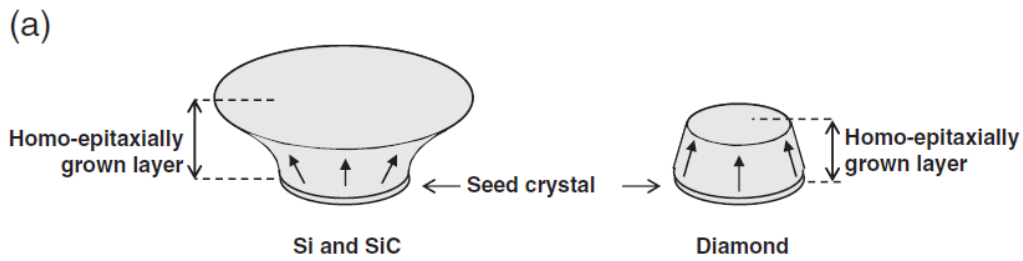


**Figure 2.1:** Enlargement of the top surface area during crystal growth of Si (left) and shrinking of the top surface area diamond growth due to the introduction of nitrogen into the feed gas.

Figure is from [21]

In addition to these techniques, it has been shown that it is possible to increase the size of an SCD film by forming a seeding block [24]. This is done by CVD growth on the {100} surface to form a cuboid followed by polishing and growth on the {010} surface. This procedure is illustrated in **Figure 2.2**, and shows that it is possible to transform a small SCD substrate into a seeding block. The largest seeding block produced so far has dimensions of half an inch [24].

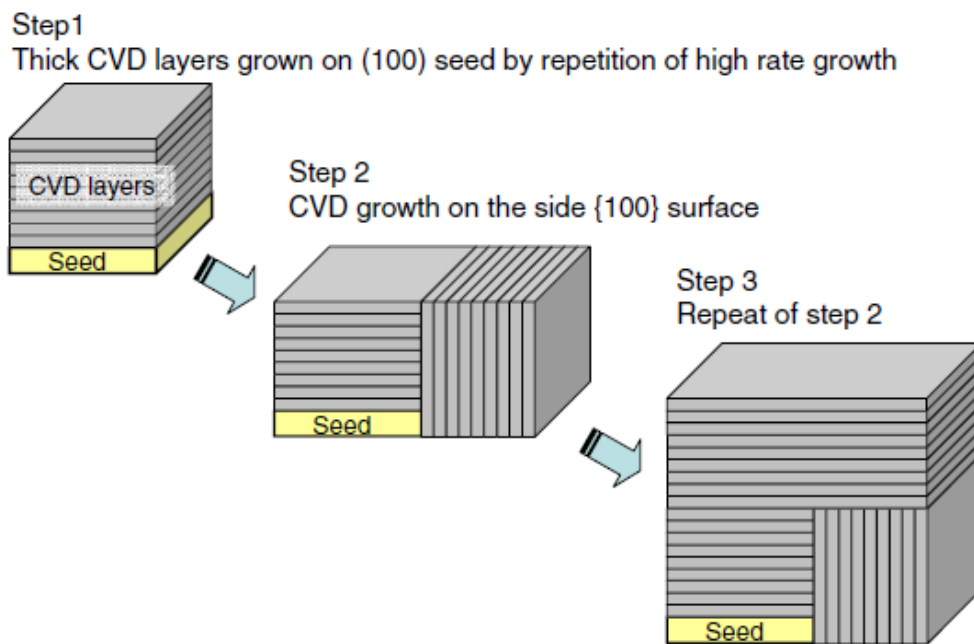


**Figure 2.2:** An illustration of the concept of 3D enlargement of a SCD seed crystal by growth on the side of the {100} surface. Figure is from [23].

These blocks can then be processed into freestanding wafers using laser cutting [21] or lift off processes [21,22] which use a high energy ion beam to produce a layer of damage beneath the top of the substrate [25,26]. This layer of diamond above the damaged layer can then be removed to create a freestanding wafer or subjected to diamond growth before it is removed from the larger block. By applying this technique to an SCD block already described, it is possible to produce many larger are clones of this seed crystal [24]. This is illustrated in **Figure 2.3**.

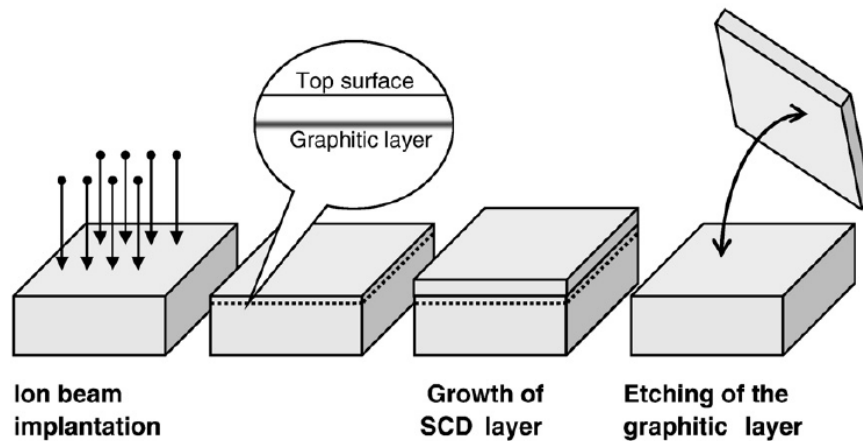


**Figure 2.3:** An illustration of a lift-off procedure using ion implantation to create a damaged layer just below a surface of a diamond block. Growth on the surface of the disconnected layer followed by selective etching of the graphite allows a freestanding wafer to be produced. *Figure is from [21]*

While these methods have been very successful, increasing the wafer size to 20 x 20 mm is very difficult. Even at a high growth rate of  $10 \mu\text{m h}^{-1}$  it would take over 1000 hours to enlarge a 0.5 inch SCD plate to 1 inch in size [21]. During these extremely long timescales, the pressure, gas flows, microwave power and substrate temperature need to be controlled with variations  $<1\%$  to ensure that the surface grows uniformly, since any large fluctuations will cause errors to occur in the growth process and ultimately lead to a PCD film [11]. For this reason, current SCD growth is limited by the precision of the reactor engineering and how much time and money can be invested in producing larger SCD films from seeding crystals [11].

For this reason, there is considerable interest in increasing the size of diamond wafers in the form of mosaic structures [27,28], shown in **Figure 2.4**. SCD is commercially available in the form of small tiles which can be arranged in order from the growth layer and join the plates together into one large wafer. This technique allows for larger areas of diamond to be produced much more rapidly than the growth of a large block seed crystal. A recent study has shown that the diamond formed at junctions between the seeds of these mosaic wafers is different to that grown on the top of the seeding crystals [27]. The crystal quality at these junctions is currently being investigated [29,30] since the differences between these regions may cause significant problems when large plates grown by the mosaic seeding method are used in electronic devices.

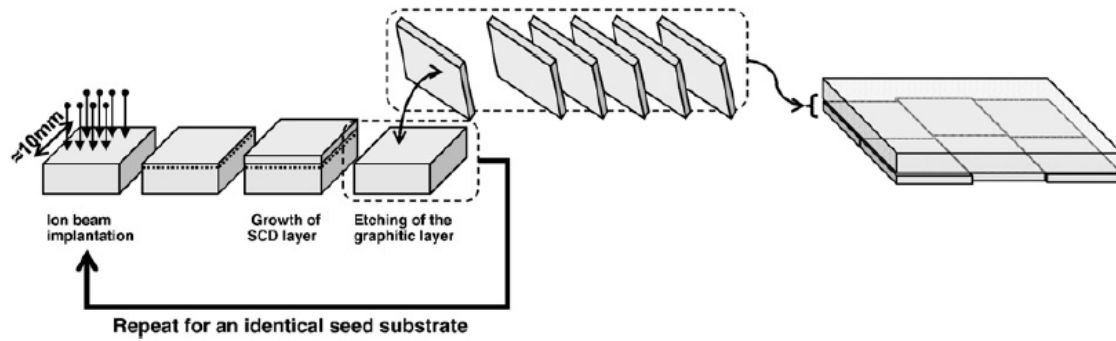


**Figure 2.4:** A procedure for fabricating multiple clones of the SCD block which can then be arranged in a mosaic structure and grown together by CVD to produce a large area wafer. *Figure is from [21].*

Since it does not seem as though high quality SCD suitable for commercial applications will be obtained at any time in the near future, other diamond materials are being considered as candidates for use in the first generation of electronic devices.

## 2.2 Alternative diamond materials to SCD

Diamond materials have been grown on non-diamond substrates since the dawn of the CVD era [30] and a number of different substrate materials have been used [31]. Recently, there has been considerable interest in the use of iridium as a substrate for CVD due to material's close match to the diamond lattice [32,33]. In general CVD growth on iridium uses a bias-enhanced nucleation (BEN) technique [34] where a negative potential is applied to cause carbon containing ions to be implanted into the surface of the substrate [12]. Since the upper layers of the substrate are rich in carbon, the diamond nuclei can register with the substrate more rapidly and hence, the long incubation periods required for the initial nucleation of diamond in standard CVD procedures is removed [12].

Optimising the CVD conditions to achieve a specific value of the  $\alpha$ -parameter has been shown to produce highly textured films following BEN on iridium [35] but most interestingly, extended diamond growth using this two-step technique has revealed that the diamond grains can coalesce, reducing the mosaicity of the films to a state where large areas of the surface appears to become singularly crystalline [36]. This material is known as quasi-SCD and an example is shown in in **Figure 2.5**.

At first glance quasi-SCD seems to be the best possible replacements of SCD, especially for NEA applications where the properties of the surface are most important. However, there are a number of issues associated with the production of these materials [12]. The first problem is that the reactors used require more complex reactor engineering than standard CVD reactors. Secondly, the growth process involves multiple stages. In commercial production, it is preferable to use procedures with minimal complexity because, in general, extra stages require extra equipment and longer processing times. Furthermore, quasi-SCD has only been achieved over

small areas in the centre of the samples [37] and so cannot currently be scaled up to suit the requirements of commercial electronic applications.

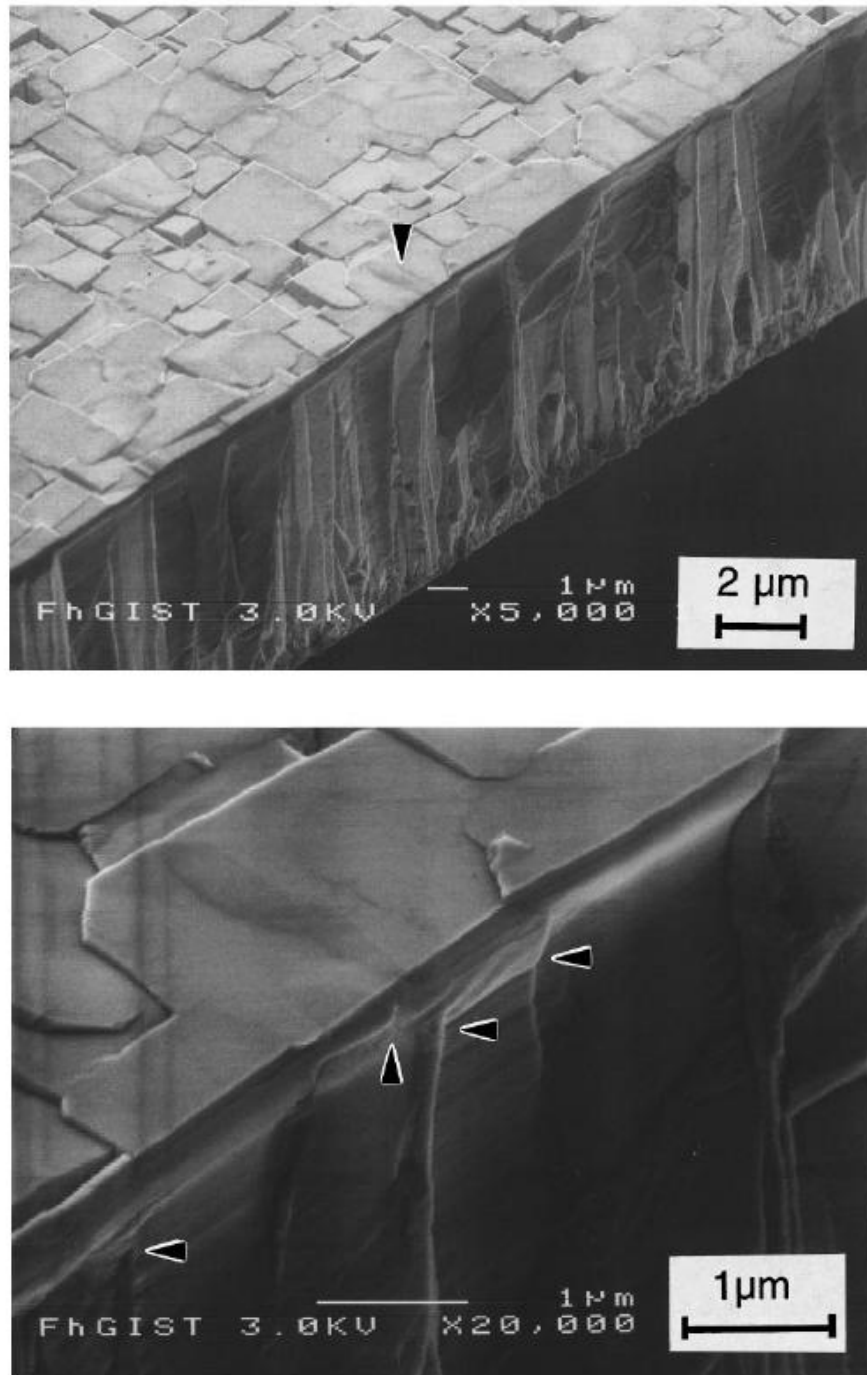


**Figure 2.5:** Cross-sectional SEM images of a 10 μm thick diamond film grown on silicon using BEN and CVD conditions optimised for  $\alpha=1$  showing coalescence of the diamond grains at the surface (top). Higher magnification at the location indicated by the arrow in the first image shows the grains overlapping to produce the appearance of larger crystallites. *This figure is from [38].*

Since materials with single crystal surfaces cannot be achieved over the areas required, MCD materials produced by standard CVD seem to be the best candidates for use in NEA

technologies. MCD can exhibit very similar properties to SCD when the crystal sizes are large [39] and has a number of advantages over SCD in that it can be grown on cheap non-diamond substrates at rates  $>1 \mu\text{m h}^{-1}$  [40]. Furthermore, large area deposition of MCD is possible by the use of an array of filaments [41] and the material can easily be doped with boron to induce p-type semiconductivity [42]. Furthermore, hydrogen termination of the diamond crystals in the PCD material can be done easily and gives the surface the desired NEA properties for use in cold cathode devices [43].

As mentioned at the end of chapter 1, this project forms part of the work towards the realisation of thermionic devices based on diamond. In these devices the diamond will be used as a cold cathode, which is integrated into an electronic system to face a collector anode [44]. A schematic of such a device is shown in **Figure 2.6**. As thermal energy from the heat source (ideally from the sun) is transferred to the diamond, the electrons are excited to the conduction band. Since this lies above the vacuum level in diamond, the electrons are emitted from the surface. These electrons cross the gap to the anode where they are collected and flow through the circuit to the load where work is done and so, thermal energy has been converted to electricity [44]. The electrons can then continue to follow the circuit back to the emitter to fill the holes that have been created by the emission of electrons across the vacuum gap.

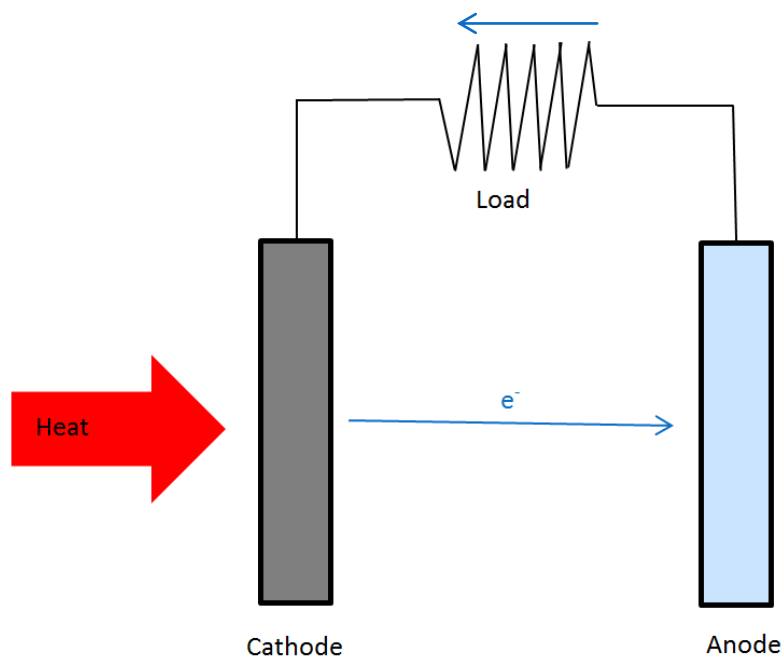


**Figure 2.6:** Schematic of a simple thermionic energy conversion device. The blue arrows indicate the direction of the electron flow. *This figure was designed by the author.*

Apart from requiring the lowest possible threshold for electron emission from the diamond material, the efficiency of thermionic energy converters will be dependent on the proportion of electrons emitted from the cathode being collected by the anode material. The ideal situation would be to have an NEA surface which emitted electrons in a uniform manner with minimal time transit spread [45]. This means the surface needs to be smooth, as illustrated in **Figure 2.7**.

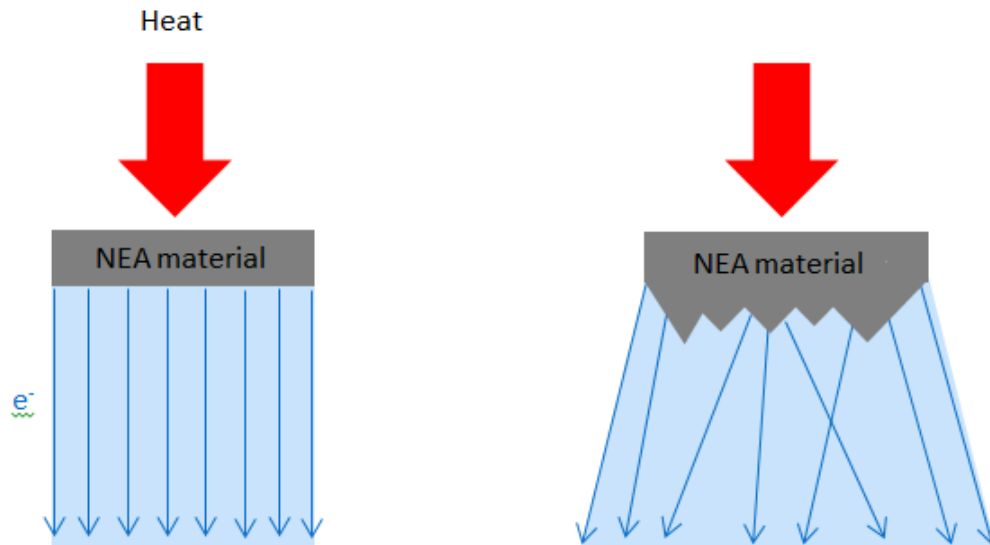


**Figure 2.7:** An illustration of emissions from a smooth diamond surface (left) and a rough surface (right), showing the average spread of the electrons emitted from the surface in response to the stimulation source. *Figure designed by the author.*

This requirement for smooth surfaces means that PCD cannot be used in its as grown form since the random orientations and non-uniform sizes of the crystallites make the surfaces of PCD very rough [46]. This means that polishing techniques will need to be incorporated into the preparation of PCD materials for use in cold cathode devices.

## 2.3 Polishing of diamond materials

A number of techniques have been developed which remove material from the surface of diamond, ranging from relatively simple lapping techniques [47] and chemo-mechanical polishes [48] to the use of exotic thermochemical polishes [49], ion beams [50], lasers [51] and plasmas [52]. There have been many good evaluations written on the range techniques for polishing diamond materials [53,54] and so, it is not necessary to review all of the techniques here.

Simple techniques such as lapping do not remove material from the surface of large area diamond materials at significant enough rates for use commercial applications [53], but the addition of reactive species to the polishing plate has been shown to improve lapping techniques dramatically, especially when an iron plate is used [55]. However, thermochemical treatments require rather complicated and expensive apparatus [56].

Furthermore, ion beams and laser polishes have been shown to produce the fantastically smooth surfaces by removing material from the surface in a step-by-step fashion [57], but removing material from the surface in this way makes the treatments very complex, long and expensive [56].

For these reasons the use of plasmas for removing material from the diamond surface is regarded as the best solution for use in commercial applications. The main advantage of plasma etching is that it can be performed using the MWCVD apparatus used to grow diamond films simply by changing the gases flowing into the reactor [58]. The most commonly used gases for plasma etching of diamond are O<sub>2</sub>, SF<sub>6</sub> and Ar [53]. Due to its high abundance in CVD environments, there has been considerable interest in the effects of hydrogen plasmas on the roughness of SCD [59,60]. However, very few investigations have reported the effects of hydrogen plasma treatments on PCD materials.

In this project, the effects of hydrogen plasma treatment on PCD diamond surfaces will be investigated under a variety of different conditions. It is hoped that this study will show that the treatment parameters can be optimised to produce the significant smoothing effects of the diamond surface and thereby confirm the suitability of hydrogen plasmas for use in the commercial production of diamond materials for NEA applications.

## References

- [1] J. Isberg, J. Hammersberg, D. J. Twitchen & A. J. Whitehead (2004), Single crystal diamond for electronic applications, *Diamond and Related Materials* **13**(2), 320-324.
- [2] N. M. P. Johnson, G. A. Ponce, R. A. Street & R. J. Nemanich (1987), Defects in single-crystal silicon induced by hydrogenation, *Physical Reviews B* **35**, 4166-4169.
- [3] N. C. Norman (1997), Periodicity and the s- and p-Block Elements, *Oxford University Press*.
- [4] P. W. May (2000), Diamond thin films: a 21<sup>st</sup> century material, *Philosophical Transactions of the Royal Society of London A* **358**(1766), 473.
- [5] J. C-M. Sung & J. Lin (2009), Diamond nanotechnology: Synthesis and Applications, *Pan Stanford Publishing Pte. Ltd*.
- [6] R. Linares & P. Doering (1999), Properties of large single crystal diamond, *Diamond and Related Materials* **8**, 909-915,
- [7] C. S. Yan, Y. K. Vohra, H. K. Mao & R. J. Hemley (2002), Very high growth rate chemical vapour deposition of single-crystal diamond, *Proceedings of the National Academy of Sciences of the United States of America* **99**(20), 123523-12525
- [8] J. Isberg, J. Hammersberg, E. Johansson, T. Wikström, D. J. Twitchen, A. J. Whitehead, S. E. Coe & G. A. Scarsbrook (2002), High Carrier Mobility in Single-Crystals Plasma-Deposited Diamond, *Science* **297**(5587), 1670-1672.
- [9] H. Okushi (2001), High Quality homoepitaxial CVD diamond for electronic devices, *Diamond and Related Materials* **10**, 281.
- [10] D. Takeuchi, H. Watanabe, S. Yamanaka, H. Okushi & K. Kajimura (2000), Homepitaxial diamond films grown by step-flow mode in various misorientation angles of diamond substrates, *Diamond and Related Materials* **9**(3-6), 231-235.
- [11] H. Okushi, H. Watanabe, S. R. S. Yamanaka & D. Takeuchi (2002), device-grade homoepitaxial diamond film growth, *Journal of crystal growth* **237-239**(2), 1269-1276.
- [12] P. W. May (2010), Chemical vapour deposition – a route to microcrystalline, nanocrystalline, ultrananocrystalline and single crystal diamond films, *Chapter 6 in*

- Carbon Based Nanomaterials, Materials Science Foundations (monograph series)* (N. Ali, A. Öchsner & W. Ahmed Eds., Trans Tech Publications Inc, Switzerland) **65-66**, 145-176. Ed.
- [13] Y. Avigal, C. Uzan-Saguy & R. Kalish (1992), Diamond homoepitaxy by hot filament chemical vapour deposition, *Diamond and Related Materials* **2**(2-4), 462-467.
- [14] P. W. May and Y. A. Makelevich (2008), From ultrananocrystalline diamond to single crystal diamond growth in hot filament and microwave plasma-enhanced CVD reactors: a unified model for growth rates and grain sizes, *Journal of Physical Chemistry C* **112**(32), 12432.
- [15] J. C. Richley (2011), Fundamental Studies of Diamond Chemical Vapour Deposition: Plasma Diagnostics and Computer Modelling, PhD thesis, Department of Chemistry, University of Bristol.
- [16] T. Teraji (2006), Chemical vapour deposition of homoepitaxial diamond films, *Physica Status Solidi A* **203**(13), 3324-3357.
- [17] C. J. Chu, M. P. D'Evelyn, R. H. Hauge & J. L. Margrave (1991), Mechanism of diamond growth by chemical vapour deposition on diamond (100), (111) and (110) surfaces: Carbon-13 studies, *Journal of Applied Physics* **70**(3), 1695-1705.
- [18] W. Crookes (1909), *Diamonds, Published by London and New York Harper & Brothers.*
- [19] <http://famousdiamonds.tripod.com/cullinandiamonds.html>
- [20] W.C. Dash (1959), Growth of Silicon Crystals Free from Dislocations, *Journal of Applied Physics* **30**, 459
- [21] H. Yamada, A. Chayahara, Y. Mokuno, N. Tsubouchi, S. Shikata & N. Fujimori (2011), Developments of elemental technologies to produce inch-size single-crystal diamond wafers, *Diamond and Related Materials* **20**, 616-619.
- [22] A. Chayahara, Y. Mokuno, Y. Horino, Y. Takasu, H. Yoshikawa & N. Fujimori (2004), The effect of nitrogen addition during high rate homoepitaxial growth of diamond by microwave plasma CVD, *Diamond and Related Materials* **13**(11-12) 1954-1958.
- [23] Y. Mokuno, A. Chayahara, Y. Soda, H. Yamada, Y. Horino & N. Fukimori (2006), High rate homoepitaxial growth of diamond by microwave plasma CVD with nitrogen addition, *Diamond and Related Materials* **15**, 455-459.
- [24] Y. Mokuno, A Chayahara, H. Yamada & N. Tsubouchi (2009), Improving purity and size of single-crystal diamond plates produced by high-rate CVD growth and lift-off process using ion implantation, *Diamond and Related Materials* **18**(10), 1258-1261.
- [25] A. Stacey, V. S. Drumm, B. A. Fairchild, K. Ganesan, S. Rubanov, R. Kalish, B. C. C. Cowie, S. Praver & A. Hoffman (2011), Improved diamond surfaces as a result of lift-off and plasma treatments as observed by x-ray absorption spectroscopy, *Applied Physics Letters* **98**, 181907.
- [26] H. Yamada, A. Chayahara, Y. Mokuno, H. Umezawa, S. Shikata & N. Fujimori (2010), Fabrication of 1 inch Mosaic Crystal Diamond Wafers, *Applied Physics Express* **3**, 0513301.
- [27] G. Janssen & L. J. Giling (1995), "Mosaic" growth of diamond, *Diamond and Related Materials* **4**, 1025.
- [28] H. Yamada, A. Chayahara, H. Umesawa, N. Tsubouchi, Y. Mokuno & S. Shikata (2012), Fabrication and fundamental characterisations of tiled clones of single-crystal diamond with a 1-inch size, *Diamond and Related Materials* **24**, 29-33.

- [29] N. Tsubouchi, H. Umezawa, Y. Mokuno, A. Chayahara & S. Shikata (2012), Lattice structure of a freestanding nitrogen doped large single crystal diamond plate fabricated using lift-off process: X-ray diffraction studies, *Diamond and Related Materials* **25**, 119-123.
- [30] B. V. Spitsyn, L. L. Bouilov & B. V. Derjaguin (1981), Vapour growth of diamond on diamond and other surfaces, *Journal of Crystal Growth* **52**, 219.
- [31] M. N. R. Ashfold, P. W. May, C. Rego & N. M. Everitt (1994), Thin Film Diamond by Chemical Vapour Deposition Methods, *Chemical Society Reviews* **23**, 21-30.
- [32] M. Schreck, F. Hörmann, H. Roll, J. K. N. Lindner, and B. Stritzker (2001), Diamond nucleation on iridium buffer layers and subsequent textured growth: A route for the realization of single-crystal diamond films, *Applied Physics Letters* **78**(2), 192-194.
- [33] K. Ohtsuka, K. Suzuki, A. Sawabe & T. Inuzuka (1996), Epitaxial Growth of Diamond on Iridium, *Japanese Journal of Applied Physics* **35**, L-1072-L1074,
- [34] J. C. Arnault, F. Vonau, M. Mermoux, F. Wyczisk & P. Legagneux (2004) Surface study of iridium buffer layers during the diamond bias enhanced nucleation in a HFCVD reactor, *Diamond and Related Materials* **13**(3), 401-413.
- [35] S. Gsell, T. Bauer, J. Goldfuß, M. Schreck & B. Stritzker (2004), A route to diamond wafers by epitaxial deposition on silicon via iridium/yttria-stabilised zirconia buffer layers, *Applied Physics Letters* **84**, 4541.
- [36] M. Schreck, A. Shury, F. Hörmann, H. Roll & B. Stritzker (2002), Mosaicity reduction during growth of heteroepitaxial diamond films on iridium buffer layers: Experimental results and numerical simulations, *Journal of Applied Physics* **91**, 676.
- [37] T. Bauer, S. Gsell, M. Schreck, J. Goldfuß, J. Lettieri, D. G. Schlom & B. Stritzker (2005), Growth of epitaxial diamond on silicon via iridium/SrTiO<sub>3</sub> buffer layers, *Diamond and Related Materials* **14**(3-7), 314-317.
- [38] X. Jiang & C. L. Jia (1996), The coalescence of [001] diamond grains heteroepitaxially grown on (001) silicon, *Applied Physics Letters* **69**(25), 3902-3904.
- [39] Y. Yamamoto, T. Imai, K. Tanabe, T. Tsuno, Y. Kumazawa & N. Fujimori (1996), The measurement of thermal properties of diamond, *Diamond and Related Materials* **6**(8), 1057-1061.
- [40] A. Cheesman (2006), Investigations into the fundamentals of gas-phase and gas-surface chemistry prevalent in the growth of chemical vapour deposited diamond, PhD Thesis, Department of Chemistry, University of Bristol
- [41] O. J. L. Fox (2011), Deposition of nanocrystalline diamond films by MW plasma CVD & Gas-Phase diagnostics using *in-situ* molecular-beam mass spectrometry and emission spectroscopy, PhD Thesis, Department of Chemistry, University of Bristol.
- [42] P. W. May, W. J. Ludlow, M. Hannaway, J. A. Smith, K. N. Rosser & P. J. Heard (2008), Boron doping of Microcrystalline and Nanocrystalline Diamond Films: Where is the Boron Going?, *Proceedings of Material Research Society Symposium* **1039**, 17
- [43] M. C. Salvadori, W. W. R. Araújo, F. S. Tiexiera, M. Cattani, A. Pasquarelli, E. M. Oks & I. G. Brown (2010), Termination of diamond surfaces with hydrogen, oxygen and fluorine using a small, simple plasma gun, *Diamond and Related Materials* **19**(4), 324-328.
- [44] J. R. Smith, G. L. Bilbro & R. J. Nemanich (2006), Using negative electron affinity diamond emitters to mitigate space charge in vacuum thermionic energy conversion devices, *Diamond and Related Materials* **15**(11-12), 2082-2085.

- [45] J. S. Lapington, D. P. Thompson, P. W. May, N. A. Fox, J. Howorth, J. Milnes & V. Taillandier (2009), Investigation of the secondary emission characteristics of CVD diamond films for electron amplification, *Nuclear Instruments and Methods in Physics Research A* **610**, 253-257.
- [46] R. Ramesham & M. F. Rose (1998), Polishing of polycrystalline diamond by hot nickel surface, *Diamond and Related Materials* **320**(2), 223-227.
- [47] C. J. Tang, A. J. Neves, A. J. S. Fernandes, J. Grácio & N. Ali (2003), A new elegant technique for polishing CVD diamond films, *Diamond and Related Materials* **12**(8), 1411-1416.
- [48] C. D. Ollison, W. D. Brown, A. P. Malshe, H. A. Naseem & S. S. Ang (1999), A comparison of mechanical lapping versus chemical-assisted polishing and planarization of chemical vapour deposited (CVD) diamond, *Diamond and Related Materials* **8**(6), 1083-1090.
- [49] W. C Chou, C. L. Chao, H. H. Chien, K. J. Ma & H. Y. Lin (2007), Investigation of Thermo-Chemical Polishing of CVD Diamond Film, *Key Engineering Materials* **329**, 195-200.
- [50] P. W. Leech, G. K. Reeves, A.S. Holland & F. Shanks (2002), Ion beam etching of CVD diamond film in Ar, Ar/O<sub>2</sub> and Ar/CF<sub>4</sub> gas mixtures, *Diamond and Related Materials* **11**(3-6), 833-836.
- [51] E. Capelli, G. Mattei, S. Orlando, F. Pinzari & P. Ascarelli (1999), Pulsed laser surface modification of diamond thin films, *Diamond and Related Materials* **8**(2-5), 257-261.
- [52] G. S. Sandu & W. K. Chu (1989), Reactive ion etching of diamond, *Applied Physics Letters* **55**(5), 437-438.
- [53] A. P. Malshe, B. S. Park, W. D. Brown & H. A. Naseem (1999), A review of techniques for polishing and planarizing chemically vapour-deposited (CVD) diamond films and substrates, *Diamond and Related Materials* **8**, 1198-1213.
- [54] H. Y. Tsai, C. J. Ting & C. P. Chou (2007), Evaluation research of polishing method for large area diamond films produced by chemical vapour deposition, *Diamond and Related Materials* **16**, 253-261.
- [55] M. Yoshikawa & F. Okuzumi (1997), Hot-iron-metal polishing machine for CVD diamond films and characteristics of the polished surfaces, *Surface and Coatings Technology* **88**(1-3), 197-203.
- [56] Y. Chen & L. C. Zhang (2009), On the Polishing Techniques of Diamond and Diamond Composites, *Key Engineering Materials* **404**, 85-96.
- [57] A. M. Ozkan, A. P. Malshe & W. D. Brown (1997), Sequential multiple-laser-assisted polishing of free-standing CVD diamond substrates, *Diamond and Related Materials* **6**(12), 1789-1798.
- [58] F. Silva, R. S. Sussmann, F. Bénédic & A. Gicquel (2003), Reactive ion etching of diamond using microwave assisted plasmas, *Diamond and Related Materials* **12**(3-7), 369-373.
- [59] O. M. Küttel, L. Diederich, E. Schaller, O. Carnal & Louis Schlapbach (1995), The preparation and characterization of low surface roughness (111) and (100) natural diamonds by hydrogen plasma, *Surface Science Letters* **337**, L812-L818.
- [60] B. D. Thoms, M. S. Owens, J. E. Butler & C. Spiro (1994), Production and characterisation of smooth, hydrogen terminated diamond C(100), *Applied Physics Letters* **65**(23), 2957-2960.

# CHAPTER 3

## Diamond from a low pressure solid state source

---

In addition to investigating the effects of hydrogen plasmas on PCD surfaces, a secondary study will be performed to determine whether the presence of metallic layers on the surface of the diamond film can enhance the polishing effects of the plasma treatment. This idea has been inspired by the work of a group led by Rustum Roy at Pennsylvania State University, who discovered a potentially useful method of diamond formation, which bridges the gap between HPHT and CVD. This technique is known as the low pressure solid state source (LPSSS) technique [1]. This chapter will present an overview of LPSSS.

LPSSS uses hydrogen plasmas to treat various forms of carbon mixed with a range of metal powders and has been shown to grow diamond very easily [2], and in some cases did not require diamond seeds [1]. In these experiments it was shown that the diamond produced by LPSSS was commonly associated with metallic globules or ropes, shown in **Figure 3.1**. For this reason, it was thought that the metal was playing a crucial role in the process.

Due to the apparent importance of a metal in the process, the inventors of the LPSSS process suggested that the method may be similar to the HPHT. In an analysis of the metallic globules produced during the process it was shown that they were amorphous in structure [1] and were composed of a range of ternary  $M_xC_yH_z$  alloys which contained up to 70 atomic% carbon [3] in some cases. This provided evidence that LPSSS may be similar to HPHT since previous work had shown that the intermediate solution formed in HPHT could also contain up to 70 atomic% carbon [4].

The noble metals (Ag and Au) were found to be particularly effective in the LPSSS technique and provided an illustration of how the diamond formation progressed step-by-step [1], shown in **Figure 3.2**. However, the exact mechanism by which the diamond was forming was not clear. Despite this, Roy et al. continued to study the LPSSS process and showed that it could be used to improve the quality of cheap diamond grits (**Figure 3.3**) and also grow well-aligned epitaxial layers on {100}-oriented SCD. It was in the experiments using SCD that the enhancing role of the metal on the diamond formation process was most evident. In comparison to a LPSSS experiments without any metal, the presence of a metal was found to increase the growth rate by  $12 \mu\text{m h}^{-1}$  [1]. However, the role of the metal was still unclear.

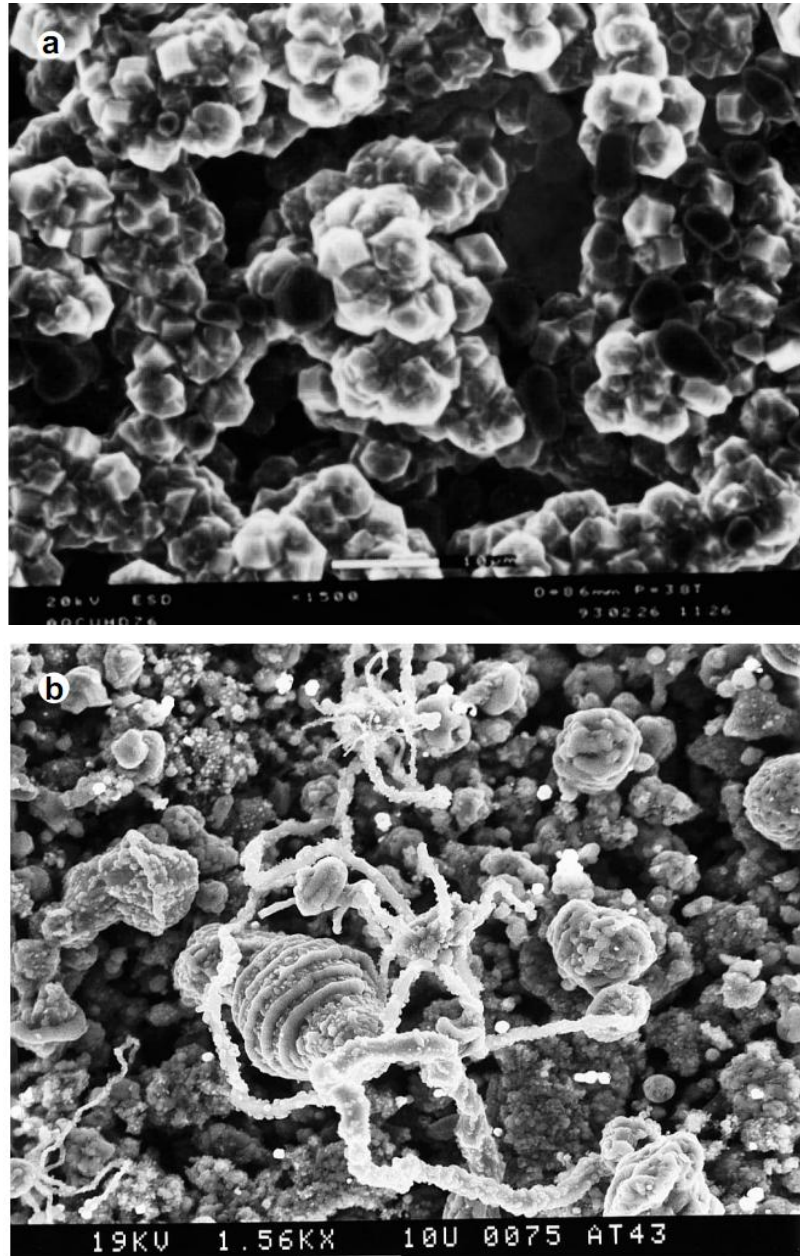


**Figure 3.1:** Example SEM images of diamond produced by LPSS associated with metallic globules (top) Diamond formed from a mixture of graphite and copper, where the diamond is associated with metallic globules. b) Diamond formed from a mixture of graphite and nickel, where the diamond is associated with metallic ropes. *Figure is from [1].*

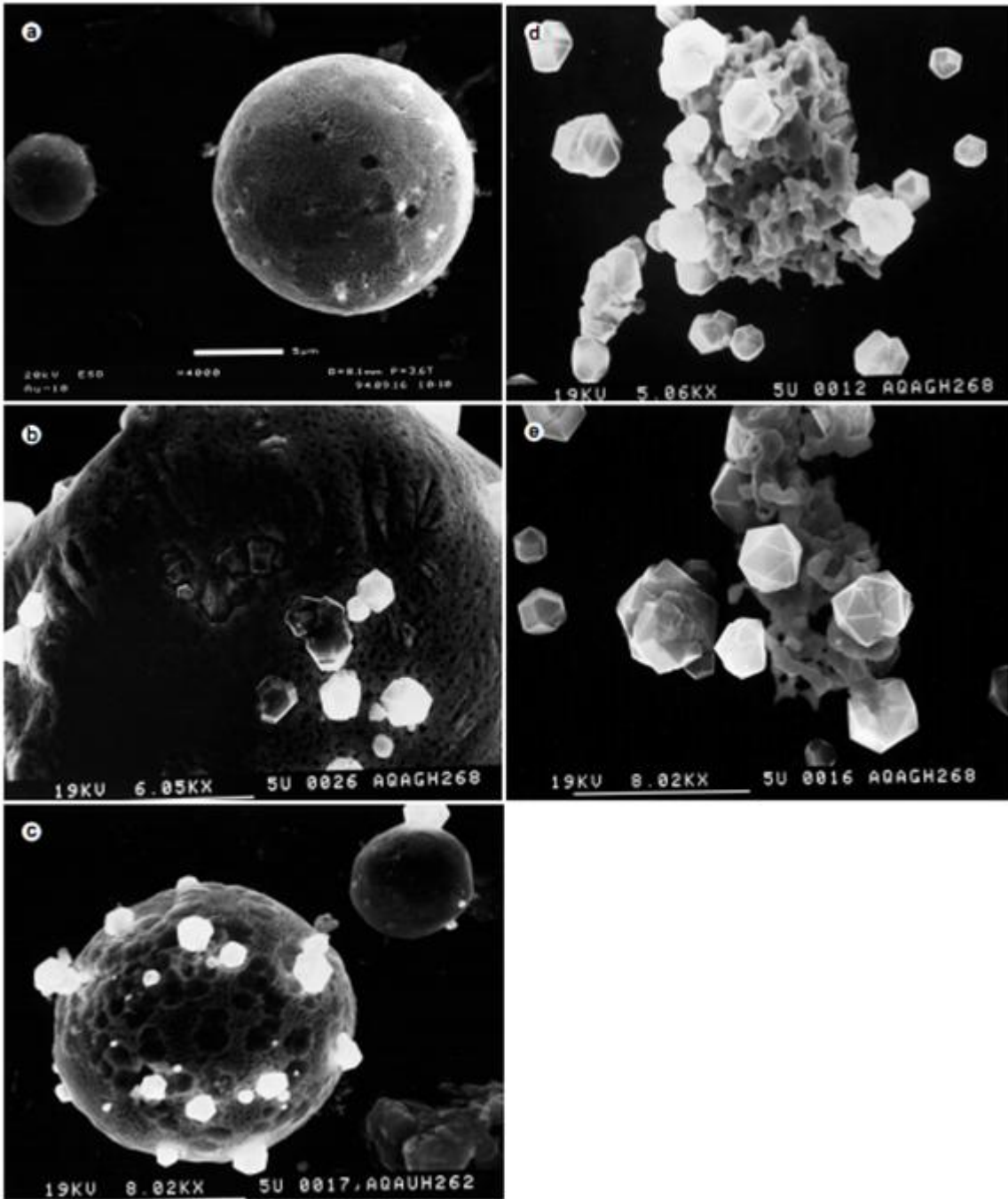


**Figure 3.2:** The production of diamond from a molten globule in an Au-C-H system formed during LPSSS. These images illustrate how diamond crystals seem to originate from within the globule. The images are in sequence from a-e. *Figure is adapted from [1].*

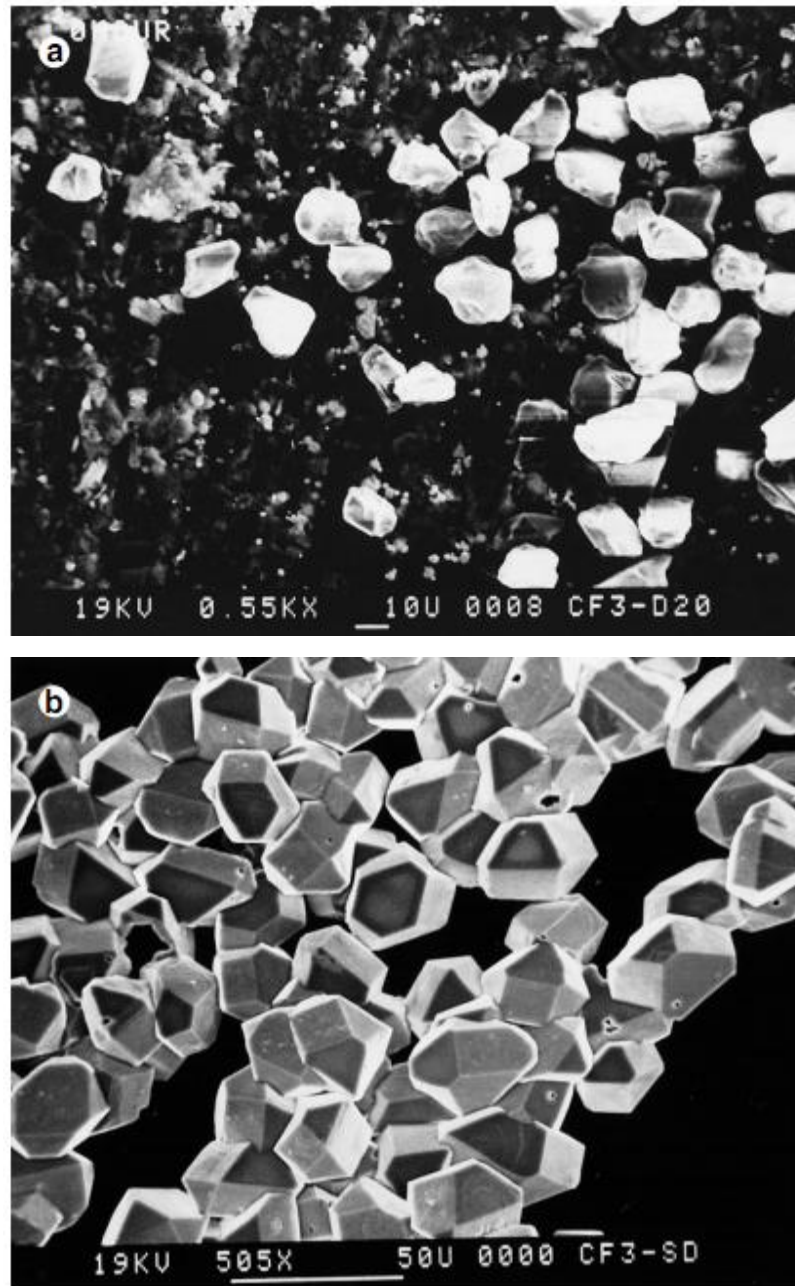


**Figure 3.3:** A diamond grit before (top) and after (bottom) LPSSS treatment. The crystals become larger and well faceted. *Figures are from [1].*

There have been several attempts to explain the results of the LPSSS process. However, claims that LPSSS is CVD where the metal enhances the nucleation rate [5] have been offset by reports of diamond formation inside metallic phases under low pressure conditions [6] and reports of the metals failing to enhance the rate of diamond growth [5] have been counteracted by reports which show a considerable increase in the growth rate in the presences of metal [6,7]. However one thing is clear, the exact mechanism of diamond formation remains unknown.

Despite the lack of a clear mechanism, the results of LPSSS techniques are still remarkable, and such treatments could prove to be very useful in the production of device grade diamond materials, once the techniques are better understood. It is hoped that the investigation into the effects of various metals on the surfaces of diamond crystals under the influence of hydrogen

plasmas will shed some light on some of the processes which may be occurring during LPSSS and act as a first step towards a detailed investigation into the process.

## References

- [1] R. Roy, K. A. Cherian, J. P. Cheng, A. Badzian, C. Langlade, H. Dewan & W. Drawl (1997), Precipitation of diamond from  $Me_xC_yH_z$  solutions at 1 ATM, *Materials Research Innovations* **1**, 117-129.
- [2] R. Roy, H. S. Dewan & P. Ravindranathan (1993), Diamond synthesis via a low-pressure solid-state-source process, *Material Research Bulletin* **28**(9), 861.
- [3] R. Roy, H. S. Dewan, K. A. Cherian, J. P. Cheng, A. Badzian, W. Drawl & C. Langlade (1995), Precipitation of diamond from metallic liquids below 1 atm, *Materials Letters* **25**(5-6), 191-193.
- [4] A. A. Giardini & J. E. Tydings (1962), Diamond synthesis: Observations on the mechanism of formation, *The American Mineralogist* **47**, 139
- [5] M-S. Wong, C-A. Lu, H-K. Chang, T-S. Yang, J-H. Wu & Y. Liou (2000), Diamond synthesis via C-H metal precursors processed in hot filament chemical vapour deposition and microwave plasma chemical vapour deposition, *Thin Solid Films* **337-338**, 274-279.
- [6] K. Mallika, R. C. Devries & R. Komanduri (1999), On the low pressure transformation of graphite to diamond in the presence of a 'catalyst-solvent', *Thin Solid Films* **339**(1-2), 19-33.
- [7] C-C. Hung, C-C. Lin & H-C. Shih (2002), The formation and characterisation of diamond crystallites by microwave plasma enhanced chemical vapour deposition a comparison of gaseous and solid carbon sources as precursors, *Materials Research Innovations* **6**, 122-127.

# CHAPTER 4

## Experimental techniques and apparatus

---

### 4.1 The reactor

This project used a MWCVD reactor based on an ASTeX design (**Figure 4.1**) with a process chamber specially made by Element Six for the Bristol Diamond Group [1]. A schematic and photograph of this reactor can be seen in **Figure 4.2**. This reactor uses microwave radiation at 2.45 GHz produced by a 1.5 kW magnetron to produce a plasma from the gaseous reagents. A detailed description of the operation of this reactor can be found in reference [2].

For this investigation PCD samples were placed onto a Mo substrate holder in the centre of the reactor and treated with pure hydrogen plasma. The temperature of the samples was monitored using a two wavelength optical pyrometer which is mounted to the chamber.

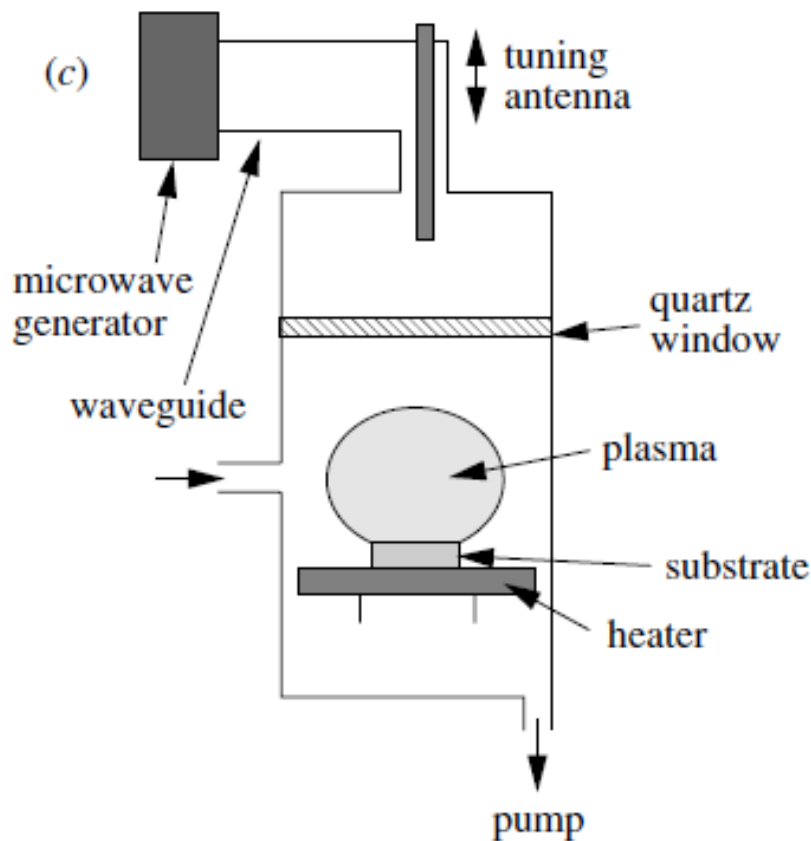


**Figure 4.1:** Schematic of an ASTeX design MWCVD reactor. *Figure from [3].*



**Figure 4.2:** A photograph of the MWCVD reactor in the Bristol Diamond Group.

## 4.2 Optical emission spectroscopy

Optical emission spectroscopy (OES) is a technique often used in the diagnostics of low pressure plasmas used in CVD [4]. The technique is based on the emission of photons in the visible region of the electromagnetic spectrum as the result of various species within the plasma relaxing from excited states.

In this work, hydrogen plasma was used to treat diamond samples at a variety of different conditions. Hydrogen plasmas are easily identifiable due to their purple glow which is the result of photon emission at four different wavelengths in the visible region which make up part of the Balmer series [5], shown in **Figure 4.2**.



**Figure 4.2:** The lines in the emission spectrum of the hydrogen atom in the visible region of the electromagnetic spectrum. This series of spectral lines is known as the Balmer series. *Figure from [6]*

The Balmer series is one in a series of spectral line emissions from atomic hydrogen and is the result of electron transfer from excited states with  $n \geq 3$  to  $n = 2$ , where  $n$  is the principle quantum number of the electron [7]. Since transferring an electron to a state with a lower principle quantum number reduces the energy of that electron, the excess energy is released in the form of a photon (obeying the first law of thermodynamics). The wavelength of the photon emitted during the transition is related to the energy gap between the electronic states by

$$E = \frac{hc}{\lambda}$$

where  $E$  is the difference in energy between electronic states with different principle quantum number,  $h$  is Planck's constant,  $c$  is the speed of light and  $\lambda$  is the wavelength of the photon emitted.

This means that transitions from electronic states with different principle quantum numbers produce photons with different wavelengths. The emissions from hydrogen in the Balmer series are shown in **Table 4.1**.

**Table 4.1:** Details on the various transitions of electrons between states with different principle quantum number which cause photons to be emitted from the hydrogen atom in the Balmer series [8].

Transition in terms of $n$	$3 \rightarrow 2$	$4 \rightarrow 2$	$5 \rightarrow 2$	$6 \rightarrow 2$
Name	H <sub><math>\alpha</math></sub> (H-alpha)	H <sub><math>\beta</math></sub> (H-beta)	H <sub><math>\gamma</math></sub> (H-gamma)	H <sub><math>\delta</math></sub> (H-delta)
Wavelength / nm	656.3	486.1	434.1	410.2
Colour	Red	Cyan	Blue	Violet

In the Bristol Diamond Group OES spectra are taken with an Oriel Instaspec IV spectrometer and an optic fibre which was pointed directly at the centre of the plasma through one of the windows in the chamber. The spectra in this investigation were background corrected and collected over 500 accumulations of data collected by 20 ms exposures. An example optical emission spectrum can be seen in **Figure 4.3**.

One important thing to remember about OES is that the data does not give quantitative data and so absolute concentrations of species in the plasma cannot be determined [4]. OES can therefore only be used to look at variations in species within different plasmas relative to one another. Furthermore, OES only provides information about the excited species emitting photons in the visible region, so does not provide any information about non-emitting, neutral or ground state species in the plasma as well as not probing any highly excited atomic state species [4].

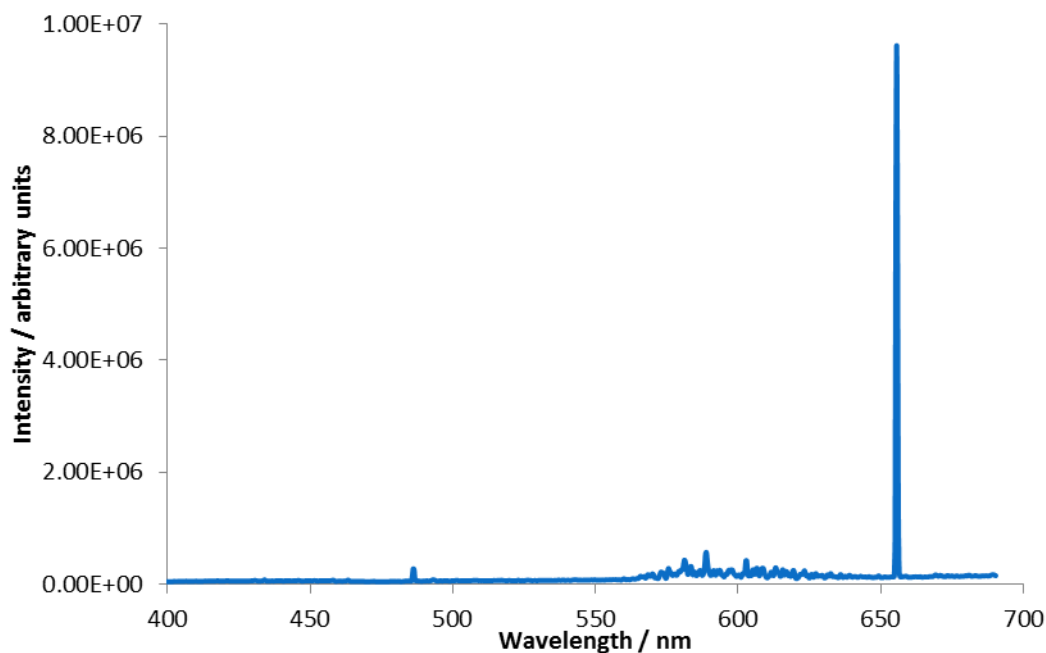


**Figure 4.3:** A typical optical emission spectrum of hydrogen plasma showing very intense H $\alpha$  emission and much lower intensity emissions from other atomic hydrogen species. This specific spectrum was obtained for a hydrogen plasma at a pressure of 83 Torr, microwave power of 1 kW and a hydrogen flow rate of 500 sccm.

### 4.3 Raman spectroscopy

Raman spectroscopy is a widely used absorption spectroscopy technique in materials science which relies on the inelastic scattering of light by a molecule in response to radiation from a monochromatic laser [9]. The technique requires no sample preparation and is non-destructive.

When laser light interacts with the electron clouds of molecules, the absorption of photons excites the molecules from the ground state to high energy virtual states. These virtual states have a very short lifetime and the energy of the molecule quickly falls back to lower energy states, however, upon relaxation the molecules may not return to their original state and thus occupy higher rovibrational levels in the molecule [10]. As discussed for OES, as relaxation occurs a photon characteristic of the transition is emitted and so, elastic and inelastic scattering of the laser light produces photons of different wavelengths. This is principle is shown in **Figure 4.4**. The difference in energy between these photons is known as the Raman shift, which is usually reported in wavenumbers with units of  $\text{cm}^{-1}$ . The wavenumber ( $\tilde{\nu}$ ) of a photon is related to its wavelength ( $\lambda$ ) by

$$\tilde{\nu} = \frac{1}{\lambda}$$

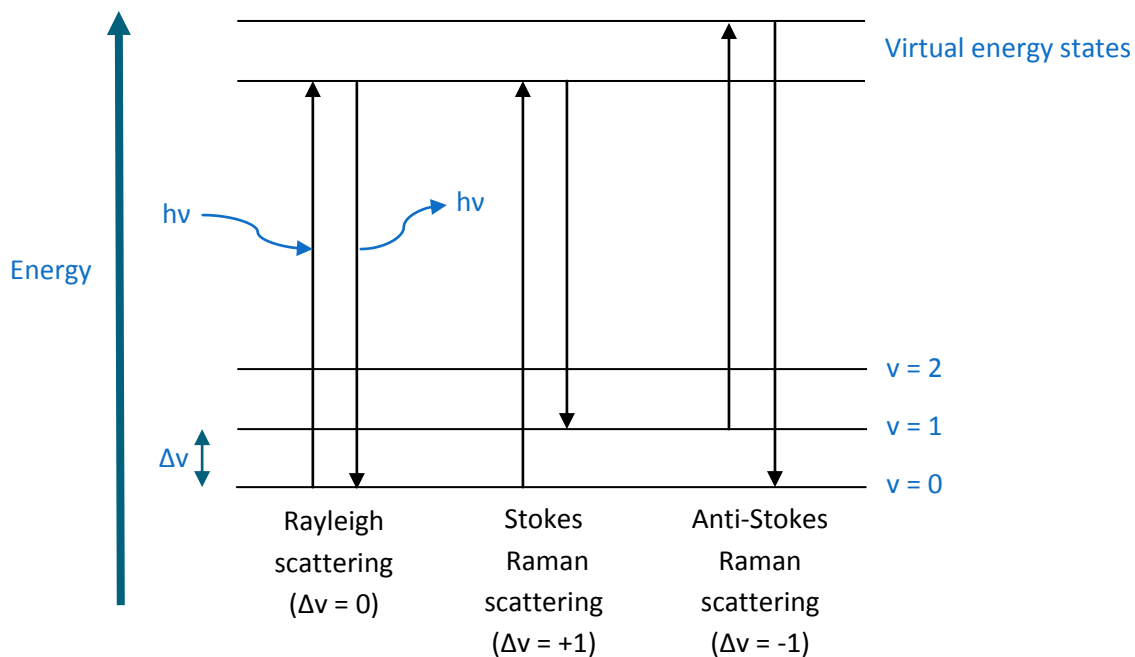


**Figure 4.4:** A vibrational energy level diagram showing how different types of scattering arise following excitation of a molecule using a monochromatic light source. When photons are absorbed, molecules are excited to high energy virtual states. As the molecules relax to lower vibrational levels, the excess energy is emitted as a photon. If a molecule returns to its original state, the scattering will be elastic and is known as Rayleigh scattering. If a molecule does not relax back to its original state then the photon emitted from the molecule will be different to that absorbed. This inelastic scattering is known as the Raman effect. The Raman effect can manifest itself in two ways depending on whether the difference between the final vibrational state is higher energy than the original state, known as Stokes scattering, or if the final vibration state of the molecule is lower energy than the original state of the molecule, known as Anti-Stokes scattering. *This figure was designed by the author using information from [7,10].*

The Raman shift is particularly useful since it gives information about the energy spacing of various modes in the molecules. For a giant covalent structure such as diamond, the entire lattice vibrates in vibrational modes known as phonons [11]. To be Raman active, the vibration of the molecule must cause a change in polarisability as the atoms move through their equilibrium positions [12]. Diamond shows one main Raman active vibration which leads to a sharp peak at a Raman shift of  $1332 \text{ cm}^{-1}$  [2,9,11]. This can be seen in the Raman spectrum of SCD in **Figure 4.5**.

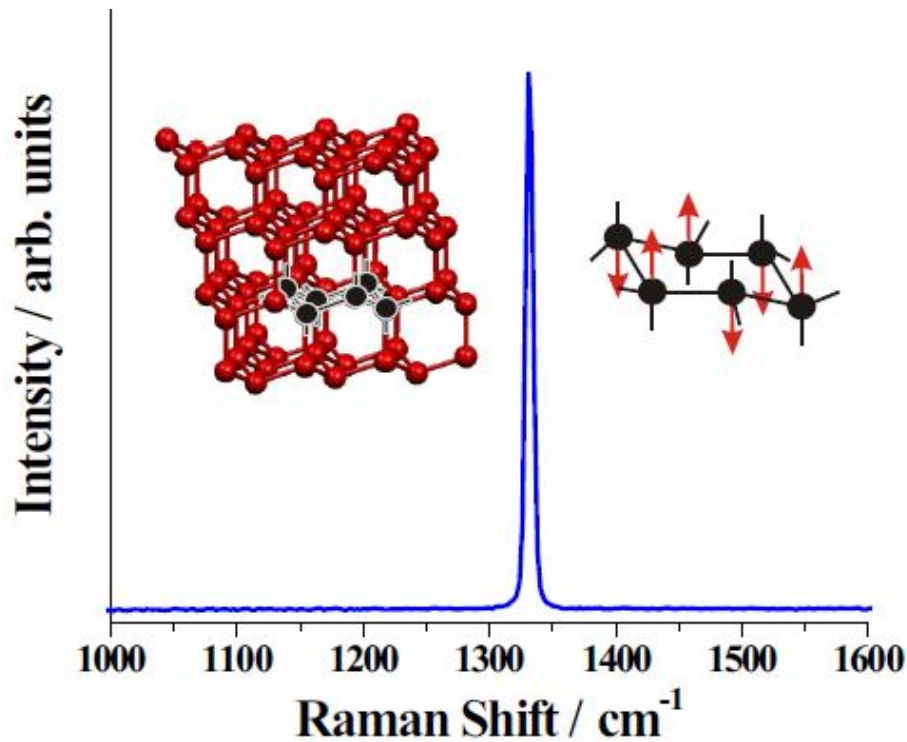


**Figure 4.5:** Raman spectrum of SCD showing the structure of diamond and the nuclear motions involved in the Raman active mode. *Figure from [11].*

Raman spectroscopy can also be used to distinguish between SCD and various forms of PCD, since non-diamond materials also have Raman active modes. The major non-diamond material considered in these investigations is graphite, which has a characteristic Raman shift at  $1580\text{ cm}^{-1}$  [9]. Since the graphite in PCD is not a large continuous single crystal the graphite peak is fairly broad. Furthermore, the Raman scattering intensity of non-diamond materials are higher than that of diamond and so graphitic material can mask the diamond signal, making the film seem of worse quality than it may actually be. A typical Raman spectrum of MCD used in this investigation is shown in **Figure 4.6**, and it is clear that there is some scattering due to non-diamond material in MCD.

In the Bristol Diamond Group, Raman spectroscopy is performed at room temperature using a Renishaw 2000 instrument and CCD detector. The Raman spectra in this investigation were taken using a UV He:Cd laser at 325 nm.

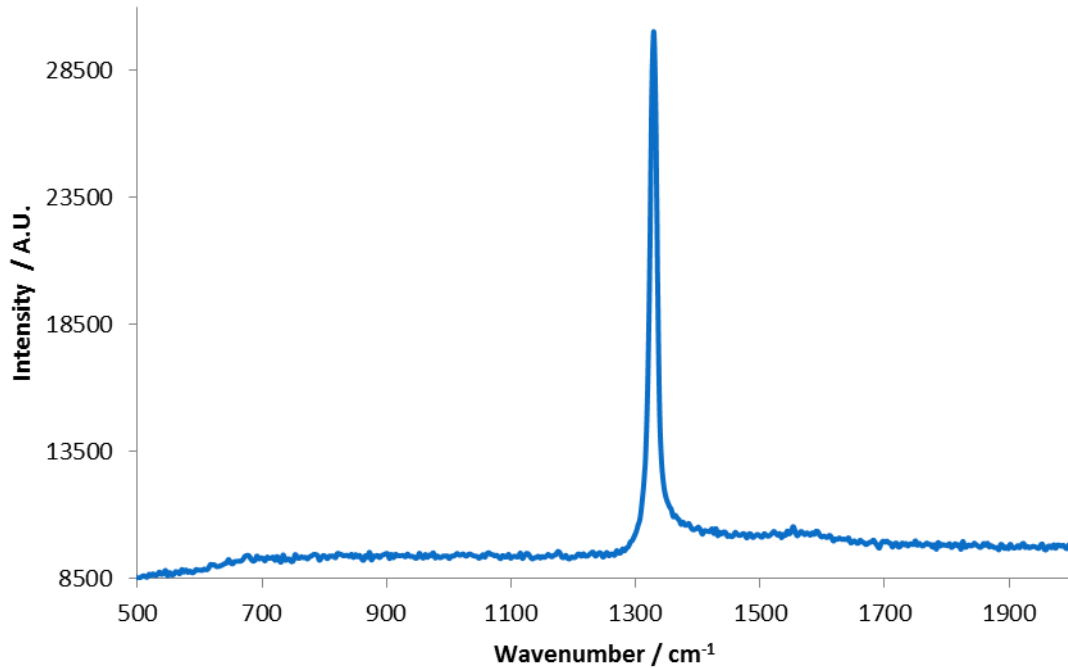


**Figure 4.6:** Raman spectrum of the growth side of a MCD sample from this work, taken using a UV laser.

#### 4.4 Scanning electron microscopy

Scanning electron microscopy (SEM) is a widely used technique in the field of materials science for characterising the morphology of surfaces. In this technique a beam of electrons are focussed onto the sample by a series of optics (lenses and scan coils). Scanning this electron beam across the surface of the sample has a number of consequences, but in general it is secondary electrons which are captured and detected to produce an image of the surface [10,13]. A schematic of a typical microscope used for SEM is shown in **Figure 4.7**

The standard procedure for SEM is to coat the sample in a highly conductive layer such as gold to prevent a build-up of charge on the surface. In this work, such coatings were not used since the samples needed to be analysed using further techniques and in some cases were required for further treatments.

In these investigations a JEOL5600V thermionic emission microscope was used to obtain SEM images of the diamond samples.

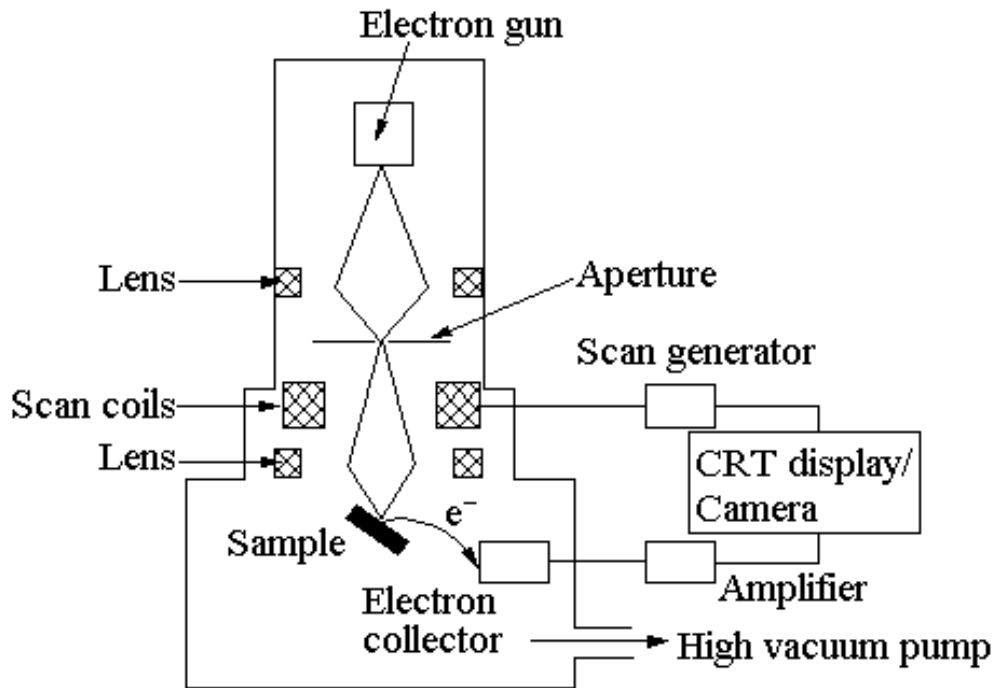


**Figure 4.7:** Schematic of a scanning electron microscope. *Figure is from [12].*

## 4.5 Atomic-force microscopy

Atomic-force microscopy (AFM) is a scanning probe microscopy technique which uses a silicon cantilever with a sharp tip to scan the surface of the sample, enabling the topography of materials to be studied at high resolution [2,14]. The basic procedure of AFM is to drag this sharp tip across the surface and measure the deflection in the cantilever caused by the topography of the surface. A typical AFM apparatus is shown in **Figure 4.8**.

In this investigation, tapping mode AFM was used to investigate the surface roughness of PCD samples before and after treatment in hydrogen plasma. In this mode the tip is made to oscillate using a small piezo-crystal in the tip holder and, as the distance between the tip and the sample is reduced, the amplitude of the oscillation reduces due to Van der Waals forces and electrostatic interactions between the tip and the surface [15]. This allows an image of the surface topography to be produced by measuring the force of periodic contacts between the tip and the surface of the sample.

Due to the roughness and hardness of PCD surfaces, producing AFM images is problematic since the cantilever tips degrade rapidly during scanning [2]. Since only intermittent contact is used in tapping mode AFM, this technique prevents rapid degradation of the cantilever tips and allows good AFM images to be produced [16]. The degradation of the cantilever tips can be reduced further by adjusting the scan parameters such as the scan rate and scan size. Typical scans performed in this work took these factors into consideration and a typical set of parameters used are shown in **Table 4.2**.

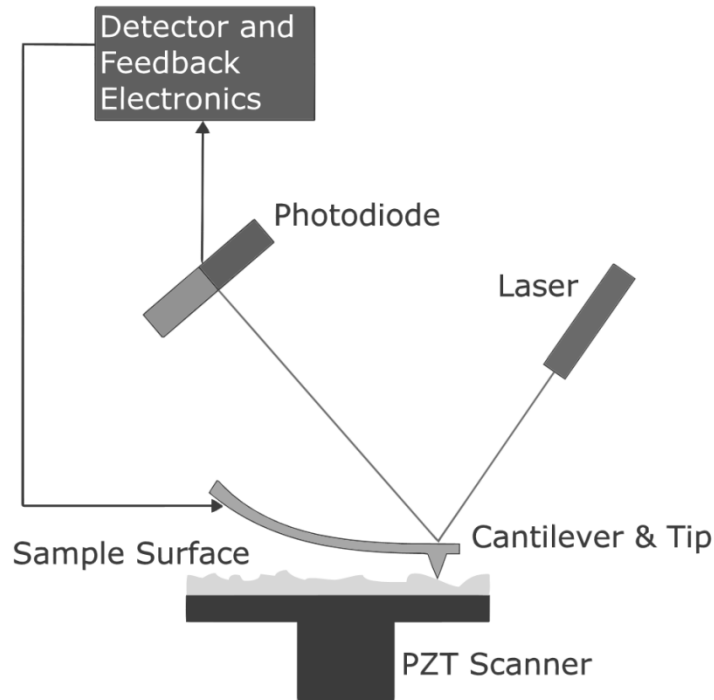


**Figure 4.8:** Schematic of an atomic force microscope. *Figure from [17].*

**Table 4.2:** Typical AFM parameters used in this work.

Scan size / $\mu\text{m}$	10 $\mu\text{m}$
Scan rate / Hz	0.5-1.0 Hz
Samples per line	512
Lines	512
Aspect ratio	1.0
Integral gain	0.3-1.0
Proportional gain	0.5-2.0
Amplitude set-point	0.2-0.3 V

The instrument used to produce AFM images in this investigation was a Bruker Multimode AFM with a Nanoscope V controller module. Gwyddion software [18] was used to analyse the AFM data and provided measurements of the root mean squared (RMS) surface roughness.

## 4.6 Diamond samples

A 10x10x1 mm<sup>3</sup> Element-Six produced, boron-doped PCD film was cut into 2x2x1 mm<sup>3</sup> samples using the Oxford Laser Systems laser cutter in the Bristol Diamond Lab, which uses a high power

laser to process materials into specific shapes and patterns. After being scribed with the desired grid pattern, the samples were snapped into individual samples using pliers and batch cleaned in hot  $\text{H}_2\text{SO}_4$  and  $\text{KNO}_3$  for 2 hours.

Single crystal diamond samples from HPHT sources were prepared and cleaned in acid by Dr. Neil Fox in the Centre for Nanoscience and Quantum Information at the University of Bristol. Dr Fox also prepared some diamond self-assembled monolayer (SAM) samples on W using 500 nm-grade HPHT nanodiamond. In simple terms, the SAM is produced using an aggregate free suspension of nanodiamonds, which is used to deposit a layer of diamond onto a substrate. These nanodiamonds are then adhered to the substrate by annealing. Producing diamond coated surfaces in this way could be a useful alternative to CVD materials due to their low cost and the fact that they do not require an energetic input to be formed. These SAM samples and some PCD samples were coated with thin films of Ag, Cu, Fe or Ti (~50 nm thickness) for the LPSSS investigation. Examples of the metal coated samples can be seen in **Figure 4.9**.

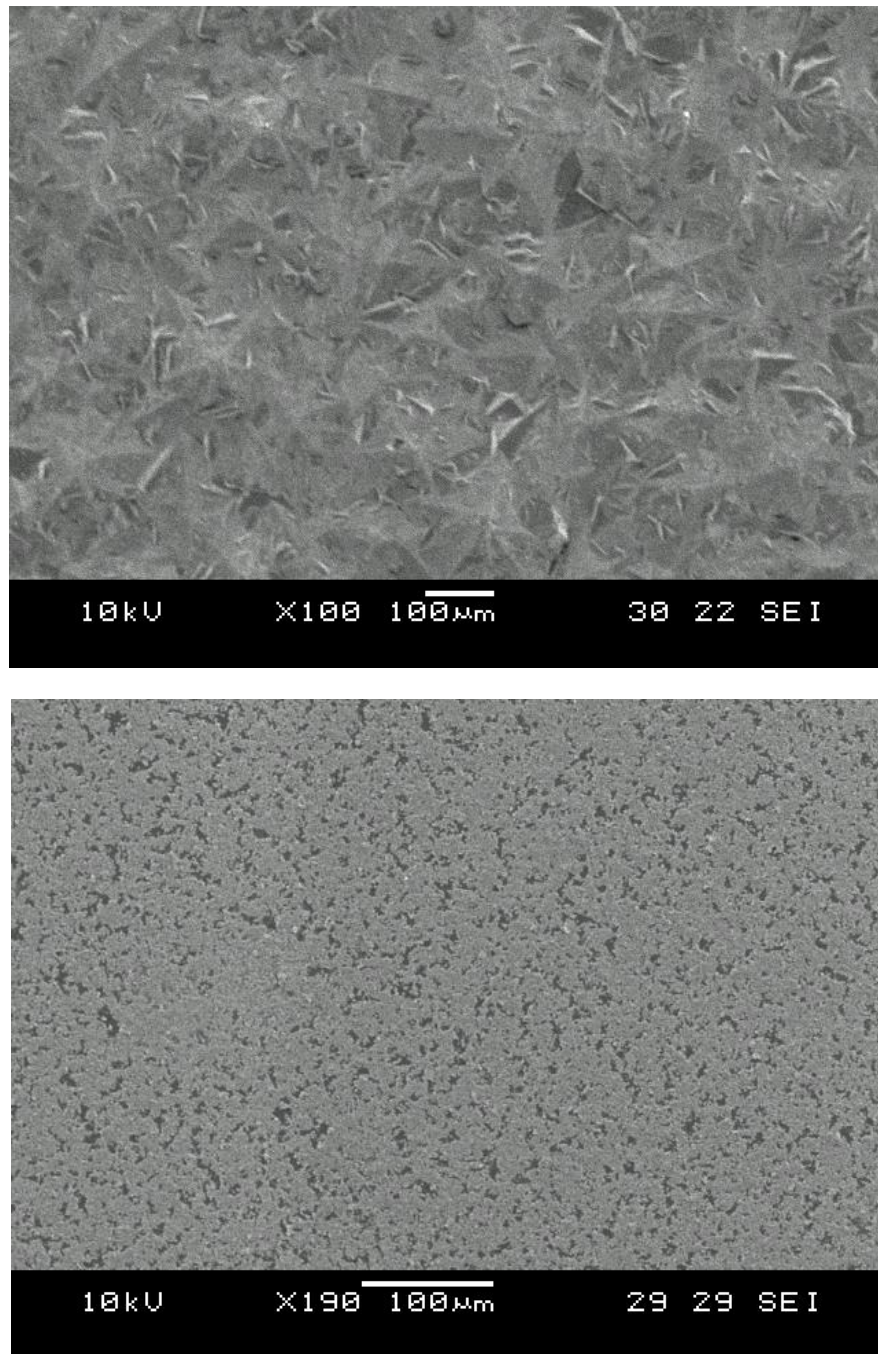


**Figure 4.9:** SEM images of metal coated PCD (top) and diamond SAM on W (bottom).

## 4.7 Manual abrasion

A few of the small PCD samples were used for manual abrasion experiments in which a diamond impregnated file was used to manually remove material from the surface of the samples. Diamond-diamond contact is a commonly used method for polishing diamond and usually makes use of small HPHT grits. The polishing mechanism is thought to be a brittle fracture process due to non-plastic deformation [19,20] in which pieces of diamond are chipped from the sample [21].

## References

- [1] A. Cheesman (2006), Investigations into the fundamentals of gas-phase and gas-surface chemistry prevalent in the growth of chemical vapour deposited diamond, PhD Thesis, Department of Chemistry, University of Bristol.
- [2] O. J. L. Fox (2011), Deposition of nanocrystalline diamond films by MW plasma CVD & Gas-Phase diagnostics using *in-situ* molecular-beam mass spectrometry and emission spectroscopy, PhD Thesis, Department of Chemistry, University of Bristol.
- [3] P. W. May (2000), Diamond thin films: a 21<sup>st</sup> century material, *Philosophical Transactions of the Royal Society of London A* **358**(1766), 473.
- [4] J. C. Richley (2011), Fundamental Studies of Diamond Chemical Vapour Deposition: Plasma Diagnostics and Computer Modelling, PhD thesis, Department of Chemistry, University of Bristol.
- [5] <http://www.differ.nl/en/node/2921>
- [6] [http://upload.wikimedia.org/wikipedia/commons/f/fb/Emission\\_spectrum-H\\_labeled.svg](http://upload.wikimedia.org/wikipedia/commons/f/fb/Emission_spectrum-H_labeled.svg)
- [7] P. Atkins & P. De Paula (2006), Atkins' Physical Chemistry, Oxford University Press (8<sup>th</sup> Ed.)
- [8] [http://en.wikipedia.org/wiki/Balmer\\_series](http://en.wikipedia.org/wiki/Balmer_series)
- [9] J. Filik (2005), Raman spectroscopy: a simple, non-destructive way to characterise diamond and diamond-like materials, *Spectroscopy Europe* **17**(5), 10-17.
- [10] D. Kealey & P. J. Haines (2002), Instant Notes - Analytical Chemistry, *BIOS Scientific Publishers Limited*.
- [11] J. Filik (2006), Fundamental Studies on the Deposition and Characterisation of Novel Diamond-like Materials, *PhD Thesis*, Department of Chemistry, University of Bristol.
- [12] C. E. Housecroft & A. G. Sharpe (2008), Inorganic Chemistry, *Pearson Education Limited* (3<sup>rd</sup> Ed.).
- [13] S. M. Leeds (1999), Characterisation of the Gas-Phase Environment in a Microwave Plasma Enhanced Diamond Chemical Vapour Deposition Reactor using Molecular Beam Mass Spectrometry, *PhD Thesis*, Department of Chemistry, University of Bristol.
- [14] F. J. Giessibl (2003), Advances in atomic force microscopy, *Reviews of Modern Physics* **75**, 949.
- [15] P. Atkins, T. Overton, J. Rourke, M. Weller & F. Armstrong (2006), Shriver and Atkins Inorganic Chemistry, *Oxford University Press* (4<sup>th</sup> Ed.).
- [16] P. Achatz, J. A. Garrido, O. A. Williams, P. Brun, D. M. Gruen, A. Kromka, D. Steinmüller & M. Stutzmann (2007), Structural, optical, and electronic properties of nanocrystalline and ultrananocrystalline diamond thin films, *Physica Status Solidi A* **204**(9), 2874.
- [17] [http://en.wikipedia.org/wiki/File:Atomic\\_force\\_microscope\\_block\\_diagram.svg](http://en.wikipedia.org/wiki/File:Atomic_force_microscope_block_diagram.svg)
- [18] <http://gwyddion.net/>
- [19] J. C. Sung & H. Lin (2009), Diamond nanotechnology: syntheses and applications, *Pan Stanford Publishing*.
- [20] K. Hayashi, S. Yamanaka, H. Watanabe, T. Sekiguchi, H. Okushi & K. Kajimura (1998), Atomic force microscopy study of atomically flat (001) diamond surfaces treated with hydrogen plasma, *Applied Surface Science* **125**(1), 120-124.

- [21] C. J. Tang, A. J. Neves, A. J. S. Fernandes, J. Gracion & N. Ali (2003), A new elegant technique for polishing CVD diamond films, *Diamond and Related Materials* **12**, 1411-1416.

# Chapter 5

## Results and discussion

---

### 5.1 Hydrogen plasma treatments of PCD

Before this investigation could begin, the decision had to be made as to which side of the samples would be treated. Due to the way in which a PCD diamond film grows, the top of the as-grown films exhibit relatively large crystals, whilst the substrate side is composed of very small diamond crystals. This can be seen in **Figure 5.1**. Small crystals are commonly applied to the substrates prior to CVD growth to enhance the rate of film deposition, since the initial nucleation of diamond blank substrates is known to require extremely long incubation times [1].

These different diamond surface morphologies result in the different sides of the sample having very different surface roughness. The growth side of the film is very rough, with jagged peaks from the large crystals, whilst the substrate side is smooth. This can be seen very clearly in **Figure 5.2**.

Since this investigation is ultimately concerned with the surface roughness of the PCD following hydrogen plasma treatments, it would be useful to acquire surface roughness data using AFM techniques. The high roughness of the growth side of the PCD samples is a significant problem when using AFM, since the large grains are beyond the travel limit through which the cantilever and tip can travel. This means that attempting to scan a highly rough PCD surface would force the cantilever beyond its working range, causing not only damage to the tip, but could also cause significant and costly damage to the piezo stage of the apparatus. For this reason, the growth side of the surface will not be investigated in the study of the effects of hydrogen plasma treatments at different experimental conditions.

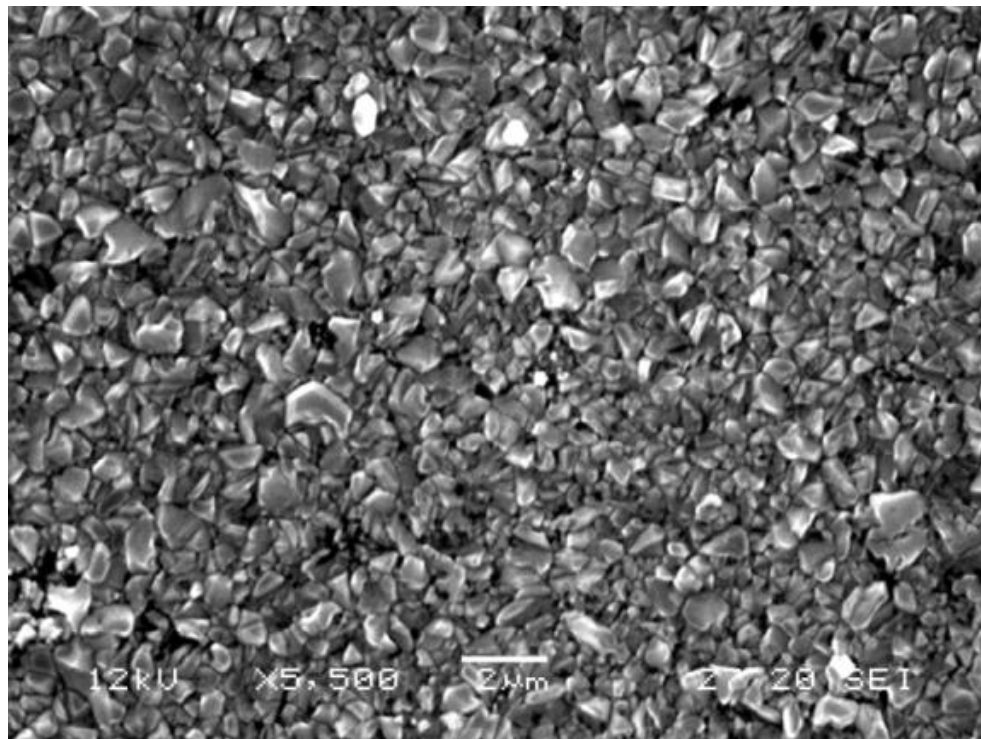
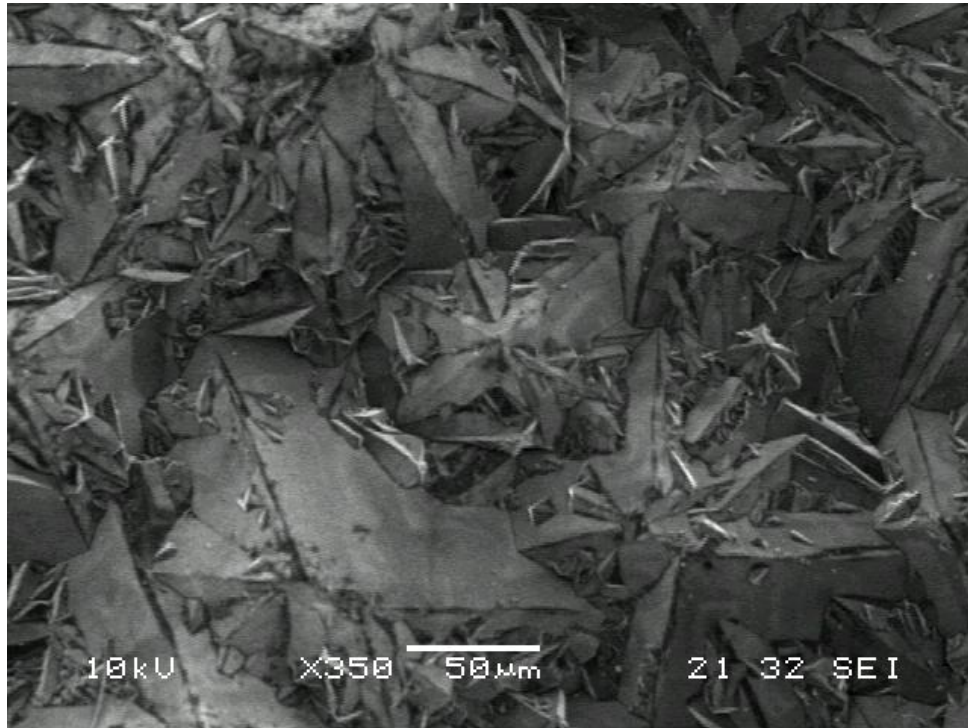


**Figure 5.1:** SEM images of the PCD samples showing the morphologies of the growth side (top image) substrate side (bottom) of the PCD samples. The growth side of the films are composed of large crystals which can be hundreds of microns in size, whilst the substrate side of the film is composed of small crystals, the largest of which are  $<2\ \mu\text{m}$  in size.

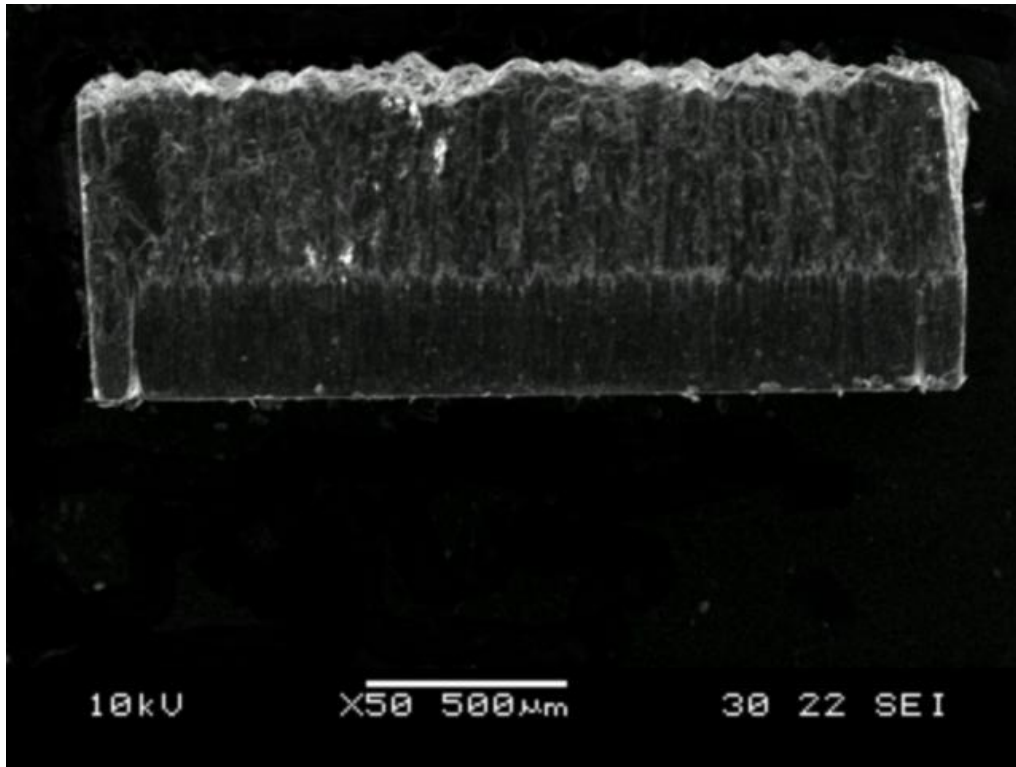


**Figure 5.2:** SEM of the PCD samples from a side on view shows that the growth side of the films are rather rough whilst the substrate side is very smooth. This image also shows the columnar structure of the film produced by CVD. The darker region towards the substrate side of the film is the result of the laser cutting of the samples; hence this region appears much more uniform than the rest of the structure.

The RMS surface roughness of the substrate side of the PCD samples was investigated using AFM and Gwyddion software [2] was used to analyse the images. Using this free software package, it is also possible to process the AFM image to produce a 3D projection of the surface. This gives a much clearer image of the morphology of the surface and example AFM images can be seen in **Figure 5.3**.

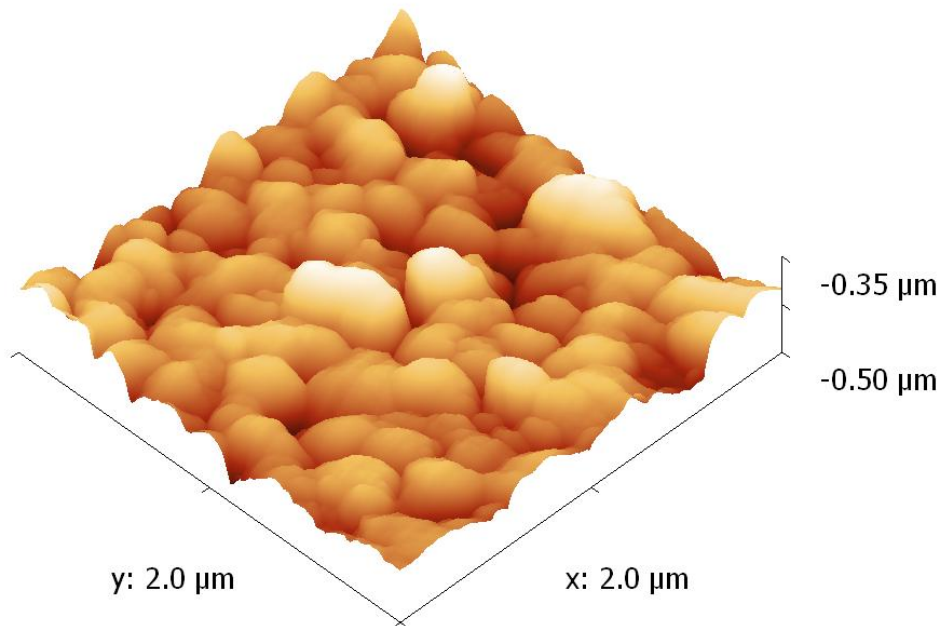
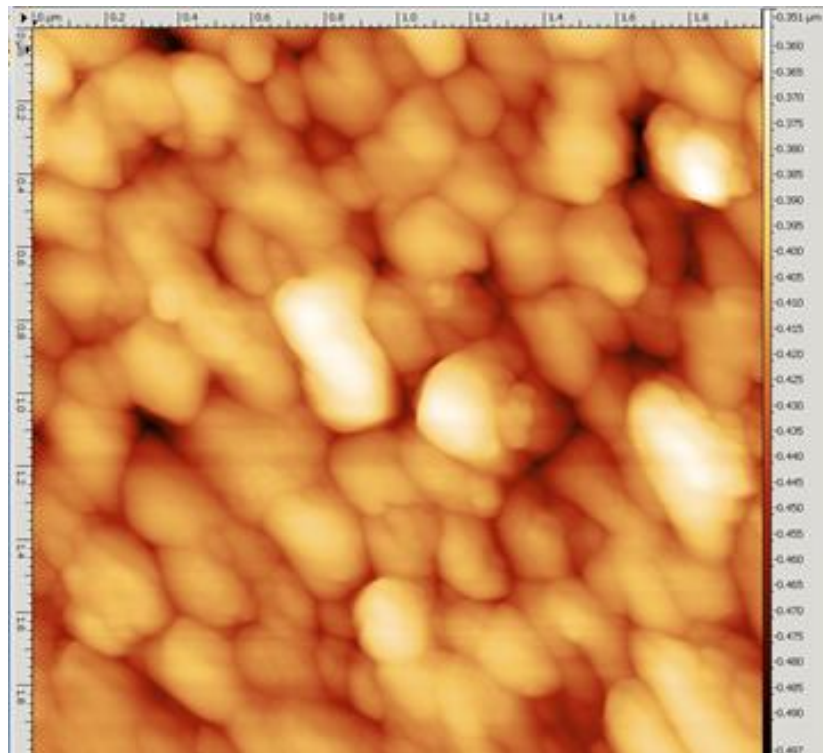


**Figure 5.3:** An example AFM image of the substrate side of PCD films obtained over an area of  $2 \times 2 \mu\text{m}^2$  showing the surface topography in 2D (top) and a 3D projection (bottom) produced using Gwyddion.

In this study, a systematic approach was used to investigate the effects of different hydrogen plasma treatments on the surface roughness of PCD samples. Various parameters such as the

reactor pressure, microwave power and flow rate of hydrogen into the reactor were varied to change the characteristics of the hydrogen plasma. The variations in the surface roughness of the PCD following these treatments were obtained using AFM over areas of  $10 \times 10 \mu\text{m}^2$ . Using this scan size, the mean RMS surface roughness of the untreated PCD was found to be 47.5 nm (obtained from 1 scan at a random location on 10 randomly selected  $2 \times 2 \text{ mm}^2$  samples). A typical AFM image of the PCD prior to treatment can be seen in **Figure 5.4** and following the treatments, the mean RMS surface roughness of the PCD was calculated from  $10 \times 10 \mu\text{m}^2$  scans at five random locations on the sample surface. The data obtained for the treated surfaces were used to observe the effects of the treatments in comparison to the original surface morphology.

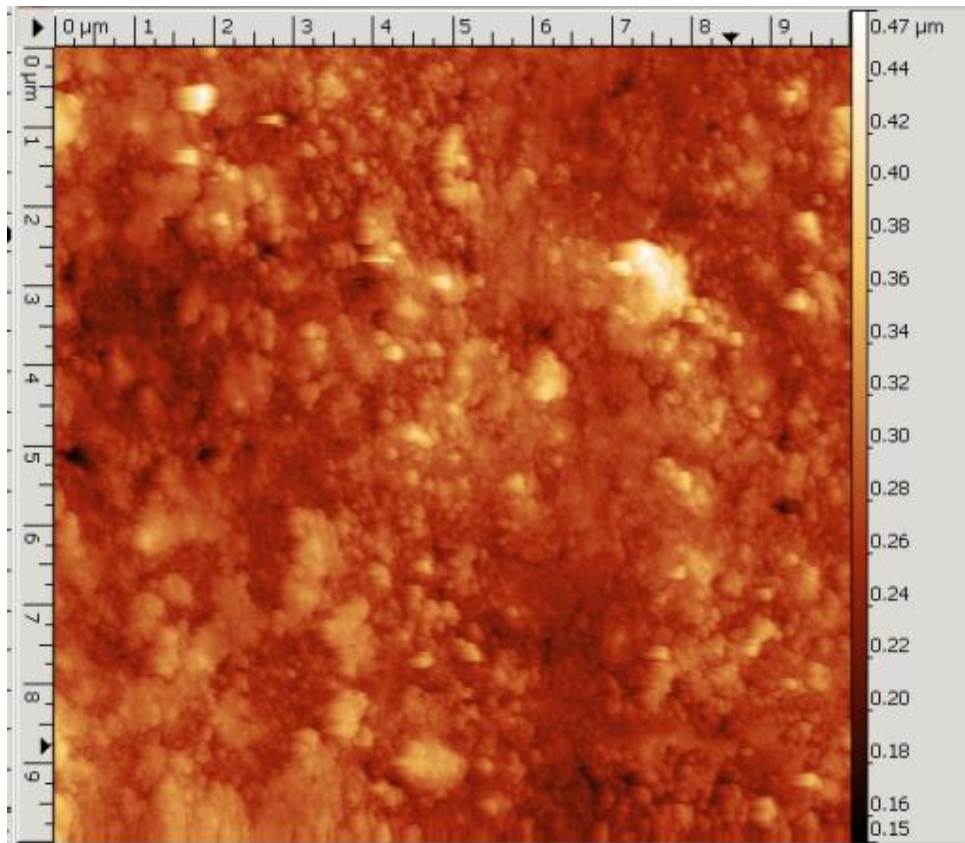


**Figure 5.4:** An example of a  $10 \times 10 \mu\text{m}$  scan obtained for the untreated PCD samples. It is clear that the surface is composed of many small diamond crystals as confirmed by SEM.

The discussion of the results obtained will begin by considering the effects of treatments at different temperatures. Since this project is aiming to control the reactions of atomic hydrogen with the diamond surface in order to promote smoothing, the treatment conditions will need to be optimised so that smoothing reactions occur at the fastest possible rate. The rate of a reaction is an important concept in physical chemistry and is well known to be dependent on temperature according to the Arrhenius equation [3] which is defined as

$$k = Ae^{\left(\frac{-E_a}{RT}\right)}$$

Where  $k$  is the rate constant,  $A$  is the pre-exponential factor (a constant dependent on the reaction being considered),  $E_a$  is the activation energy required for the reaction,  $R$  is the universal gas constant ( $8.314 \text{ J K}^{-1} \text{ mol}^{-1}$ ) and  $T$  is the temperature.

For these investigations a constant microwave power, hydrogen flow rate and treatment duration were used (1 kW, 500 sccm and 20 minutes respectively) whilst the pressure was varied. The treatment temperature was shown to increase with pressure and so it can be said that the gas temperature in the plasma increases with pressure. In addition to increasing the plasma temperature, increasing the pressure seems to decrease the size of the plasma when it is observed through the viewing window in the wall of the reactor. This decrease in the size of the plasma suggests that the atomic hydrogen species produced by dissociation of hydrogen are not able to diffuse as far from the centre of the plasma under high pressures and so emit photons due to relaxation of excited states in regions closer to the centre of the plasma. This decrease in the rate of diffusion of atomic hydrogen species can be attributed to an increase in the plasma density caused by the increase in pressure, resulting in more frequent collisions during the Brownian motion of the gaseous species [3]. These more frequent collisions mean that the species diffuse away from the centre of the plasma more slowly.

The increased concentration of gaseous species in the reactor as a result of the increased pressure means that the microwave energy from the magnetron will be distributed over more species. This leads to an increase in the average kinetic energy of the particles, which leads to the increase in temperature. OES data shown in **Figure 5.5**, also confirms that the energy is being spread over more species at high pressures since there is an increase in the emission from atomic hydrogen species which will form due to dissociation of hydrogen. This data also indicates that lower energy excited states are formed preferentially over highly excited states since the emission intensity due to  $H_{\alpha}$ -emission and other low energy transitions increases whilst  $H_{\delta}$ -emission decreases. It is possible that due to the energy being spread to more species in the centre of the plasma, there is not sufficient energy being transferred to dissociate atomic hydrogen to form highly excited states. Furthermore, it is possible that such highly excited states of atomic hydrogen are quenched by the increased frequency of collisions with other gas phase species under high pressures conditions before they can emit a photon.

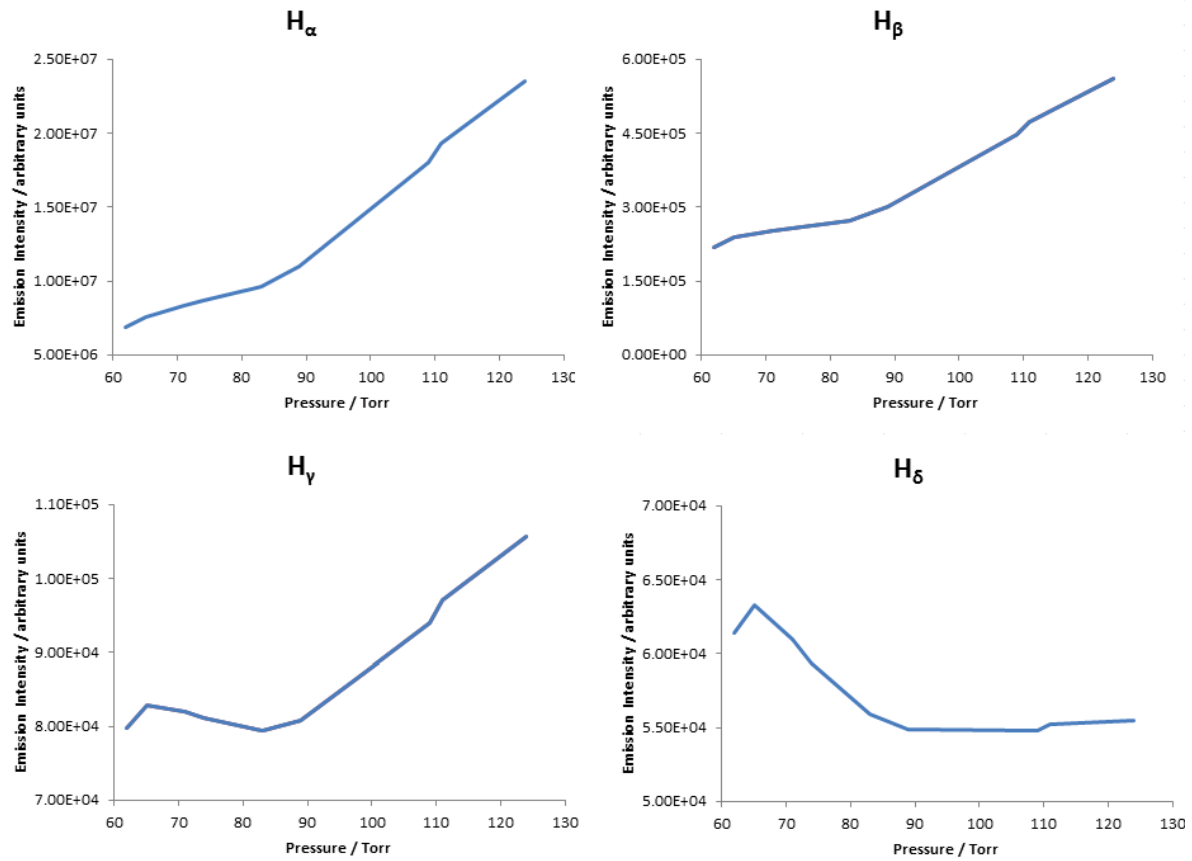


**Figure 5.5:** Data obtained from optical emission spectroscopy of the hydrogen plasmas produced using a MWCVD reactor which was used to treat PCD at different pressures/temperatures on hydrogen plasma. The emissions from various atomic hydrogen species have been plotted against the reactor pressure to show the behaviour of each species within the plasma as the conditions are changed.

The variation in the surface roughness of PCD following hydrogen plasma treatment at different pressures and constant power and flow rate are shown in **Figure 5.6**. This data is presented as the variation of the surface roughness of the PCD with different temperature hydrogen plasma treatments and the way in which this data was collected was mentioned in a previous chapter. The relationship between the pressure and treatment temperature has also already been described.

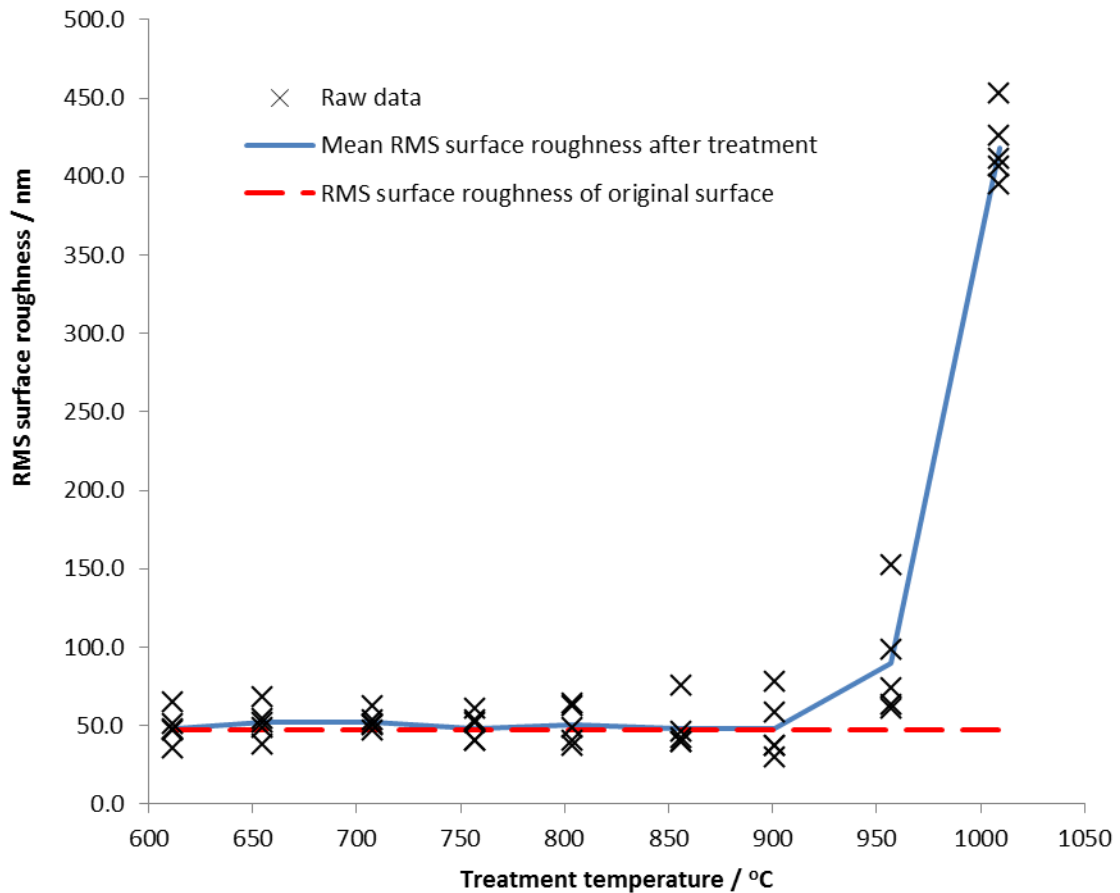


**Figure 5.6:** A plot of the variation in the RMS surface roughness of PCD diamond samples obtained using AFM following treatments in hydrogen plasma at various temperatures.

It is evident that the variation in the surface roughness following hydrogen plasma treatments at different temperatures has two major trends: a significant increase in the surface roughness at treatment temperatures  $>900^{\circ}\text{C}$  where the surface becomes rough on a scale of hundreds of nanometres and a region where the surface roughness is increased very slightly in comparison to the original sample on a scale of tens of nanometres. This suggests that there is a transition to a different regime at high temperatures.

The PCD sample treated at  $1000^{\circ}\text{C}$  has become incredibly rough according to AFM, and SEM reveals that the surface is covered in a considerable amount of non-diamond material, as well as large craters and trenches being present on the sample. These results can be seen in **Figure 5.7**. Raman spectroscopy of this sample confirmed that the surface had become highly graphitised by the treatment. This could be deduced due to the broad band at  $1550\text{ cm}^{-1}$  indicated in **Figure 5.8**. The broadness and small size of this band suggests that the graphite is not one continuous crystal [4]. Furthermore, no diamond peak can be seen at  $1332\text{ cm}^{-1}$  following the treatments. This observation, combined with the presence of small grains of non-diamond material observed by SEM, indicates that the formation of graphitic phases must be occurring on the surfaces of the diamond crystals.

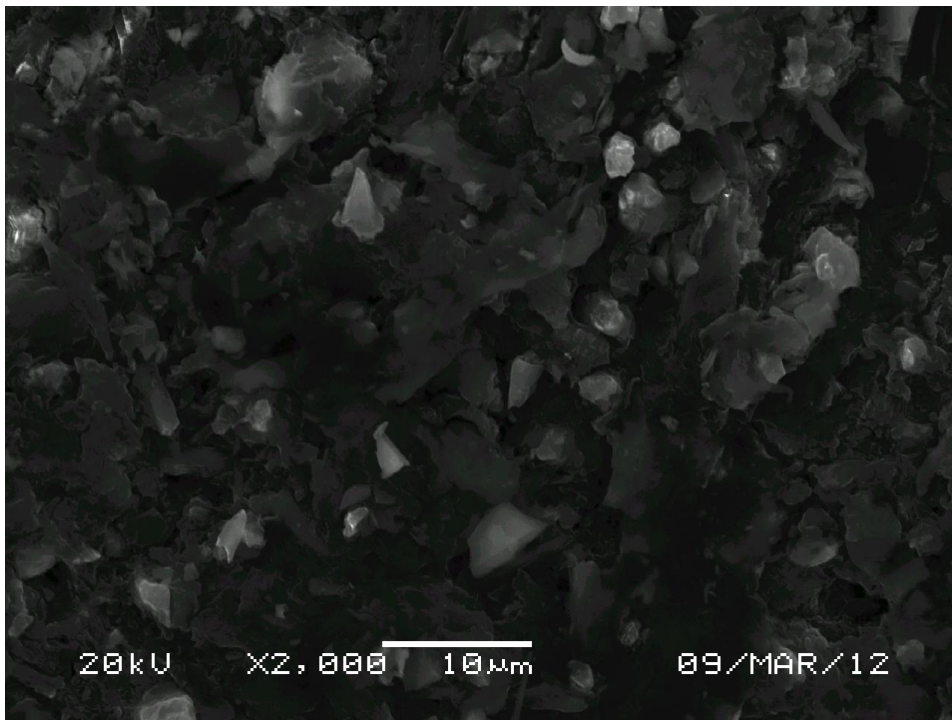
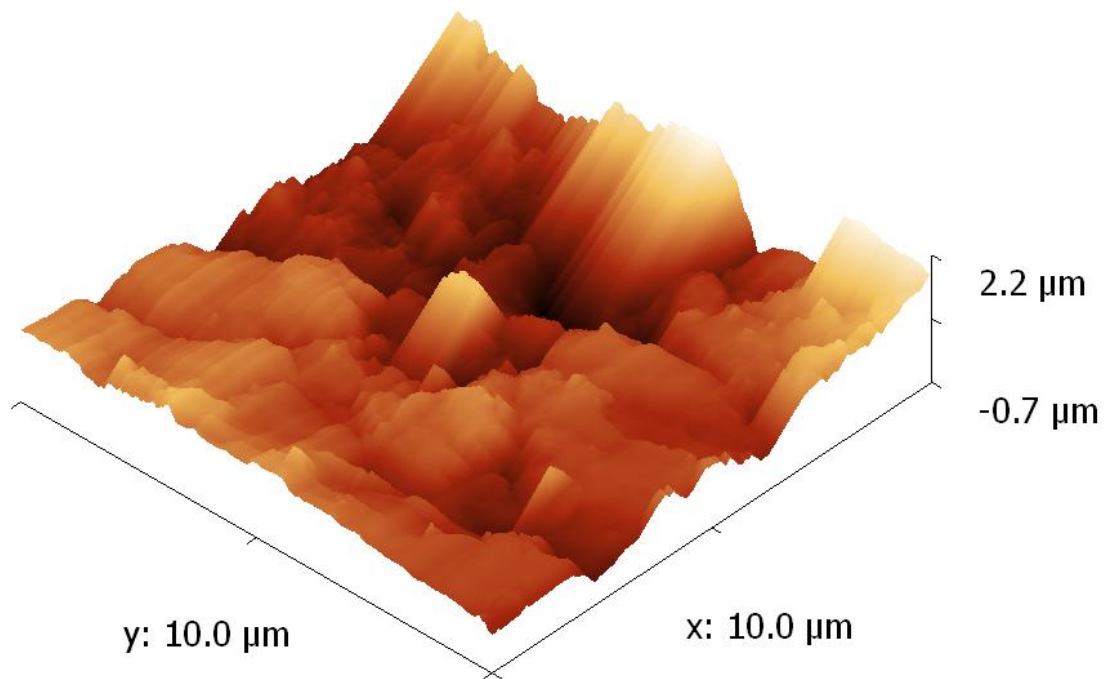


**Figure 5.7:** A 3D projection produced using Gwyddion shows that the PCD surface becomes rough following hydrogen plasma treatment at 1000°C (top). SEM of this sample (bottom) shows that this rough surface is no longer composed of small diamond crystals and a significant amount of non-diamond material has formed. In addition to non-diamond phases forming, deep craters and trenches can be seen.

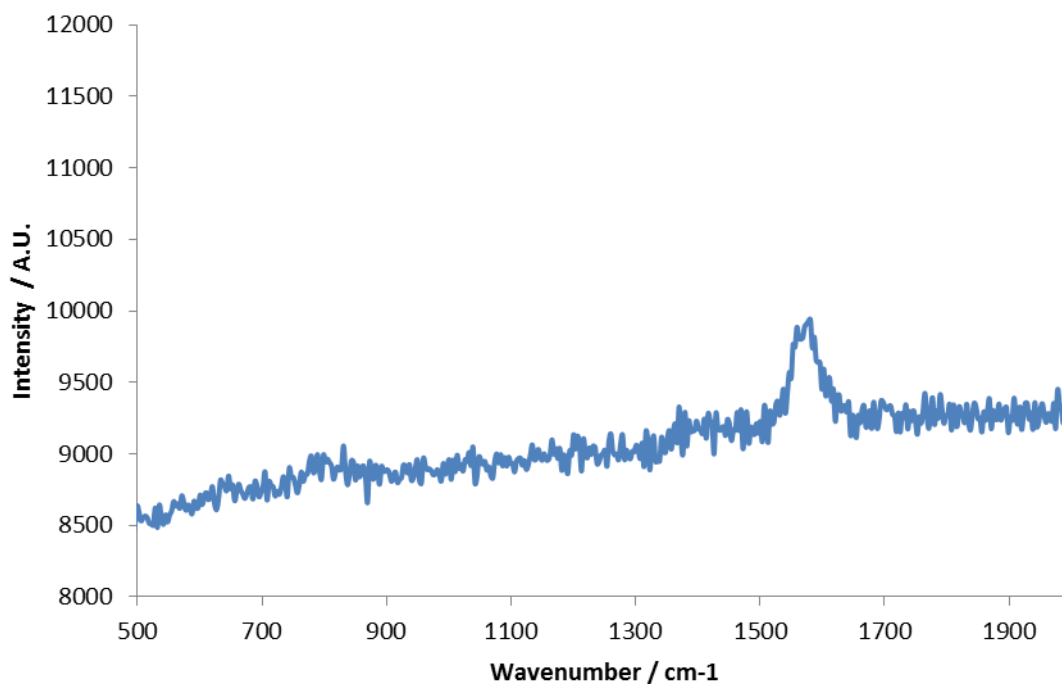


**Figure 5.8:** Raman spectroscopy of the PCD sample treated for 20 minutes in hydrogen plasma at 1000°C produces a spectrum with a broad peak centred at 1580 cm<sup>-1</sup> due to graphitic material and no diamond peak can be observed at 1332 cm<sup>-1</sup>.

The transformation of diamond to graphite under the treatment conditions can be explained quite simply by the fact that graphite is the more thermodynamically stable phase under the experimental conditions [5]. This means that any of the diamond material with a high enough energy to overcome the large free energy barrier will form graphite. By considering the way in which the distribution energy between different states (the Boltzmann distribution [3]) changes with temperature it is obvious that at high temperatures an increased proportion of the diamond will have sufficient energy to be converted to graphite. This is illustrated using the distribution of kinetic energy between particles at different temperatures in **Figure 5.9**, but the same principles apply to other forms of energy which a molecule may possess. For the purposes described here, it is the variation in the vibrational energy with temperature which is of particular interest.

Atomic hydrogen also plays a role in enhancing the rate of graphite formation [6]. At high temperatures, the high flux of atomic hydrogen and high rate of hydrogen abstraction from the surface will produce a large number of radical sites on the surface. These radical sites are highly unstable, which causes their high reactivity in the growth of diamond by CVD, and not all of them will be stabilised by re-termination of the lattice with hydrogen [7]. To stabilise these highly unstable sites a change in hybridisation can occur, changing the sp<sup>3</sup> hybridisation to the more stable sp<sup>2</sup> configuration and so it is possible for large areas of unstable sites to be stabilised by forming graphitic phases [6]. The increased vibrational energy of the lattice at high temperatures may play a further role in this effect, since the chair of diamond can become more planar through some vibrational mode. By considering the stretching of the {111} plane of diamond in these vibrations, it is clear to see that the graphite structure can be formed [8]. This

indicates that the rate of graphitisation depends on the vibrational energy of the diamond lattice.

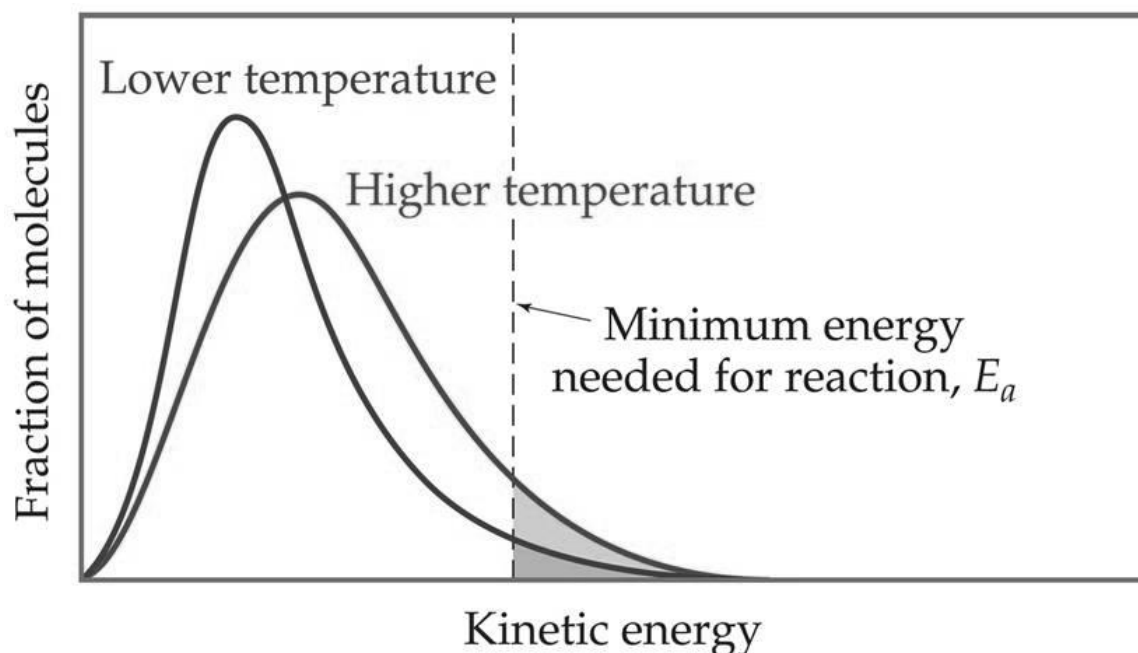


**Figure 5.9:** An illustration of the variation of the Boltzmann distribution with increasing temperature. It is clear that at higher temperature the average energy of the molecules increases and also the number of molecules with higher energy increases. This diagram also indicates the minimum energy required for a specific reaction and how at high temperatures, more molecules will be able to undergo the reaction. Figure is adapted from [9].

Graphitisation of diamond following exposure to hydrogen plasma at room temperature using an RF plasma discharge has previously been reported [6]. In that study, an increased proportion of  $sp^2$  hybridised C-H and C=C bonds were observed by Fourier transform infrared spectroscopy following exposure to the plasma.

In addition to graphitisation, this work has shown that craters and trenches are formed on the surface at high temperatures. This behaviour can be attributed to a high rate at which atomic hydrogen etches non-diamond material whilst the etching of diamond is quite slow [10]. Furthermore, at high temperatures, the rate of this etching will be very fast. Since there is a considerable amount of graphitic material located at the grain boundaries, these regions of the surface will be etched incredibly quickly by atomic hydrogen. This etching process essentially removes the material which bonds many of the crystallites together and so, after etching, the grain boundaries become wide trenches and dislocations become apparent on the surface. An example of a dislocation from treatment at 950°C is shown in **Figure 5.10**. A dislocation is a crystal which has not grown to become part of the PCD film. Therefore removing the graphitic materials causes these crystals to become loose in their sites on the surface and, as the sample is transferred to a vial for storage, can easily be shaken from its position. This leaves a crater in the surface.

The formation of trenches can also be attributed to the etching of grain boundaries, but in this case it is most likely the relaxation of strain at the surface upon etching which causes trenches to form. This strain in the PCD structure is the result of the diamond material being bonded together non-diamond material and the high defect density of the material [11]. As a matter of fact defects have been shown to be present in SCD produced by CVD [12]. As the etching progresses, the 'glue' is removed and so the crystals strain reduced. This leads to extra space between the crystallites producing a trench.

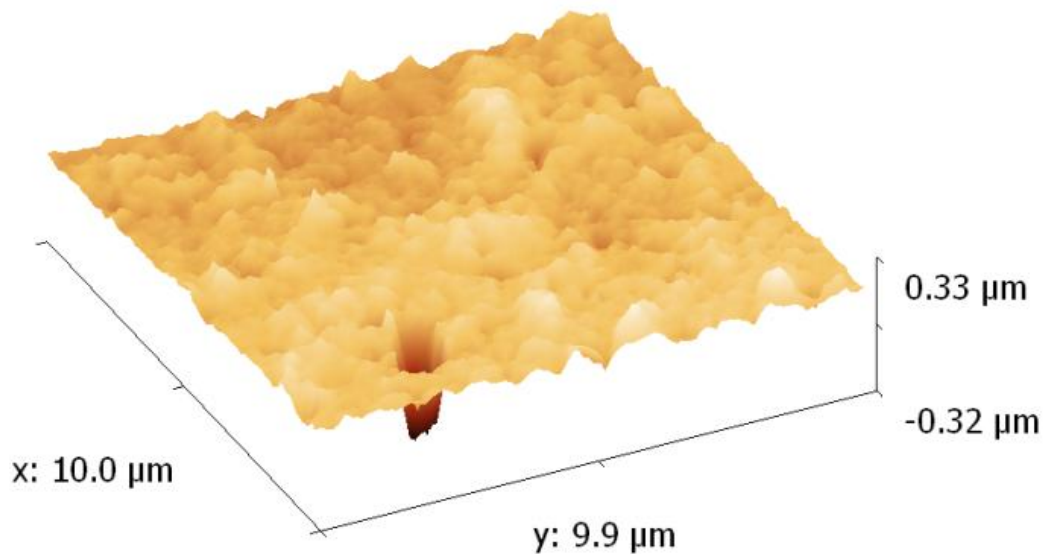


**Figure 5.10:** A 3D-projection of a PCD sample following treatment at 950°C showing a large crater formed by the loss of a dislocated seed crystal from the surface.

Since the variation in the surface roughness of PCD has been explained for the high temperature regime, the processes occurring in the region where slight roughening of the surface is observed will now be described. A comparison of AFM images obtained for the PCD prior to treatment and following hydrogen plasma treatments indicates that the increased surface roughness observed following all hydrogen plasma treatments is the result of atomic hydrogen etching non-diamond material at the grain boundaries. This is easily identifiable since the grain boundaries are very clearly pronounced following the treatments, as can be seen in **Figure 5.11**. Additionally, it should be noted that the width of these grain boundaries increases with treatment temperature and this can again be related to the release of strain in the PCD structure as a result of non-diamond material being etched from the sample. With increasing temperature, the rate of etching will inevitably increase and so, more 'glue' is removed from the sample. As a result, the crystals can move slightly from their original position in the as grown film and the magnitude of this displacement is therefore related to the amount of non-diamond material removed. From these images it is also clear that the columnar structure of the films becomes more apparent with the increased rate of etching.

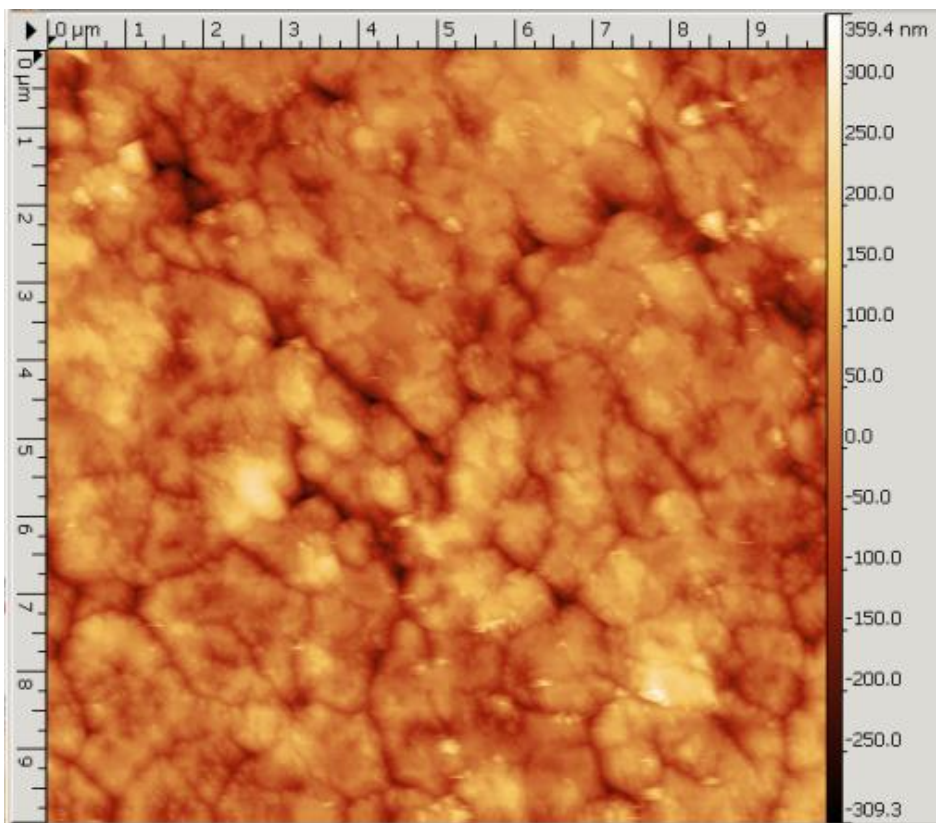
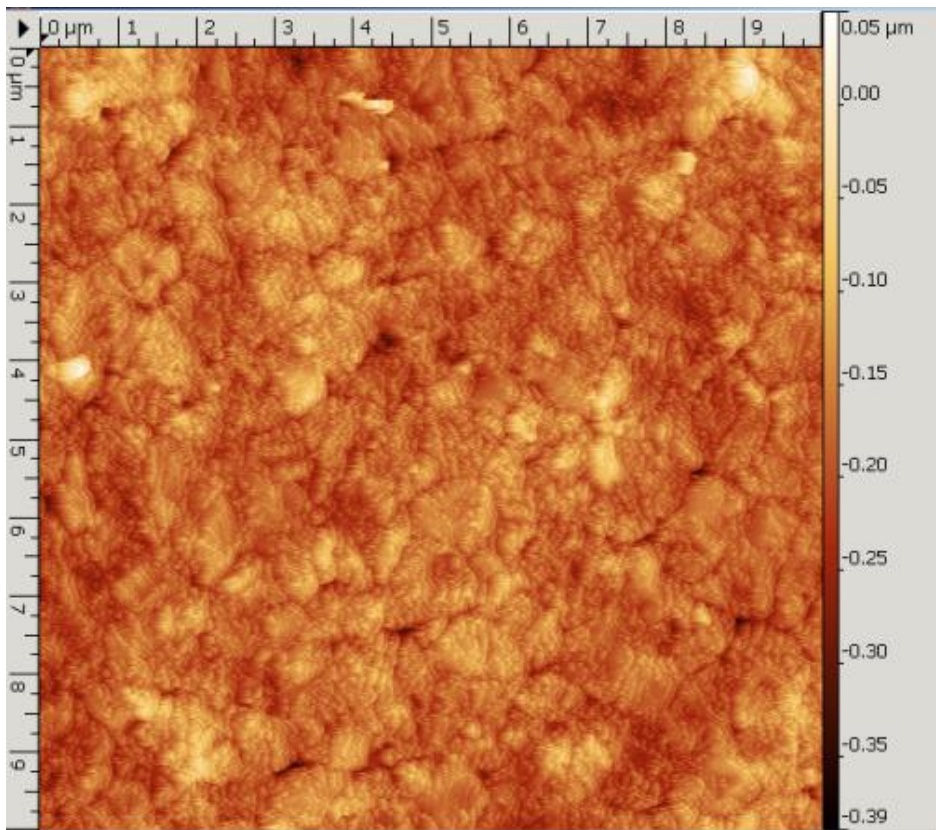


**Figure 5.11:** AFM images for PCD samples treated at 800°C (top) and 900°C (bottom), showing grain boundaries becoming more pronounced with increasing treatment temperature.

In addition to the phenomena described which cause the surface to become rougher following hydrogen plasma treatments at different temperatures, smoothing can be observed on the diamond crystallites themselves following treatments in the 600-900°C region. After hydrogen plasma treatment, the edges of the crystals can be seen to become more rounded and it can also be noted that the uneven texture of the original surface (i.e. bumpy surface) seems to be reduced by hydrogen plasma treatments. In particular it should be noted that the number of tall peaks is reduced significantly by hydrogen plasma treatment. This can be deduced by the size of the white regions in the AFM images which denote tall peaks.

The role of atomic hydrogen in this smoothing of the diamond surface is not immediately clear and there has been much discussion on the dominant smoothing mechanism of hydrogen plasma treatments in the literature. The mechanism of smoothing due to hydrogen plasma treatments will be described in another section of this discussion.

The apparent decreased surface roughness following hydrogen plasma treatment at 900°C compared to treatment at 700°C shown in **Figure 5.6** seems to be quite an interesting result, since it suggests that with higher temperatures the rate of smoothing reactions increases whilst the rate of etching at the grain boundaries remains relatively unaffected. By considering simple reaction kinetics this seems to be plausible. However, from **Figure 5.11**, it is clear that the grain boundaries are getting considerably wider with increasing treatment temperature and so the etching of the grain boundaries must not be occurring at the same rate in both cases. The only obvious difference from this image is that the crystals are not composed of so many small bumps at 900°C compared to 800°C. This effect could not be seen using SEM due to the microscope not being capable of the resolution required.

Making a conclusion as to whether this effect is due to the hydrogen plasma treatment or just caused by slight differences in the AFM parameters used is not clear. This apparent trend could also be attributed to the way data was collected for the experiments. Since only five scans of the sample surface were obtained, a total area of 500  $\mu\text{m}^2$  out of 4  $\text{mm}^2$  has been analysed for each sample. This is only 2.5 % of the entire surface. This suggests that the data obtained may not be entirely representative of the surface of the samples as a whole and so, some strange trends in the data may not be the result of the treatment and will be due to uncharacteristic data which does not provide the bigger picture.

This problem could easily be alleviated by investigating a larger proportion of the surface, whether that is by collecting more scans or scanning over larger areas. The latter approach would not be preferable since the AFM used for these investigations collects the topographical information from 512 lines made up of 512 points per line. This means that scanning over larger areas causes the spacing between points and lines to be larger and so it is possible that a great deal of topographical information about the surface would not be collected. This was one of the reasons for small scan sizes being used in this investigation, allowing a more accurate image of the surface to be produced. Furthermore, scanning over large areas increases the risk that the tip will snag on a rough part of the surface and be damaged. For this reason, it is recommended that lots of small area scans are collected for future projects wishing to observe the trends in surface roughness following treatments.

Continuing with the systematic investigation into the effect of different parameters on hydrogen plasma treatments of PCD, the effect of the hydrogen flow rate into the reactor was investigated using a constant treatment temperature, reactor pressure and microwave power, as well as constant treatment duration (800°C, 82-84 Torr, 1 kW and 20 minutes respectively). When the flow rate is changed there is no visible change to the size of the plasma, however OES confirms that the composition of the plasmas are dependent on the flow rate of hydrogen into the reactor. This can be seen in **Figure 5.12**.

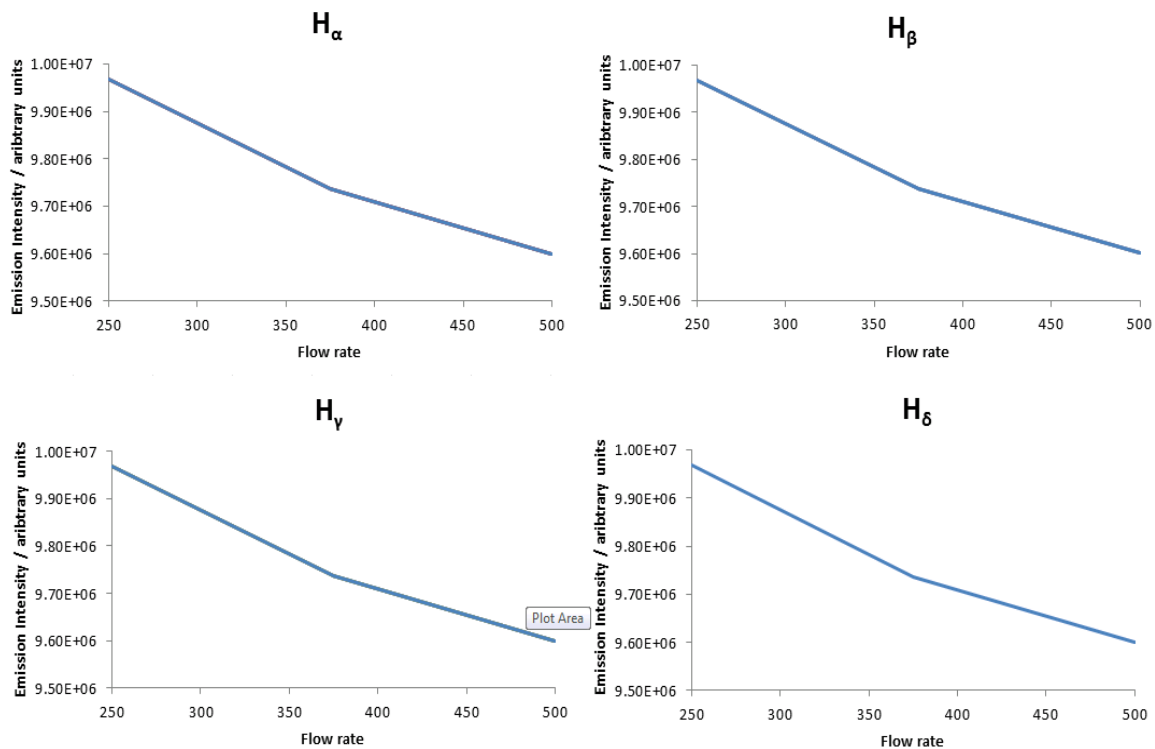


**Figure 5.12:** OES of different atomic hydrogen species within hydrogen plasmas formed at different flow rates of hydrogen into the reaction chamber.

From the OES data, it is clear that the emission intensity of various atomic hydrogen species decreases with increasing flow rate. As with the discussion of the effects of increasing the pressure on the plasma, this effect can easily be explained by considering the concentrations of various species at the centre of the plasma. Since the MWCVD system was maintained at roughly the same pressure in each of these experiments, the pressure exerted on the reactor walls by the various H species in the plasma must be the same. This suggests that the concentration of H in any form in the reactor must roughly be the same for each of the plasmas. The key difference is that new hydrogen is flowing into the reactor at different rates and so the gases already in the chamber are being removed to maintain the constant pressure. This means that at lower flow rates, atomic hydrogen species are not being removed by the exhaust valve as quickly as they would be at high flow rates. This in turn leads to more atomic hydrogen species possibly being present in the plasma which can emit photons in the visible region of the spectrum, leading to an increase in the intensity of emission.

In addition to this, the flow rate of hydrogen into the reactor will create concentration gradient between an area with lots of H<sub>2</sub> at the gas inlet and an areas with little H<sub>2</sub> in the centre of the plasma. This in turn means that the rate of diffusion from the gas inlet to the centre of the plasma will be significantly increased at high flow rates and so, a dilution effect is seen at the centre of the plasma. The increased rate of diffusion towards the centre of the plasma could also cause quenching of the excited state H by more frequent collisions and so it would be expected that the plasma size would decrease. This was not observed. For this reason, the dilution of species at the centre of the plasma seems to be the most likely explanation of why the emission intensities of atomic hydrogen species decrease with increasing flow rate.

The effect of hydrogen plasma treatments at different flow rates on the surface roughness of the PCD is shown in **Figure 5.13** and indicates that variation of the flow rate of hydrogen into the reaction chamber during hydrogen plasma treatments has very little effect on the surface roughness of the PCD.

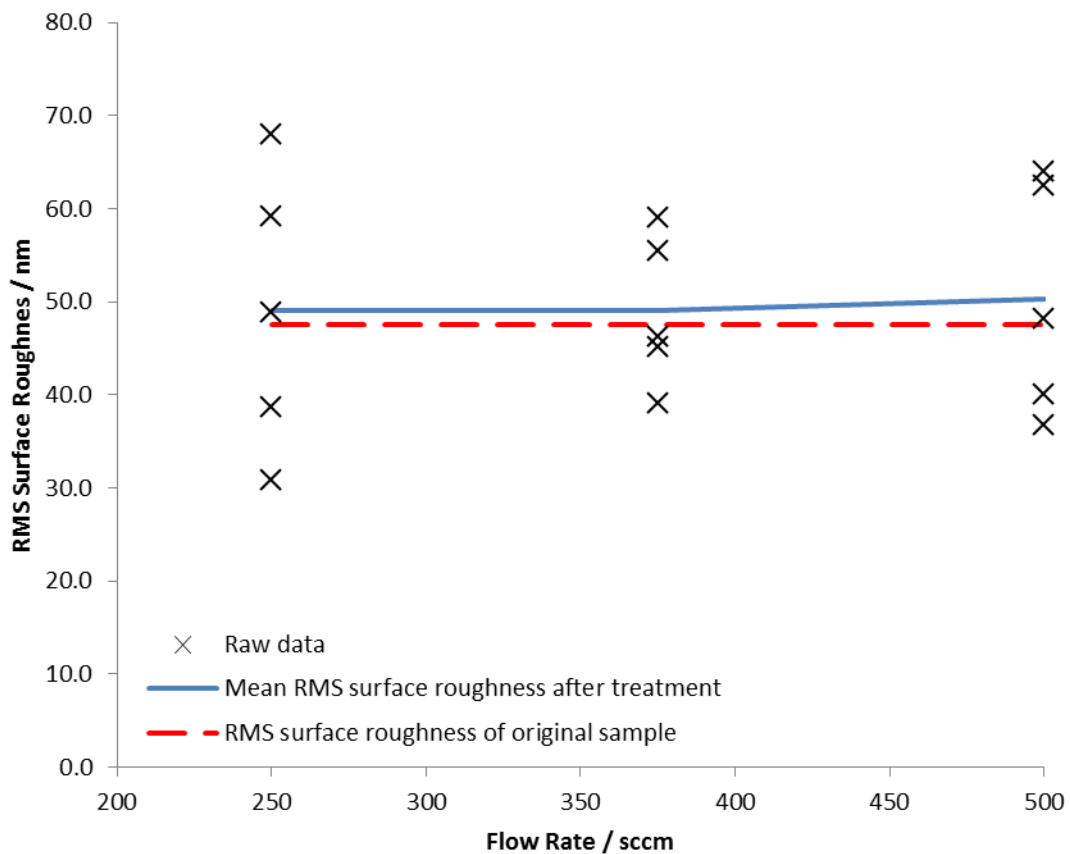


**Figure 5.13:** the variation in the surface roughness of PCD after treatments at constant temperature hydrogen plasmas with different flow rates.

As with the treatments at different temperatures, exposure of PCD samples to hydrogen plasmas causes roughening of the surface due to the etching of non-diamond material at the grain boundaries. This can be deduced by the mean RMS surface roughness of the samples following treatment being higher than that of the original sample. In the AFM data obtained, there were no differences in the widths of the grain boundaries following the different

treatments. This suggests that the rate of etching was occurring at its maximum possible rate for a temperature of 800°C, and that increasing the proportion of atomic hydrogen at the surface did not increase the rate of reaction. This suggests that in a hydrogen plasma treatment, the flux of atomic hydrogen is very high and the surface is saturate with reactive species allowing reactions to occur at their maximum rate, as determined by the temperature. In addition to this etching of the grain boundaries, it was observed that the edges of the crystals had again become quite rounded.

This result of the flow rate not having an effect on the surface roughness of the samples supports a previous report on hydrogen plasma treatments [13]. However, this will be readdressed when the mechanism of smoothing by hydrogen plasmas is discussed later in this chapter.

The third set of investigations into hydrogen plasma treatments and the effects of different parameters looked at the effects of microwave power at constant treatment temperature, flow rate and duration (800°C, 500 sccm and 20 minutes respectively).

Power is defined as the rate at which energy is transferred, used or transformed by a system [14]. This means that at high microwave powers, more electrical energy is being transformed by the magnetron into microwave radiation and thus more microwaves are being transferred into the reaction chamber per unit time ( $1 \text{ W} = 1 \text{ J s}^{-1}$ ). This definition can be used to explain the trends observed in OES of the hydrogen plasma at different microwave powers shown in **Figure 5.14**. The first thing that can be noted from the OES data is that increasing the power increases the intensity of emission from the atomic hydrogen species in the plasma. This can primarily be attributed to an increase in the amount of energy being transferred to H<sub>2</sub> molecules to break the H-H covalent bond. This leads to an increased concentration of atomic hydrogen in the plasma.

Increasing the input microwave power also transfers energy to the gaseous species leading to an increase in their average kinetic energy. This is the cause of the increased temperature when the microwave power is increased. Since temperature increases with microwave power, the plasma density needs to be reduced by reducing the pressure. This is why the pressure was not kept constant for each treatment at different powers. Inevitably, this decision to keep the treatment temperature constant rather than the pressure will have had an effect on the plasma composition and subsequent emissions.

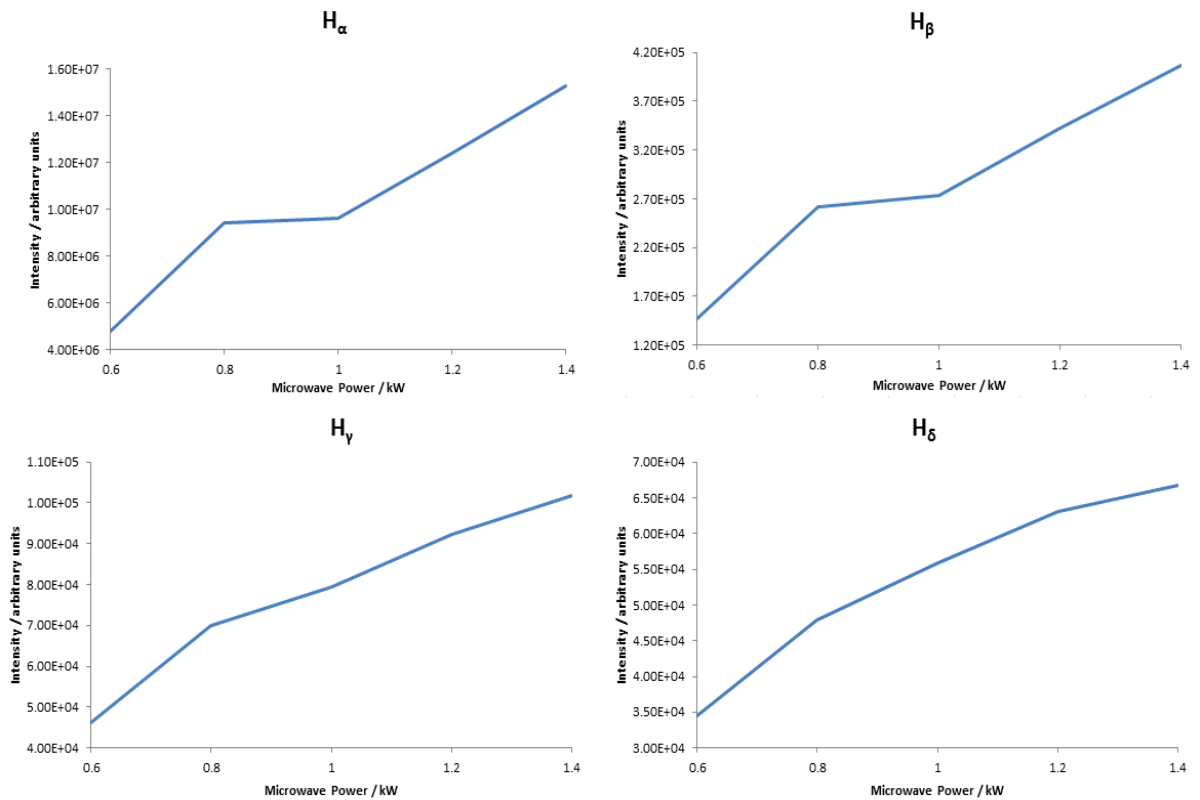


**Figure 5.14:** OES data of the emissions from various atomic hydrogen species within hydrogen plasmas at different microwave input powers and a constant hydrogen flow rate of 500 sccm. The pressure was decreased over the range 100-70 Torr as the power was increased to allow for a constant treatment temperature.

The effect of hydrogen plasma treatments at different input microwave powers and constant temperature on the surface roughness of PCD surfaces is shown in **Figure 5.16**. The most obvious trend in this data is an increase in the surface roughness of the PCD with increasing microwave power.

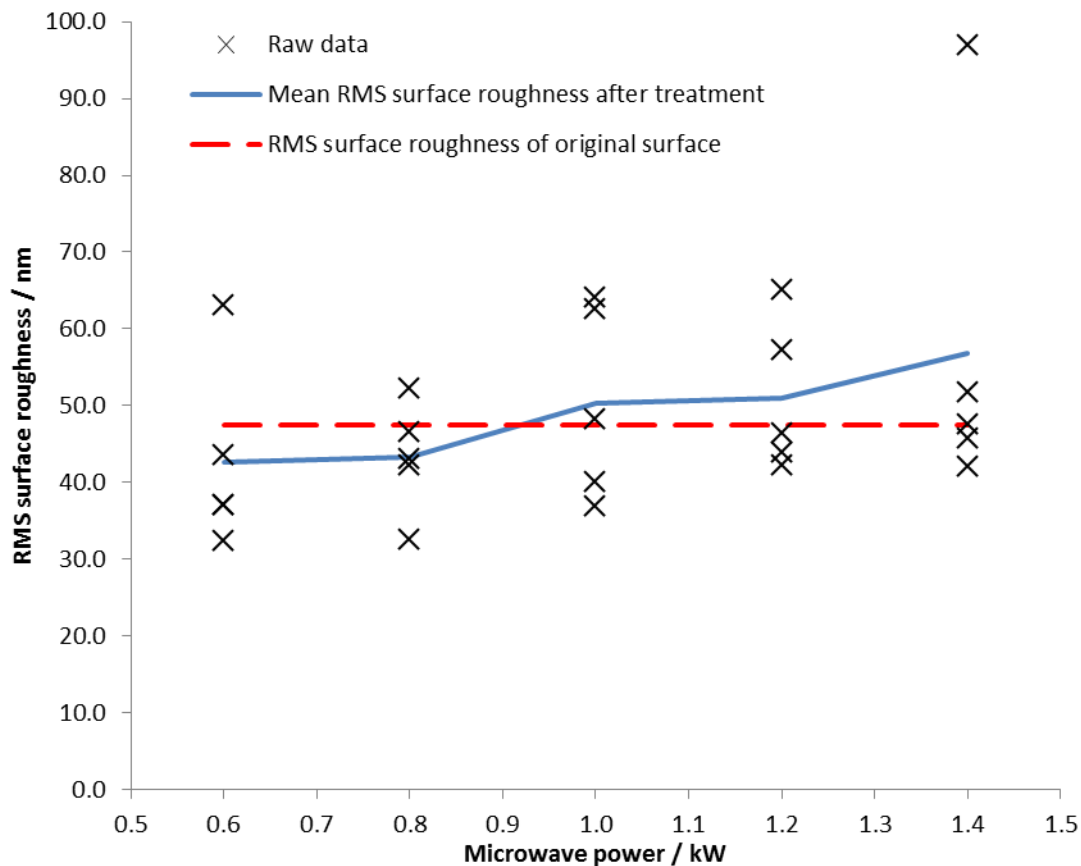


**Figure 5.16:** A plot of the variation in RMS surface roughness of PCD samples treated for 20 minutes in hydrogen plasmas at various microwave powers but the same treatment temperature and flow rate.

At microwave powers >1 kW, the roughness of the PCD is seen to increase due to hydrogen plasma treatment. Again, this can be attributed to the etching of non-diamond carbon at the grain boundaries. In addition to this, smoothing of the crystal edges is also observed. The fact that the treatments at 1.0 and 1.2 kW produce a virtually identical mean RMS surface roughness for the PCD suggests that rates of reactions at the surface are similar under both sets of conditions. Since the temperature is constant in these treatments, the proportion of H available to react with the diamond surface will be responsible for the effects observed. This indicates that despite there being less atomic hydrogen at the surface at 1 kW than at 1.2 kW, the surface is saturated with atomic hydrogen species which could react and so the surface reactions are occurring at their maximal rate. Further increases in the amount of H at the surface will not therefore enhance the rates of reaction any further. However, this trend does not continue to the sample treated at 1.4 kW.

From the AFM image in **Figure 5.17** it is clear that there are lots of small protrusions on the surface following hydrogen plasma treatment at 1.4 kW. These protrusions from the surface suggest that significant etching has occurred. The diamond crystals in **Figure 5.17** also appear to have become more ballas in morphology when compared to previous images. This could be due to the anisotropic etching similar to that which produced the thin columns. This result is in

contrast to reports in the literature which have described the evolution of etch pits on the PCD surfaces due to hydrogen plasma treatment at high microwave powers [15]. Suggest etching...

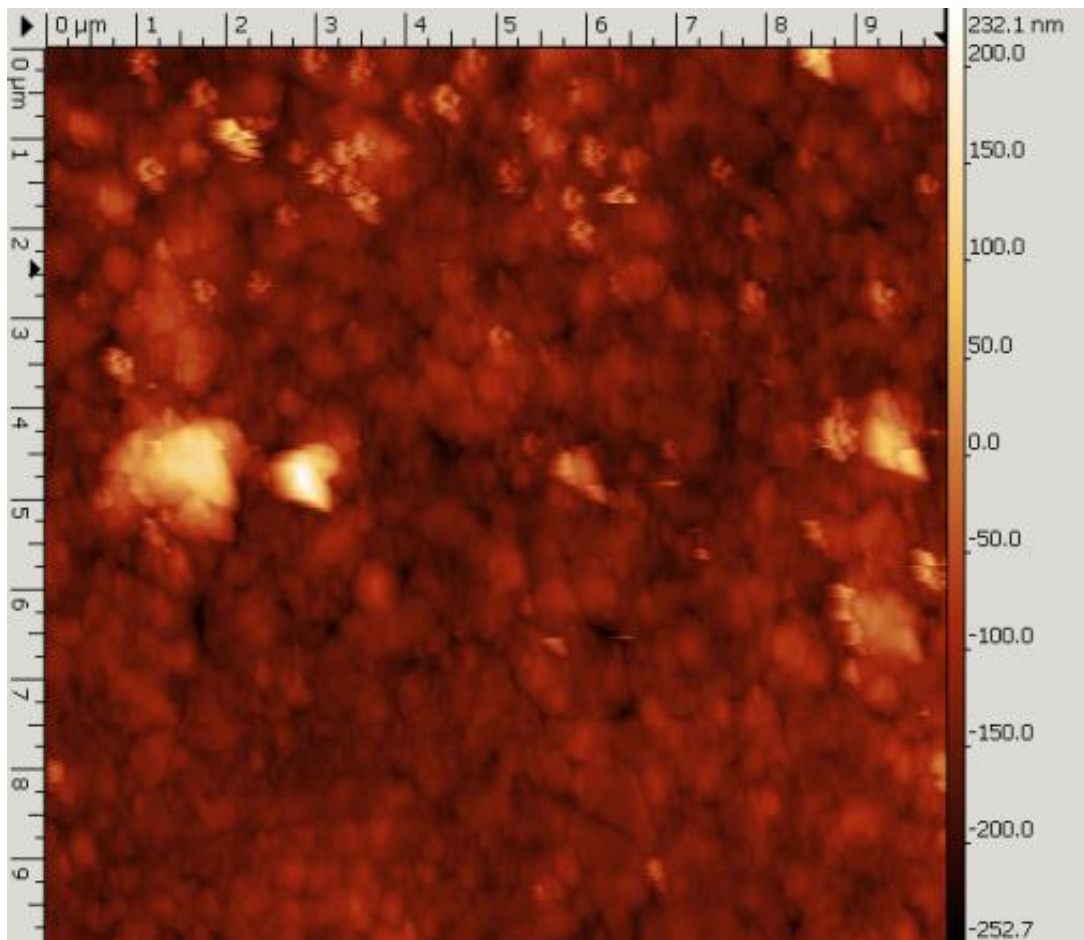


**Figure 5.17:** An AFM image of a PCD sample following hydrogen plasma treatment at 1.4 kW.

This etching behaviour is quite remarkable and seems to be specific to certain crystals on the surface. This is indicated by the presence of seemingly smooth facets at the bottom of **Figure 5.17**, slightly right of centre. The fact that this etching has not occurred equally on all of the diamond crystals could be attributed to their random orientation when deposited onto the CVD substrate.

For etching to occur the C-C bond of the diamond lattice needs to be broken, and this requires a large amount of energy [16]. Since the treatments were performed at constant temperature, the source of this energy for breaking the bond must be related to the energy state of the reactive hydrogen species. This is due to the rates of the surface reactions and average kinetic energy of hydrogen atoms colliding with the surface being constant for a given temperature. This theory of high energy atomic hydrogen species being responsible for the etching of the diamond crystals on the surface is supported by the OES data which shows that there is an increase in  $H_{\delta}$ -emission at high microwave powers. As already mentioned, OES cannot be used to observe all of the species within the plasma which may have a role to play at the diamond surface. Hydrogen atoms in states with  $n > 5$  cannot be detected since they emit photons in the UV. Ro-

vibrationally excited neutral H<sub>2</sub> molecules and ionic species such as H<sup>+</sup>, H<sup>-</sup> and larger cluster ions cannot be detected but are known to be present in the medium [17].

The exact identity of the species responsible for these highly energetic reactions is not currently known, but the increased rate of etching observed in DC-biased hydrogen plasma treatments suggests that ionic species may play a significant role in the process [18]. In the literature it has been shown that {100}-oriented surfaces parallel to the substrate are etched less efficiently from the surface than other crystal orientations [18].

The fact that the cause of such etching reactions is not known highlights that the composition of hydrogen plasmas, the interactions of the various species within the medium and also the interactions of various species produced in such a medium with the surfaces of diamond materials are still not completely understood. However, OES in this study has shown that high powers cause an increase in the number of higher energy species in the plasma and so, it can qualitatively be deduced that there will be a higher number of species with sufficient energy to overcome the high energy barrier for cleavage of the C-C bond. This means that the rates of such reactions will be higher for high power plasmas than low power plasmas, even if the samples are heated to the same temperature.

Now that the roughening of the PCD surface at high powers has been considered, the apparent smoothing observed at the opposite end of the power scale will be described. By comparing the AFM images of samples treated at 0.6 kW and 1 kW in **Figure 5.18**, it is clear that the etching of the grain boundaries is less significant for the low power plasma treatment. This can be attributed to the reduction in the number of atomic hydrogen species at the surface due to the slower rate of dissociation of H<sub>2</sub> at low microwave powers, as indicated in the OES data. However, there is no clear evidence to suggest that these surfaces are smoother than the original sample and if these images alone were analysed, it would seem as though the hydrogen plasma treatment had made the surface rougher. The most likely explanation for this apparent smoothing is the possibility that the area scanned using AFM has not been representative of the whole sample surface as previously described.

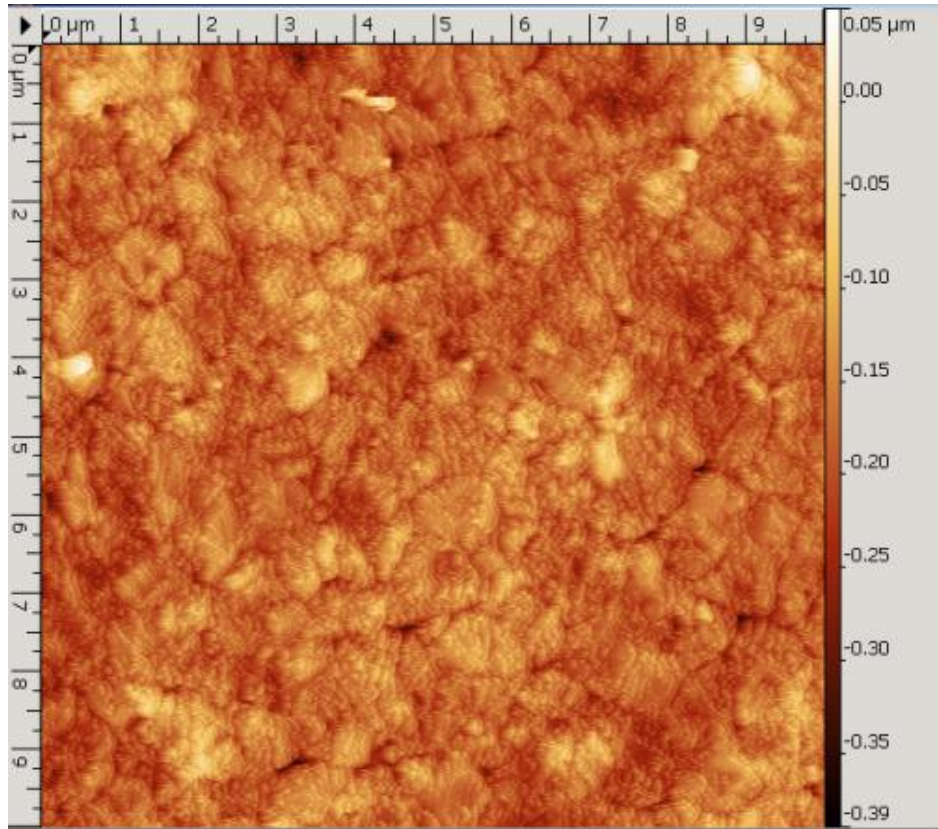


**Figure 5.18:** AFM images of PCD samples treated in hydrogen plasma at 800°C for 20 minutes at microwave powers of 0.6 kW (top) and 1 kW (bottom).

Now that the various parameters which affect the plasma composition had been observed, a final investigation into the effect of treatment duration was performed. This investigation was performed as a set of 10 minute experiments leading to a total treatment time of 1 hour, to see how the surface roughness varied at different points during the treatment. The results of this investigation can be seen in **Figure 5.19**.

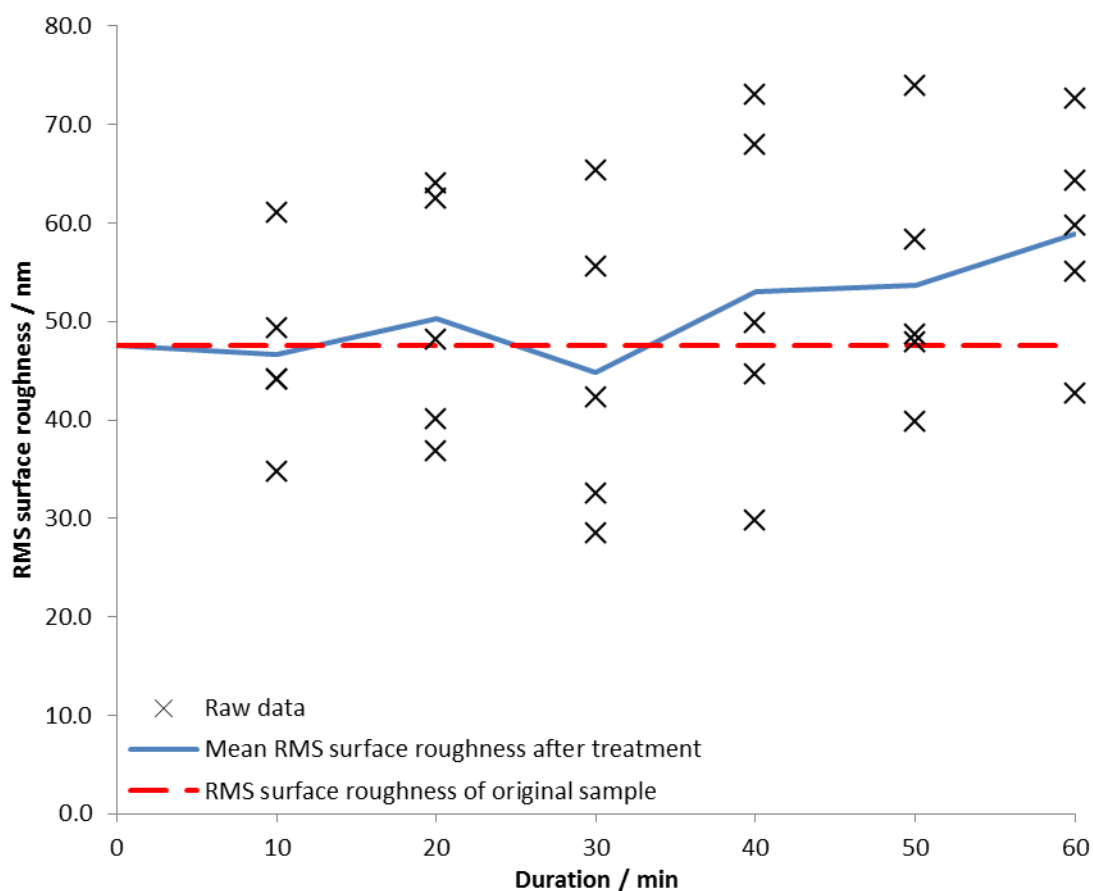


**Figure 5.19:** A plot of the variation in the RMS surface roughness of PCD treated in a series of 10 minute treatments for a total of 1 hour exposure of the sample to hydrogen plasma.

Over the course of the full hour treatment, the roughness of the PCD increases and this can be attributed to the prolonged exposure to the hydrogen plasma causing significant etching of the grain boundaries as observed following all of the hydrogen plasma treatments already reported. This etching of the grain boundaries is prominent in the both the SEM and AFM shown in **Figure 5.20**. From the AFM image the treatment also appears to have significantly altered the morphology of the crystals at the surface of the PCD over the course of the hour, revealing some larger crystals ( $<1 \mu\text{m}$ ) with a range of facets from large smooth surfaces to others which appear to be ballas and composed of small crystals.

Similar observations have been made in previous reports where smooth  $\{100\}$  facets were seen following hydrogen plasma treatments whilst  $\{111\}$  facets were etched to form smaller nanodiamond features [19]. This effect has been explained in other reports which attributed the effect to the interactions of atomic hydrogen with the  $2 \times 1$  reconstructions of the two surfaces affecting the absorption properties of hydrogen on these crystal planes [20], where the dimer bonds on the 100 surface are not broken by atomic hydrogen very efficiently and so, these surface cannot be covered fully with hydrogen. The  $2 \times 1$  reconstruction on the  $\{111\}$  surface however, is much weaker and so can be more easily broken [20]. Experiments which have

negatively biased the substrate during hydrogen plasma treatments also report a similar phenomenon [21].

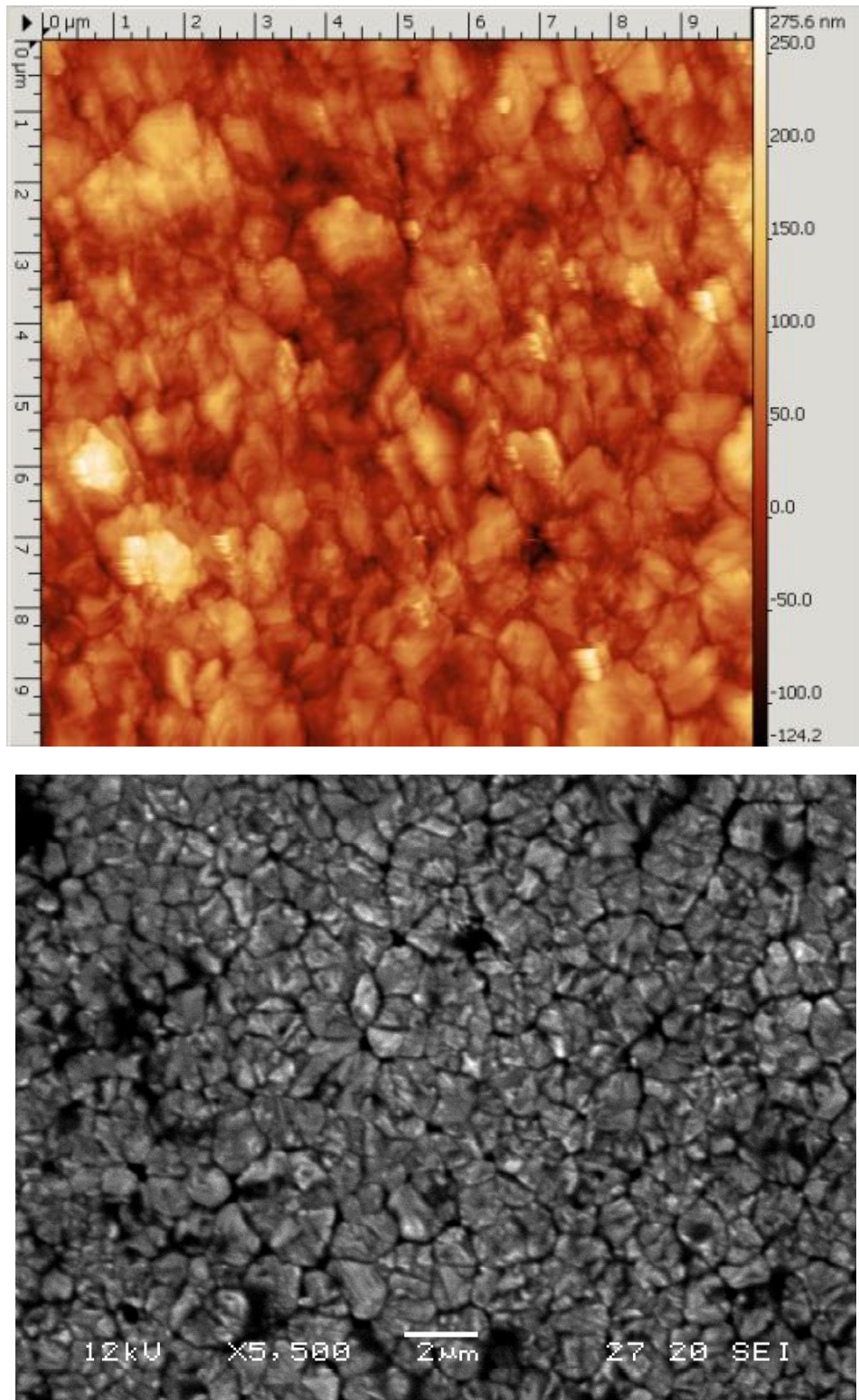


**Figure 5.20:** AFM (top) and SEM (bottom) images of the PCD samples exposed to hydrogen plasma at 800°C in a series of 10 minute treatments for a total treatment time of 1 hour.

In addition to the series of 10 minute experiments, a PCD sample was exposed to hydrogen plasma treatment for the whole hour in one single treatment. SEM of this sample reveals that upon prolonged exposure, the surface had become more highly graphitised, as can be seen in **Figure 5.20**. The cause of this graphitisation has already been described. Furthermore, the mean RMS surface roughness of the sample which was treated for 1 hour in hydrogen plasma was  $\sim 15$  nm more than that of the sample which had been treated in hydrogen plasma for the same time, except by accumulating the effects of a number of shorter treatments. This highlights an important observation that prolonged exposure to hydrogen plasma causes roughening and graphitisation of the surface. This effect of roughening of the diamond surface during long exposure to plasmas has been reported previously in the literature [23].

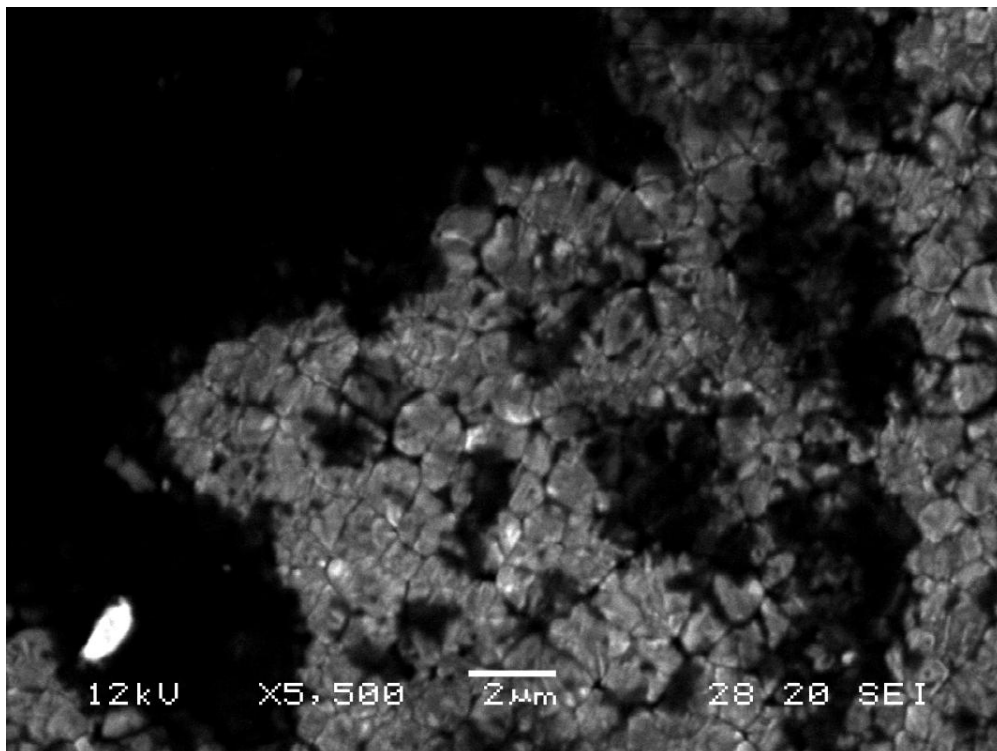


**Figure 5.21:** SEM of a PCD sample exposed to hydrogen plasma treatment at 800°C for a single 1 hour treatment shows that the surface has become covered in large areas of non-diamond material.

At this point, it is important to summarise the findings of this part of the project:

- First of all, treatment of PCD in hydrogen plasma generally causes significant removal of non-diamond material from the surface. This leads to roughening of the surface and a reduction in the integrity of the diamond film, but does improve the surface quality in terms of increasing the proportion of diamond material at the surface.
- The next most significant effect observed was graphitisation of the surface at high temperatures or following long exposure to hydrogen plasma.
- Sharp, narrow protrusions were produced on the diamond surface due to etching by highly energetic species and it was noted that the {100} facets appear to be most resistant to etching. {110} and {111} facets can be seen to be etched to form nanoscale-ballas features on the surface.

- In addition to these effects, it has been noted that the crystal edges appear to become more rounded by hydrogen plasma treatment.
- Hydrogen plasma can reduce the uneven texture of the PCD surface by removing small 'lumpy' features.

From these conclusions, it is clear that hydrogen plasma treatment alone is not an ideal candidate for producing a smooth surface on PCD. Harsher techniques need to be applied to planarise the surface. The main issue with hydrogen plasma treatment is that the grain boundaries are subject to rapid etching. This has also been an issue in a number of other studies which have attempted to use methods other than hydrogen plasmas to polish the diamond surface [24,25,26,27].

In order to prevent this, a number of masking procedures have been suggested. These techniques use a variety of materials as sacrificial layers and can produce patterned surfaces by preventing regions of the diamond from being etched [28]. These techniques have also been used to prevent the rapid etching of grain boundaries in PCD films whilst leaving the tops of the grains exposed [29]. However, as the surface becomes smoother, it gets harder to remove all traces of the masking material from the surface [30]. For this reason, and the need to apply the technique several times to achieve a flat surface, it is clear that masking procedures would preferably be avoided in a commercial setting. Furthermore, the chance of contamination being present on the diamond surface is not an option for cold cathode devices where the diamond surface is of the up most importance.

Since the investigation into the effects of hydrogen plasma treatments at different conditions has shown some that there is some smoothing occurring during the treatments, an investigation using SCD could provide a useful insight into the processes occurring on the crystals of a PCD film.

## 5.2 Hydrogen plasma treatments of SCD

For this investigation, a 3 x 3 x 1 mm<sup>3</sup> {100}-oriented SCD sample was treated at 800°C for 1 hour in hydrogen plasma at 1 kW, 500 sccm and 120 Torr. In comparison to a similar sized PCD sample, the conditions required to reach the desired treatment temperature were much higher for SCD. This is due to the superior thermal conduction properties of the single crystal material.

The morphology of the as-grown {100}-oriented diamond surface prior to treatment exhibits a number of small defects in the surface. The RMS surface roughness of the regions between these defects was obtained using Gwyddion and these surface regions were found to have a low mean RMS surface roughness of 0.4 nm. This indicates that the majority of the surface is very smooth. Almost to the level desired for device applications. However, when the pits in the surface are included, the mean RMS surface roughness of the sample was found to be 8.1 nm. This value of the surface roughness of the as-grown SCD may not be entirely accurate since it is impossible to gauge the depth of small features on the surfaces of materials using AFM. This is due to shape and dimensions of the cantilever tip, as illustrated in **figure 5.22**.

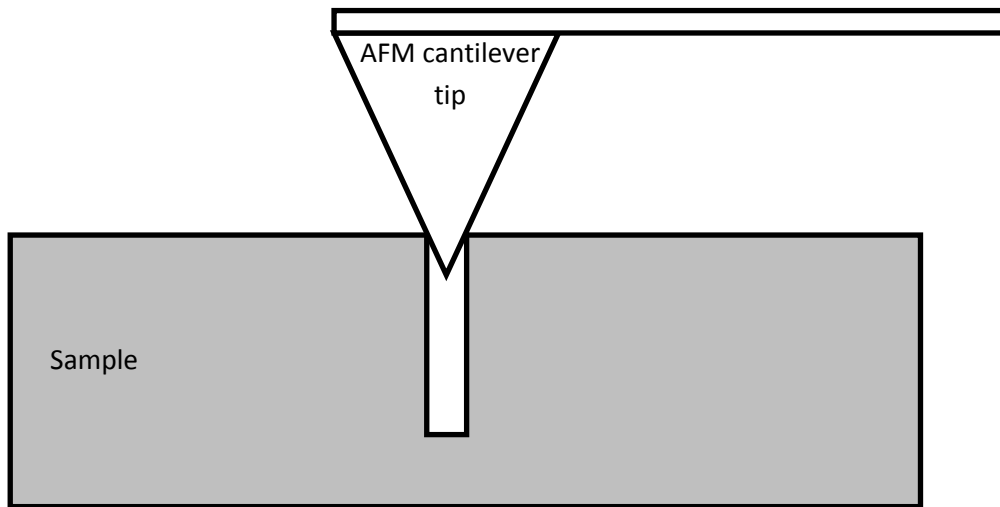


**Figure 5.22:** An illustration of how AFM cannot accurately measure the depth profile of a narrow pit-like feature on the surface of a material due to the dimensions of the cantilever tip. When this occurs the depth of the feature on the surface cannot accurately be determined. *Figure designed by author.*

Since it is difficult to assess the depth of the surface defects, it is common practice to polish the surface using lapping techniques. This procedure removes surface defects and makes the surface more uniform. Due to the fact that this process relies on the use of small diamond grits impregnated into suitable tool pieces, the smoothness which can be achieved using such techniques is limited by the size of the crystals in the abrasive [8]. Furthermore, since lapping is a non-plastic deformation process, scratches are usually produced in the surface [8]. The effects of hydrogen plasma treatments on the roughness of these polishing marks seem to have been the focus of many papers on the subject of hydrogen plasma treatments of SCD, and the results of these investigations will be described in the next section.

For this experiment, the SCD was not polished so that the effects of hydrogen plasma treatment on as-grown SCD could be investigated. It was assumed that the diamond crystals in PCD films would behave very similarly to this SCD, except the processes would occur on a much smaller scale which cannot be observed on a PCD film without using ultrahigh resolution imaging techniques.

AFM images of the SCD surface before and after treatment can be seen in **Figure 5.23** and it is clear that the surface has become much rougher following the treatment. This roughness can be attributed to the formation of square pits in the surface which consist of terraces parallel to the  $\{100\}$  orientation and steps which run parallel to the  $\{110\}$  direction (i.e. the faces of steps are vertical and perpendicular to the terraces). These square pits can be seen to be almost pyramidal in structure in the 2D AFM image shown in **Figure 5.24**.

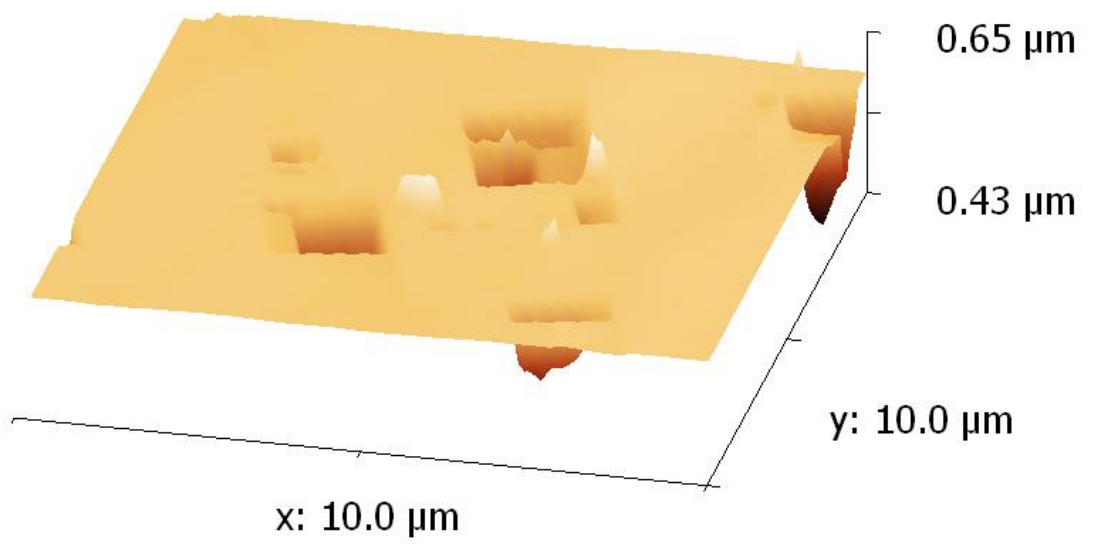
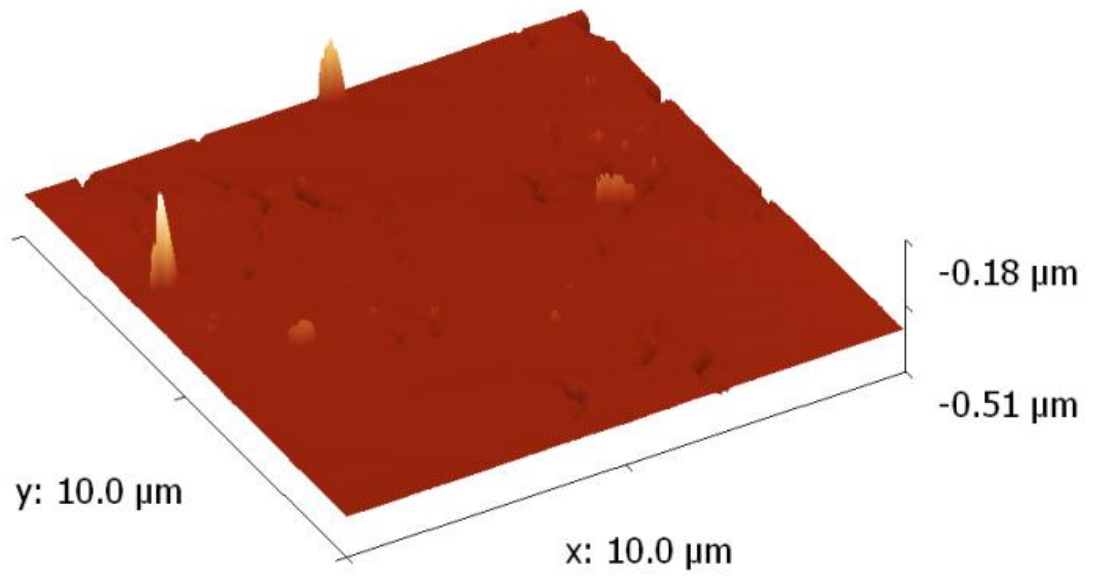


**Figure 5.23:** 3D-AFM projections of the SCD sample before (top) and after (bottom) treatment in hydrogen plasma for 1 hour at 800°C.

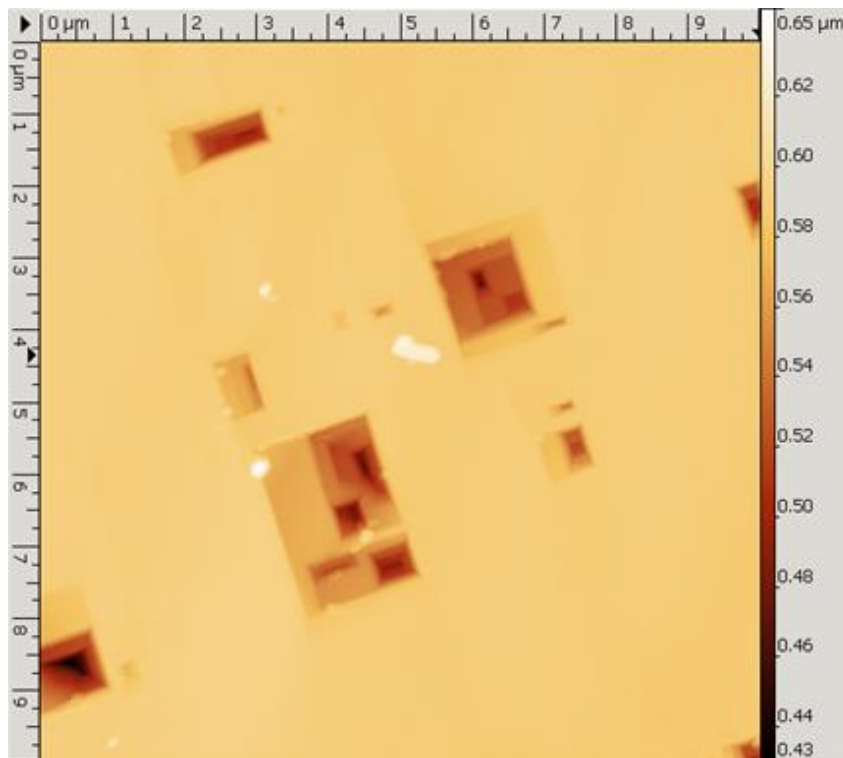


**Figure 5.24:** An AFM image of SCD following hydrogen plasma treatment for 1 hour at 800°C.

These observations suggest that that diamond material is being etched from the surface at the sharp edges of the defects and that this regression of the step flow growth process will continue with further hydrogen plasma treatment. From **Figure 5.24** it is clear to see that if the treatment was continued, the pits in the surface would merge together and it would be highly likely that the majority of the upper diamond layers would be removed, leading to a reduction in the depth of the pits. Further treatments would result in the same process repeating many times over until only atomic steps remained on the surfaces. To be able to achieve this in this investigation, it was clear that the sample would need to be treated for very long treatment durations to produce a smooth surface.

An additional point of interest is the fact that the hydrogen plasma treatment has produced rectangular pits all with parallel step edges. Considering the original state of the surface and the seemingly random shape of the defects in the surface, this is quite remarkable and suggests that the regression of the step growth propagates along the edge of a step rather than etching material randomly from the surface.

Nonetheless, this short investigation has provided an insight into the way in which the morphology of the SCD changes en route to the formation of an atomically smooth surface. This result will now be compared with previous reports in the literature to determine the main mechanism by which hydrogen plasmas reduce the roughness of diamond surfaces.

### 5.3 The smoothing mechanism of hydrogen plasma treatment on SCD

So far in this study, hydrogen plasma treatments have been shown to smooth the sharp edges of small diamond crystals in PCD films, as well as producing pits on SCD which clearly originate from anisotropic reactions at defective sites in the surface of the material. It has also been proposed that longer treatments would cause these pits in the surface to merge and continue to increase in size until the top layers of the surface have been removed to reveal a smooth surface. The major question in the mechanism of these processes is whether the diamond surface becoming smoother due to the removal of material from the surface or whether material is simply being redistributed. This has been a widely discussed question since the early work in the 1990s which showed that hydrogen plasmas could routinely be used to smooth {100}-oriented natural diamonds [31].

In the literature there are two mechanisms proposed to explain the smoothness of SCD following hydrogen plasma treatments. These are hydrogen atom-assisted surface diffusion (also known as hydrogen atom-assisted surface migration) and etching by atomic hydrogen.

Hydrogen atom-assisted surface migration (illustrated in **Figure 5.25**) was proposed as the dominant mechanism of smoothing caused by hydrogen plasma treatments in 1995 [13]. This was due to experiments in which natural diamond powders were shown to become well faceted without a change in mass [32]. This apparently ruled out etching as the possible smoothing mechanism since the crystal size did not change. The authors of this report also ruled out the possibility that an etching and recombination mechanism may have caused the smoothing of the diamond crystals, and there were a number of reasons for this.



lattice [32]. Following this logic, it was reasoned that this would mean that small isolated diamond crystals would undergo etching and so get smaller, whilst closely packed particles would experience regrowth [33]. Since this was not observed, that was one tick against etching and recombination as the mechanism of smoothing.

The second argument against etching and recombination was based on the idea that increasing the flow rate would have caused the etch products to be removed from the reactor more quickly [13,32,33], thus leading to a decreased rate of recombination and so etching only would be observed. Again this was shown not be the case and well faceted crystals were produced at all of the flow rates investigated. Similar observations to these literature reports have been made in this project, where it has been shown that the flow rate has no effect on the surface roughness of PCD in hydrogen plasma treatments. In this work, OES has shown that at low flow rates the emission intensity from atomic H species in the centre of the plasma increases and it was suggested that this was due to a less rapid dilution effect caused by new H<sub>2</sub> flowing into the reactor more slowly. The explanation for why the surface roughness does not vary with changing the flow rate was then attributed to the surface being saturated with H under any plasma conditions. This meant that the rates of the various surface reactions were occurring at the maximum possible rate according to the treatment temperature, which was the same in all cases. Since the starting material in each experiment was from the same original sample, the fact that the surface reactions were occurring at the same rate, despite a higher proportion of atomic hydrogen being present at low flow rates, produced very similar results.

It is the author of this projects belief that the dismissal of etching and recombination is not justified by the arguments used in the literature. The main point to consider is that the rates of diffusion away from the surface will depend on the volume of the reactor (i.e. the total number of possible paths away from the surface). The MWCVD system used in this project has a volume of ~1 L [34], which means that from the perspective of a small particle, there are a phenomenal number of possible routes away from the surface and very few which stay close to the surface over an extended timeframe. This means that the etch products will diffuse away from the surface very rapidly and so, adjusting the flow rate by a minute amount in relation to the volume will have no effect on the rate of diffusion of the etch products. For this reason, it is proposed that etching should be reconsidered as the dominant mechanism of surface smoothing by hydrogen plasma treatments.

The only factor in support of hydrogen atom-assisted surface migration which cannot be argued against is that the literature shows that the samples did not change significantly in mass. In recent years, there has been considerable interest in modelling the growth of SCD with H-assisted surface migration playing a major role in step-flow growth [35]. By modelling these reactions computationally, it has been shown that when a CH<sub>2</sub> group migrates across the surface and becomes incorporated into a six membered ring at a concave step edge, this group becomes locked in position. This agrees well with early work in the field [36] and shows that diamond can grow in a step flow manner by the addition of carbon species to the lattice followed by H-assisted surface migration to find suitable sites at step edges for incorporation into the diamond lattice.

In hydrogen plasma treatments, there is no carbon containing precursor in the gas phase and so, new carbon material is not being added to the lattice. For H-assisted surface migration to be the dominant mechanism there must be a lot free CH<sub>2</sub> groups on the diamond surface. For the {100} surface in particular, this is known not be the case due to a reconstruction of the surface to minimise the steric repulsions between the CH<sub>2</sub> groups on the surface. This is known as a 2 x 1 reconstruction [37]. For this reason, smoothing by surface migration alone does not seem feasible, especially on {100}-oriented surfaces which have already been mentioned as being more resistant to etching than other facets. For this reason, there needs to be a regression of the diamond growth process to produce pendant groups which can migrate. This 'ring-opening' is effectively an etching effect.

In terms of experimental evidence, there seems to be much more support for the idea that etching is the main mechanism of surface smoothing by hydrogen treatments [38,39] with many reports being published around the same point in time as the report which suggested that H-assisted surface migration was the dominant mechanism of surface smoothing by hydrogen plasma treatment.

Many publications have reported the formation of pyramidal pits with square-symmetry on {100} surfaces [40,41,42,43,44] like those observed in this project. Computational modelling based on etching reactions during the CVD of {100}-oriented diamond have also been shown to provide a good prediction of the growth rates and morphologies seen experimentally when growing SCD with smooth surfaces [45].

The sides of the pits in the literature are reported to be comprised of (111) facets [41,46] and the edges are parallel to the {110} direction, as found in this study. The etch pit density has been shown to be related to the dislocation density [43] and has also been shown to decrease with an increase in the misorientation angle of the diamond surface [40]. Macro-steps observed in this project related to literature reports where steps appeared on the {100}-oriented SCD surface [47].

The reason for etching at step edges can be explained very simply by considering the bonding of the atoms at a step edge [45]. At a step edge (and the surface), the atoms are not as highly coordinated as atoms found in the bulk of the material. This means that fewer of the strong C-C covalent bonds are formed and so the atoms at a step edge are held onto the lattice more weakly. This means that the amount of energy required to remove this atom from the surface is much lower than other atoms in the bulk of the material. Furthermore, at a step edge, the number of bonds exposed to the atomic hydrogen is higher than that for an atom on a flat surface. This allows for atomic hydrogen to attack from many different angles. This would greatly increase the likelihood of the atom being removed from the surface of the diamond.

Once an atom has been removed from a step edge, the etching will propagate along the step edge since the newly exposed atom will be even less coordinated to the lattice and so can be even more easily removed. This is illustrated in **Figure 5.26** where cubes are used to represent the atoms on the surface and show in a simple way how the etching along a step edge can propagate due to a lower number of bonding interactions with the lattice.

For etching to be possible, hydrogen atoms need to insert into the C-C bond and cause cleavage to leave a pendant radical species on the surface, as shown in **Figure 5.27**. These radical species are higher in energy than pendant methyl groups and so have a lower barrier to removal from the surface [34,35,36,45]. This means that subsequent attack by hydrogen atoms will release the radical back into the gas phase and leave two unactivated lattice sites.

However, as already mentioned several times previously, the diamond surface tends to reconstruct itself to reduce steric interactions between the hydrogen atoms terminating the dangling surface bonds. Atomic hydrogen plays a further role in breaking this reconstruction and thus reducing the coordination of the surface atoms to the lattice by forming a dihydride [48]. This surface dihydride is shown being etched in **Figure 5.27**.

Once a carbon radical has been removed from the surface, it is possible that it may reattach to the surface at an activated lattice site. At this point the atom may migrate across the surface, become incorporated into the lattice or be etched away a second time. If a carbon atom adds to a pendant radical to produce a long alkyl chain on the surface, then facile  $\beta$ -scission reactions can occur and remove more material from the surface [34,49]. The mechanism of  $\beta$ -scission is shown in **Figure 5.28**.

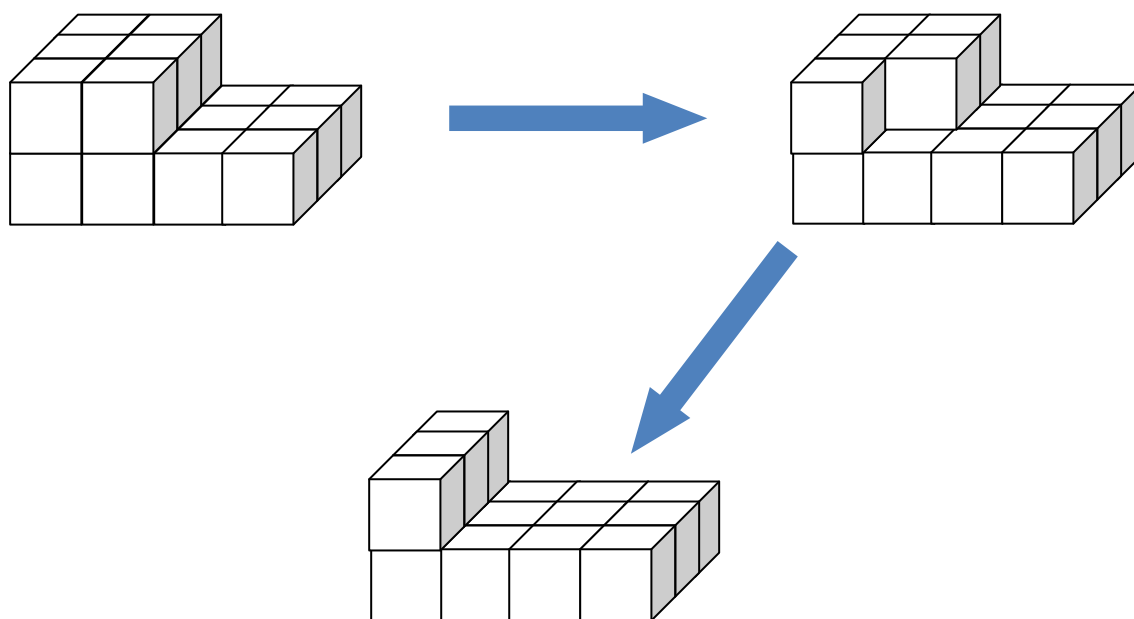


**Figure 5.26:** A simple illustration of etching at a step edge (top left). The cubes represent atoms and the number of faces exposed at the step represents the proportion of C-C bonds exposed to the plasma. Etching removes an atom and reveals further bond to the plasma which could be etched (top right). These under-coordinated atoms are rapidly etched away in a regression of the step flow growth process (bottom). *Figure designed by author.*

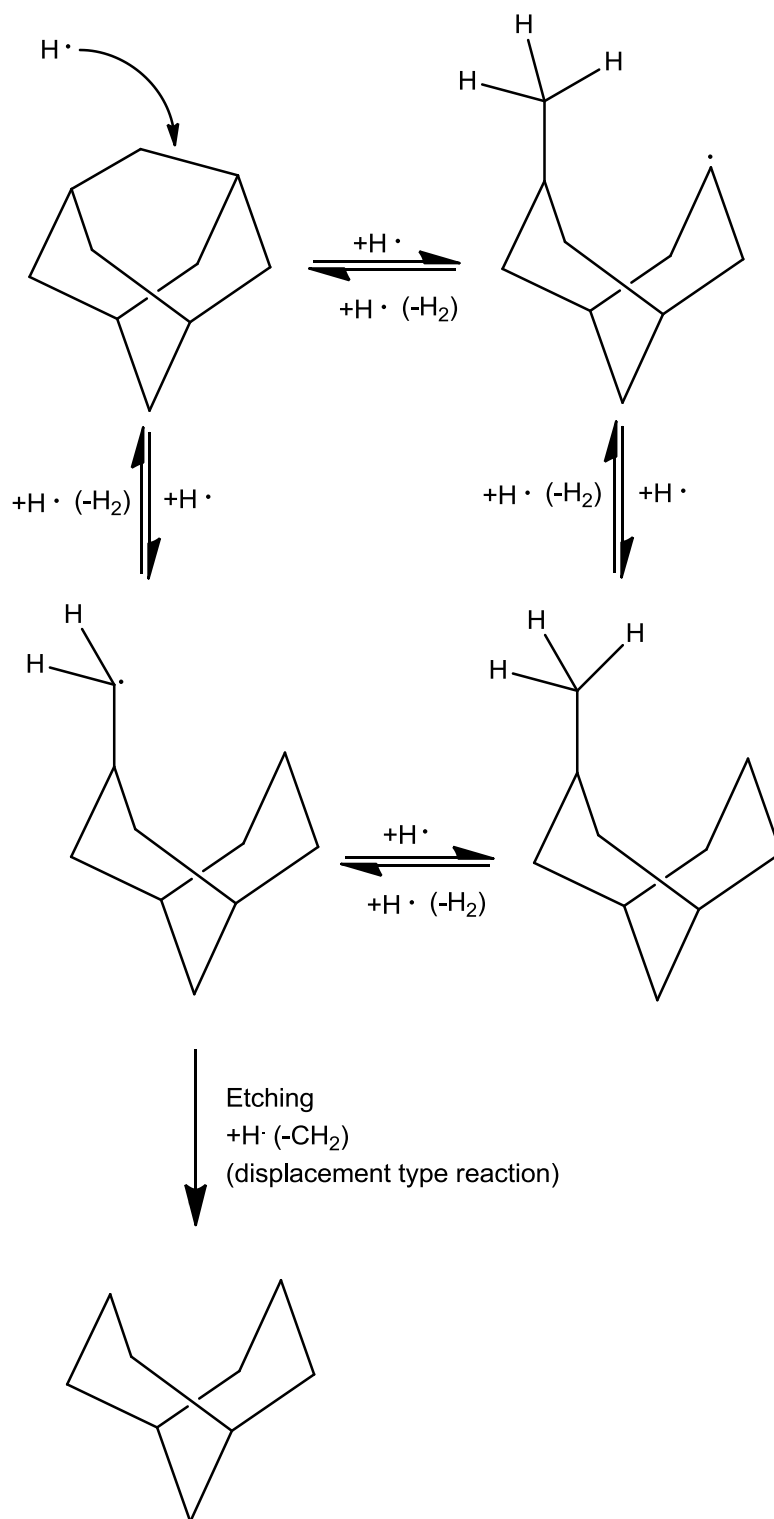


**Figure 5.27:** The mechanism of etching by atomic hydrogen on the diamond surface, showing the regression of diamond growth and the pendant species produce being removed via a radical intermediate. *Figure designed by author.*

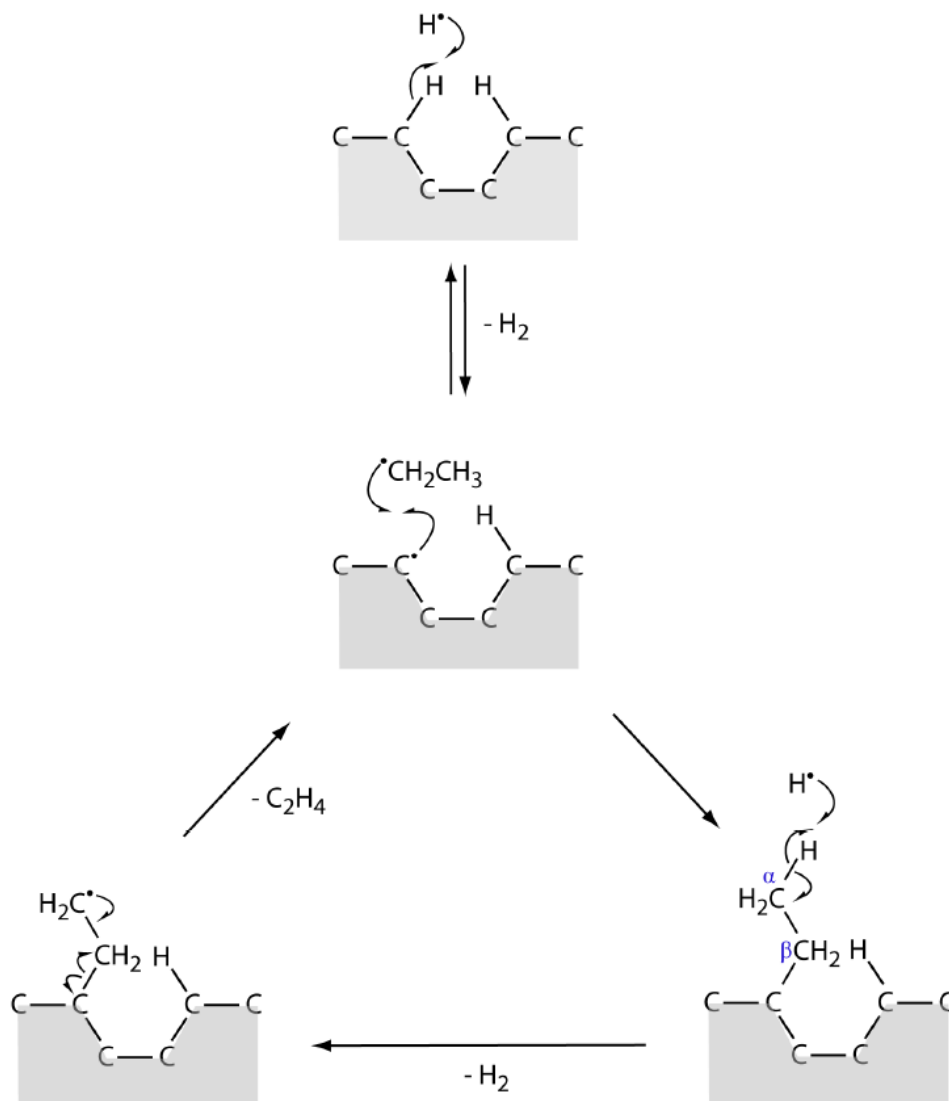


**Figure 5.28:** The mechanism of  $\beta$ -scission [34].

## 5.4 Hydrogen plasma treatment of PCD and manual abrasion

Since hydrogen plasma treatments alone did not seem to be the solution to the problem of producing planar PCD surfaces at reasonable rates and the use of masking materials to prevent the rapid etching of the grain boundaries was not considered as the best option, interest was taken in improving the rate of manual polishing through the use of a hydrogen plasma pre-treatment.

From the previous experiments in this work, it was shown that hydrogen plasma treatments at high temperatures or long durations cause non-diamond materials to form and accumulate on the surface of the PCD sample. Since this material is much 'softer' than diamond, an abrasion technique would be able to remove material from the surface at a much higher rate leading to the production of planar surfaces with much shorter polishing times.

The main advantage in using a treatment such as this is that it can easily be performed at the end of CVD diamond growth, without the need to move the sample to another apparatus or even switch the reactor off. The only action that would need to be taken is to stop the flow of the carbon containing gas into the reactor and adjust the parameters to achieve the desired hydrogen plasma treatment conditions.

The use of pure hydrogen plasma at the end of CVD growth is actually a standard operation procedure for producing high quality of diamond materials [34]. The goal of this exposure to hydrogen plasma at the end of CVD growth is to remove any non-diamond impurities from the surface of the sample. For this reason, performing the same procedure as a pre-treatment to abrasion, rather than a mild cleaning procedure, has no obvious drawbacks. Furthermore, if the diamond material is destined to be polished once it has been grown, there is no need to spend the time cleaning the surface with hydrogen plasma at the end of growth.

This demonstration of the potential for hydrogen plasma treatments as pre-treatments uses a diamond file to manually polish the growth sides of PCD films. As mentioned in a previous chapter, the larger crystal sizes of the growth side of PCD films are more attractive than small crystals since films composed of large crystals exhibit properties more similar to SCD due to a smaller proportion of non-diamond material in the film.

For these experiments, a PCD sample was clamped in a small vice and polished using the diamond impregnated file in the same direction until the surface was optically smooth. An optically smooth surface (at least in this project) was achieved when there were no obvious peaks left on the surface of the diamond when the sample was viewed using a CostMad pocket microscope at 100x optical zoom. The growth side of a PCD sample before and after 30 minutes of manual abrasion using a diamond file can be seen in **Figure 5.29**.

Since the growth side of the PCD sample had not been treated in hydrogen plasma in the previous investigations of this work, a PCD sample was exposed to hydrogen plasma at 1000°C for 20 minutes to observe the effects on the surface. The result of this treatment can be seen in **Figure 5.30** and shows that the surface had become highly graphitised and the grain boundaries had become very deep. When an attempt was made to polish this material using the diamond file, the sample disintegrated under the pressure of the vice. It was clear that this treatment was much too long and has severely diminished the structural integrity of the film, more than observed for the substrate side of the film. This is due to the differences in the structure of the two sides of the film. Due to the larger crystal sizes at the growth surface of the PCD films, the holding of the grains in certain positions by the non-diamond 'glue' at the grain boundaries puts a large amount of strain on the surface on the columnar crystals. At high temperatures it has already been shown that this material becomes removed rapidly and so the grains are able to relax into positions where they are not strained. This leads to the wide grain boundaries observed in **Figure 5.30**. For this reason another PCD sample was treated at 1000°C in hydrogen plasma for 5 minutes. This sample was not etched so intensely and so, did not disintegrate in the vice. This sample was polished using the diamond file in the same manner as the untreated sample.

An optically smooth surface, similar to that of the untreated sample polished for 30 minutes, was achieved on this treated sample after only 15 minutes of polishing using a diamond file, the

final result of the procedure is shown in **Figure 5.31**. This 50% reduction in the polishing time to achieve an optically smooth surface is very significant from an industrial point of view where the use of such techniques would translate into reduced running costs and time demands. Furthermore, the SEM images also seem to reveal that there is less diamond debris produced by polishing after high temperature hydrogen plasma treatment, this could suggest that the polishing after hydrogen plasma treatment was more uniform.

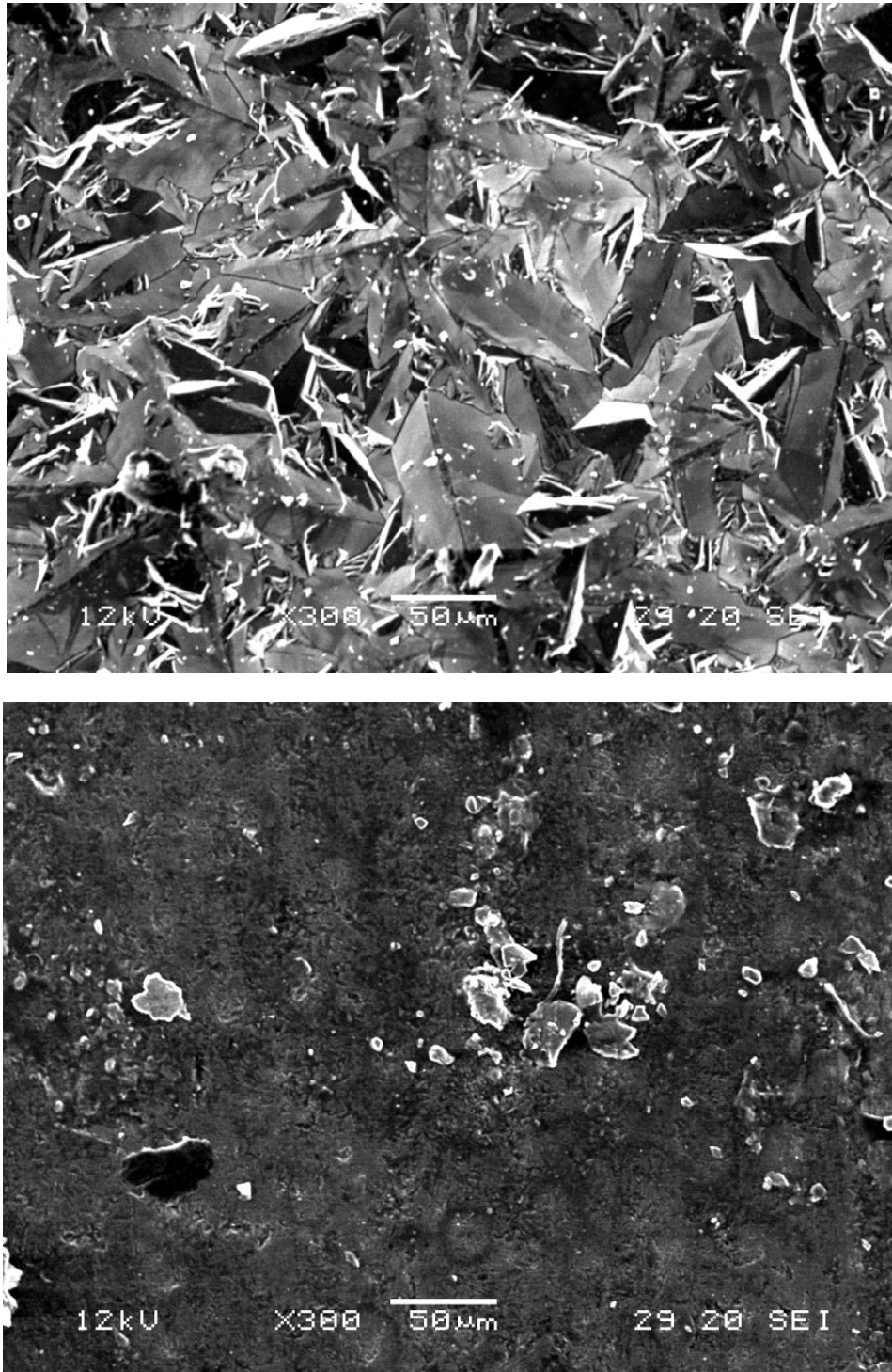


**Figure 5.29:** SEM images of the growth side of PCD diamond samples before treatment (top) and after polishing using a diamond file for 30 minutes (bottom).

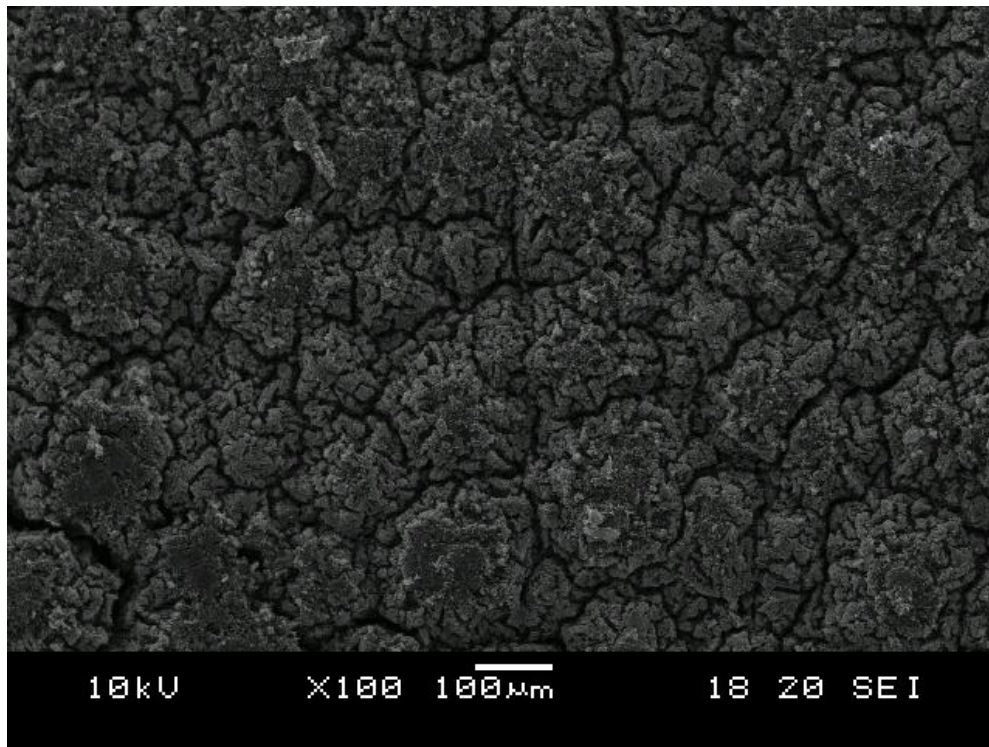


**Figure 5.30:** An SEM image of the growth side of a PCD film exposed to hydrogen plasma at 1000°C for 20 minutes.

As an indication of the reduction in the surface roughness which had been achieved using the combination of a short plasma treatment and manual abrasion of the diamond surface, this sample was analysed using AFM and was shown to have a mean RMS surface roughness of 145 nm. As described at the start of this chapter, the growth side of thick PCD films cannot normally be studied using AFM because the crystals on the surface are simply too large for the instrument to measure. Therefore, being able to produce an image such as that shown in **Figure 5.32**, highlights how effective hydrogen plasma treatments are as a pre-treatment to polishing of the diamond surface using conventional lapping techniques. Furthermore, it is predicted that performing the same procedure on larger scales would also yield significant improvements in the polishing time required to make the films more planar.

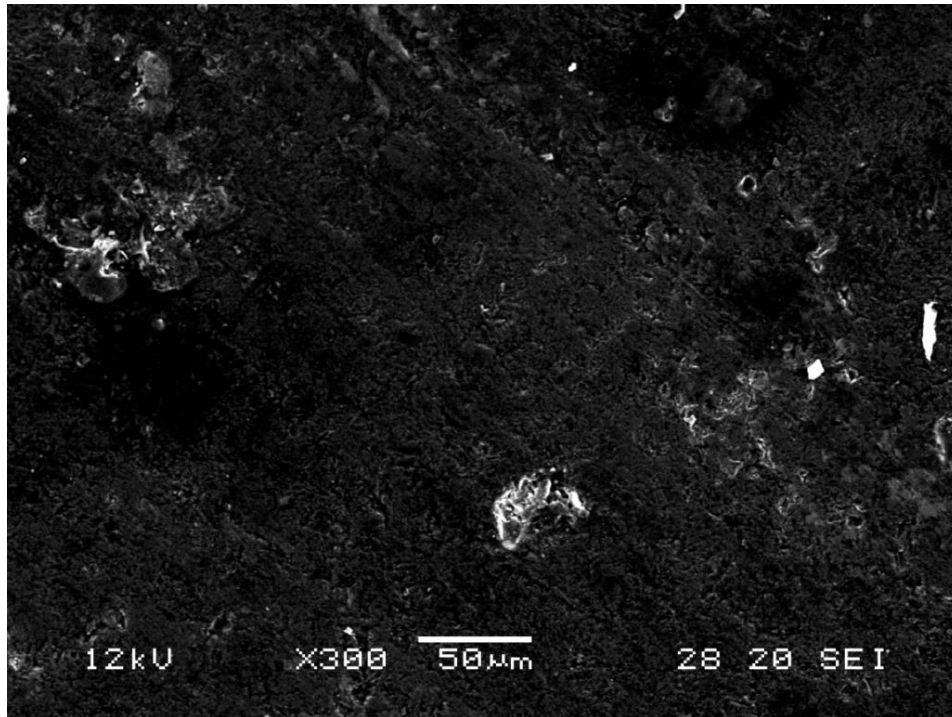


**Figure 5.31:** An SEM image of the growth side of a PCD film following graphitisation in hydrogen plasma at 1000°C for 5 minutes and manual polishing using a diamond file for 10 minutes.

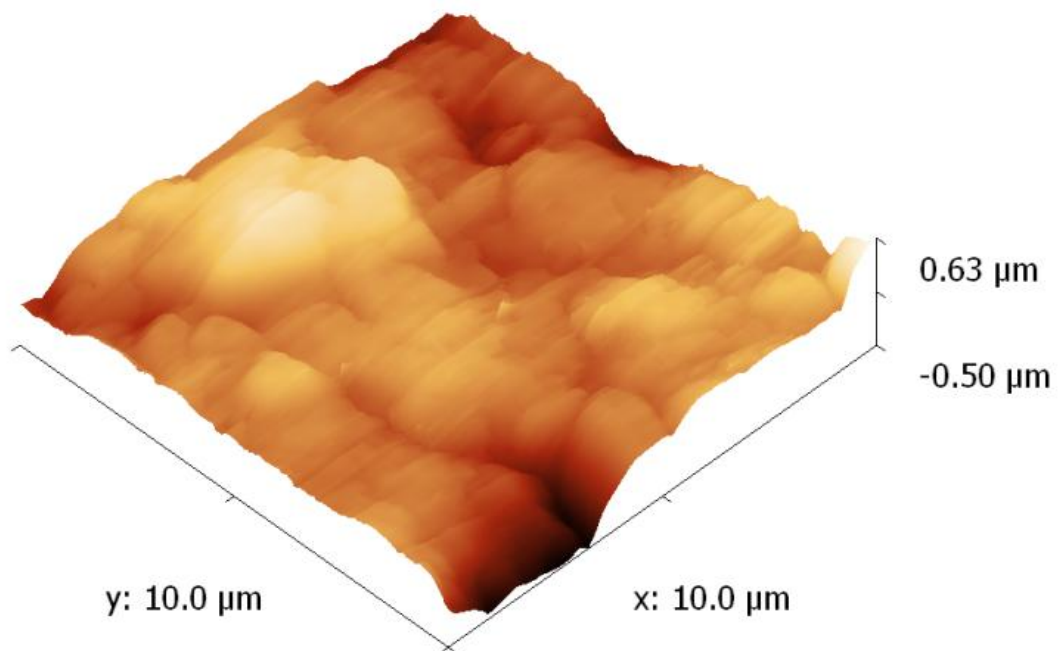


**Figure 5.32:** A 3D-AFM projection of the growth side of the PCD sample following manual polishing for 30 minutes using a diamond file.

In addition to use as a pre-treatment, hydrogen plasmas could also be used to treat the polished PCD surfaces. This was not performed in this work, but is expected to produce similar results to the treatments of the substrate side of PCD films which have already been described in this

work, where the etching of grain boundaries leads to significant roughening of the surface, along with rounding of the grains and some smoothing of the crystal facets.

## 5.5 LPSSS-style treatments

Before the LPSSS-style treatments of the metal coated samples were performed, it seemed clear that different temperature treatments would be required for each of the different metals being used, owing to their different standard melting points and the apparent requirement of LPSSS for a molten metal phase. Unfortunately, Roy et al did not report any specific information about LPSSS treatments using different metals and instead chose to present a temperature range into which all of the experiments fitted. This temperature range was reported to be 750-1100°C [50].

A further factor to be considered before the treatments could be performed was that the pressure during the treatments is significantly lower than standard pressure (760 Torr) and so the melting points of the metals may be lower than their standard melting points. The effect of pressure on the melting point of a pure substance is well depicted by the solid-vapour phase boundary seen phase diagrams, and the principles behind phase transitions can be found in many fundamental physical chemistry textbooks [3]. This meant that phase diagrams of the pure metals used in this investigation needed to be obtained in order to estimate the melting point of the metal under the experimental conditions.

Unfortunately, finding phase diagrams of the pure metals proved to be very difficult since modern metallurgy is primarily concerned with binary phases where more than one element is present in the material leading to alloys with very different properties to either of the pure substances [51]. Only the phase diagram for pure iron was found and this is shown in **Figure 5.33**.

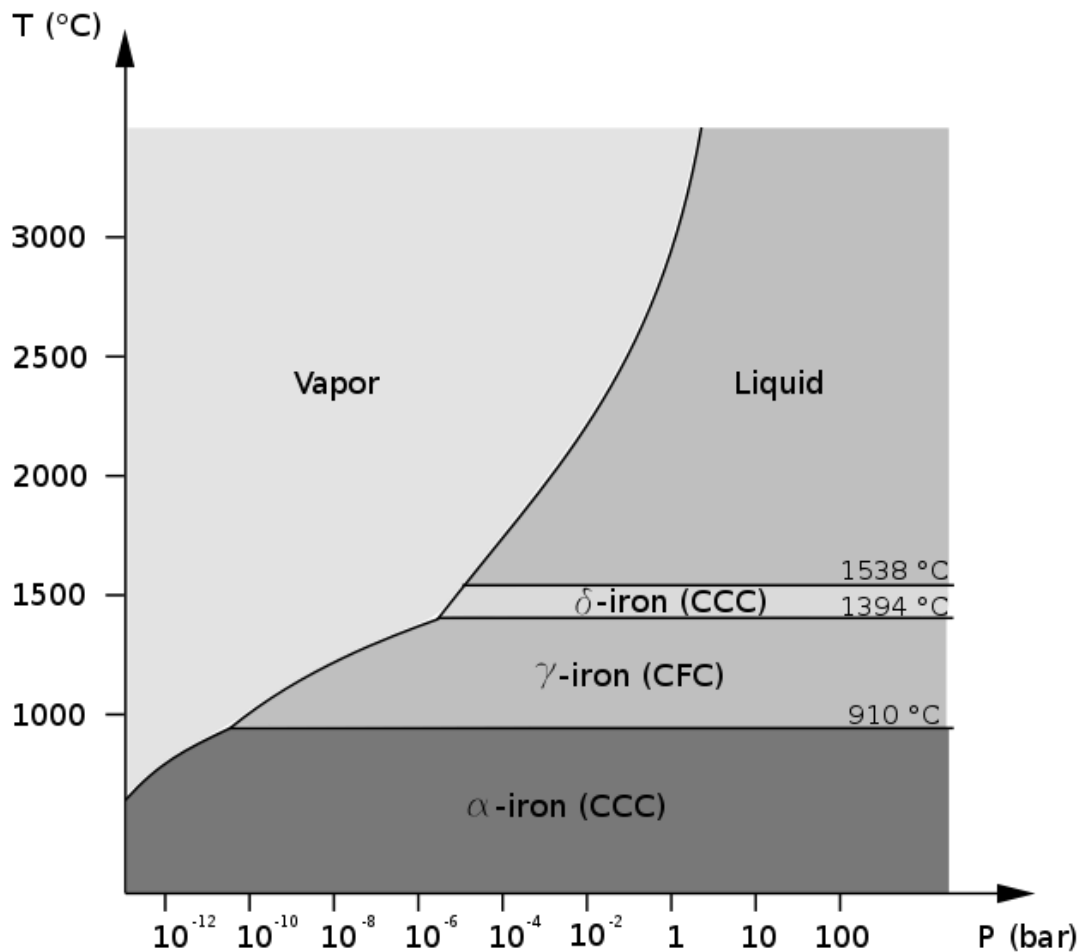


**Figure 5.33:** The phase diagram of pure iron. *Figure was adapted from [52].*

100 Torr is equivalent to 0.13 bar and so from **Figure 5.33** it is clear that the experimental pressures are well within the region where iron undergoes a melting transition (i.e. does not sublime). Furthermore, since the solid-liquid boundary appears to be horizontal, the melting point of iron in these experiments can be assumed to be the same as the standard melting point of the material. This assumption was extended to include the other transition metals used in this investigation.

As a way of confirming that these assumptions were reasonable the melting transition for each metal was considered using a thermodynamic approximation of the solid-liquid boundary of a phase diagram for a pure substance. The derivation of this approximation can be found in Atkins' Physical Chemistry [3] and where it is shown that two points on the solid-liquid boundary are approximately related by

$$p_2 \approx p_1 + \frac{\Delta_{fus}H}{T_1 \Delta_{fus}V} (T_2 - T_1)$$

where  $p_1$  and  $T_1$  are the pressure and temperature respectively at 'point 1' on the phase boundary,  $p_2$  and  $T_2$  are the pressure and temperature respectively at 'point 2',  $\Delta_{fus}H$  is the

enthalpy of fusion for the substance and  $\Delta_{fus}V$  is the change in molar volume when melting occurs. This equation can then be rearranged in a number of steps to give

$$T_1 \approx \frac{\Delta_{fus}HT_2}{(\Delta_{fus}V(p_2 - p_1) + \Delta_{fus}H)}$$

which could then be used to estimate the melting temperature of the metals at 100 Torr if  $\Delta_{fus}H$  and  $\Delta_{fus}V$  were deduced.

For these approximations it was assumed that  $\Delta_{fus}V$  would be approximately the same at 100 Torr as at 760 Torr since the metal structure is very tightly packed and is not expected to expand greatly with reduced pressure. Furthermore, it was assumed that  $\Delta_{fus}H$  was the same for both sets of conditions. The results of these calculations can be seen in **Table 5.1**, and confirms that the metals should melt at their standard melting points under the experimental conditions.

**Table 5.1:** Shows the standard melting points of the metals used in this investigation alongside the predicted melting points under the experimental conditions.

Metal	Standard melting point / °C (from ref [53])	Predicted melting point at 100 Torr / °C
Ag	961	961
Cu	1084	1084
Fe	1536	1536
Ti	1670	1670

For this reason, the decision was made to treat the SAM samples at 750°C (the lowest temperature in the range reported in the literature) for 1 hour (the shortest treatment duration reported). In this first series of treatments, the power had to be increased throughout the treatment to maintain the desired treatment temperature and this resulted in the maximum possible microwave power of the reactor being used (1.5 kW). Since the treatment conditions could not be adjusted any further, the samples were left to be treated in the hydrogen plasma for the remainder of the hour. At the end of these treatments, the sample temperatures were found to be in the range of 650-690°C.

This reduction in the sample temperature indicated that the metals were evaporating from the sample surfaces during the treatment. When these samples were removed from the reactor, it was obvious that the metal films had been removed from the surface. This removal of the metals from the surfaces of the samples could be explained by two processes: the evaporation of metal species from a liquid phase or etching of the metals by atomic hydrogen. At first glance, etching by atomic hydrogen seemed to be the most likely explanation since it had already been shown that the metals were not expected to melt under the experimental conditions. This etching of metals by atomic hydrogen has been reported previously in the literature during experiments using metals as masks for reactive ion etching [29,54].

Analysis of the treated samples by SEM reveals some very interesting results and this discussion will begin with the silver coated SAM sample, which showed that the majority of both the metal and diamond layers were removed during the treatment in hydrogen plasma. This result confirmed that the hydrogen plasma conditions used were too extreme and had etched most of the material from the surface. Towards the edge of the sample however, it is possible to see that a small proportion of the diamond was still present on the surface as well as small areas of silver (Figure 5.34). The possibility that the hydrogen plasma was etching material from the surface at high power seemed to be the most plausible explanation of the experimental result since no evidence of a liquid phase could be seen on the sample. Furthermore, in previous investigations in this project, it was shown that diamond crystals in PCD films could be etched significantly by hydrogen plasmas, possibly due to ion bombardment of the sample with hydrogen species.

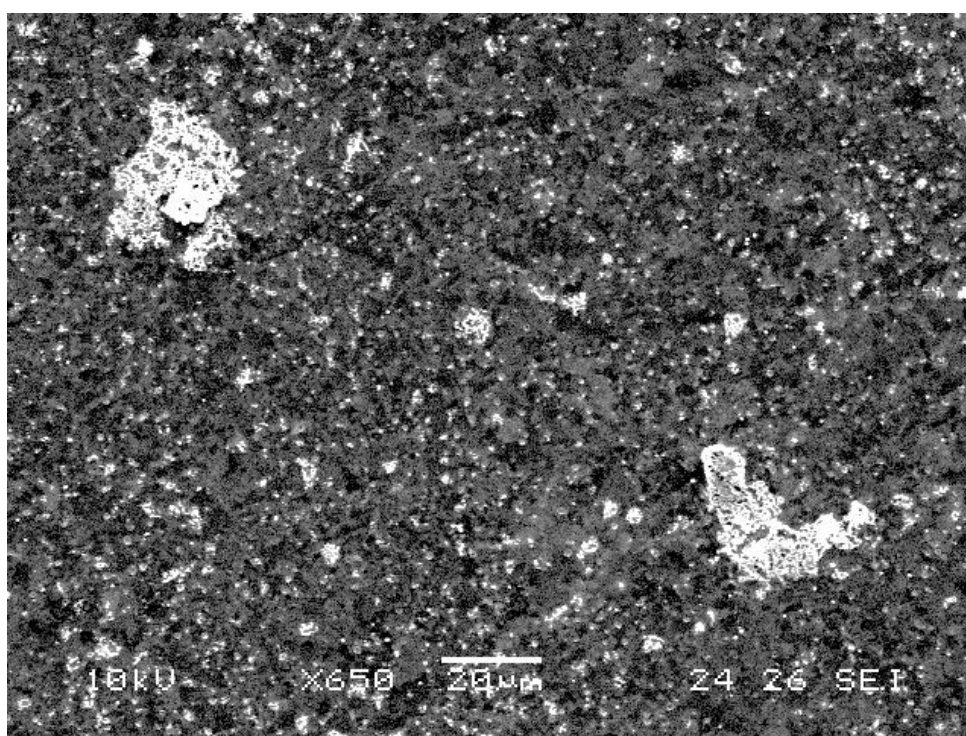


**Figure 5.34:** SEM of the silver coated SAM sample treated in hydrogen plasma at 1.5 kW for 1 hour shows that the majority of the diamond and metal layers had been removed from the surface. This image was taken at the edge of the sample and shows that only small patches of silver and very few diamond particles have remained on the surface. To clarify, the white dots are the diamond nanoparticles which have been hydrogen terminated during the treatment and thus appear very bright in SEM.

The conclusion that some of the diamond crystals were etched from the substrate can be dismissed by looking at the copper coated sample which shows that the entire diamond layers remains on the surface following treatment (Figure 5.35). This indicates that the SAM of diamond in the silver sample had not been annealed properly to ensure the crystals adhere strongly to the substrate. This meant that the treatment provided sufficient thermal energy to cause the attraction between the colloid residues and diamond particles to break and so, large

amounts of the diamond material will most likely have simply fallen off of the surface when the sample was transferred to a glass vial at the end of treatment. In addition to showing that the diamond layer remains on the surface when properly annealed, **Figure 5.35** shows that small metallic globules of Cu were formed on the surface of the sample.

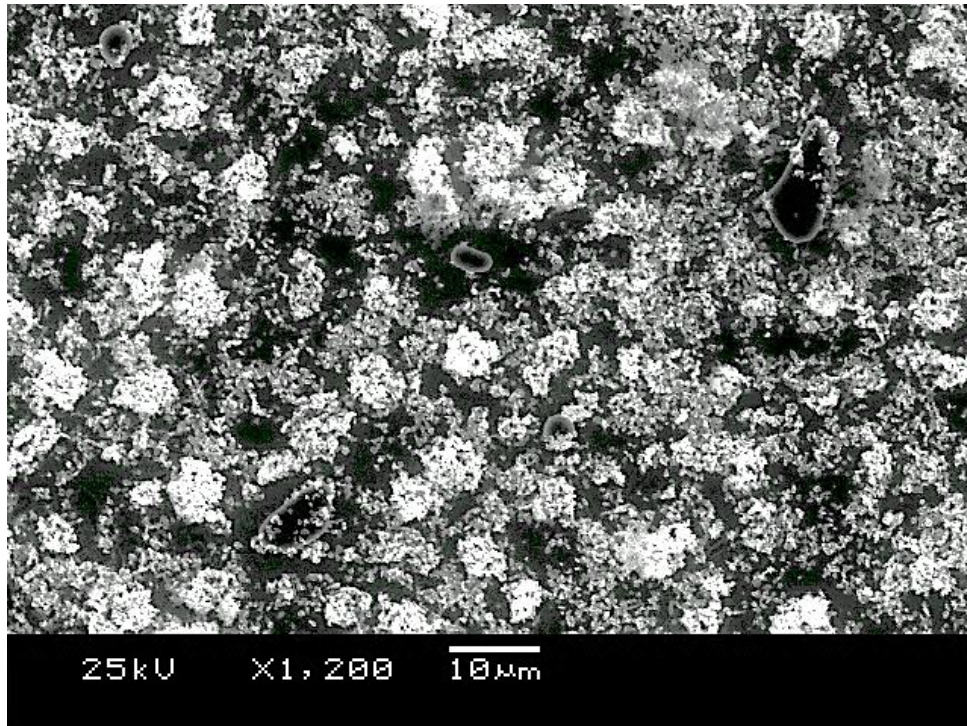


**Figure 5.35:** SEM of the silver coated sample treated in hydrogen plasma at 1.5 kW for 1 hour indicates that the diamond layers are not removed if they are properly annealed and also shows metallic globule on the sample.

SEM of the iron coated sample (**Figure 5.36**) shows that the diamond layer had again not been properly annealed and so the majority of the diamond particles had fallen from the substrate when the sample was moved. However, it was also evident that the iron had produced an increased number of larger globules than seen on the surface of the copper coated sample and it was noted that these iron globules appear to have a significant number of diamond particles on their surfaces.

SEM of the titanium coated sample again confirms that the diamond layer is not removed by the treatment when properly annealed. In addition to this, number and size of the globules produced on the Ti surface were the largest of all the samples, as shown in **Figure 5.37**. Furthermore, it is also clear that the Ti globules have absorbed more diamond nanoparticles onto their surfaces than those found on the Fe-coated sample.

From this first series of treatments vacuum annealing of the diamond layer onto the substrate has been shown to be a very important factor in the preparation of diamond nanoparticles for use in technological applications. To check that the other samples were suitably annealed, a small piece of Mo wire was used to scratch a small section of the surfaces. If a sample was found to scratch easily, it was not used for in further investigations.

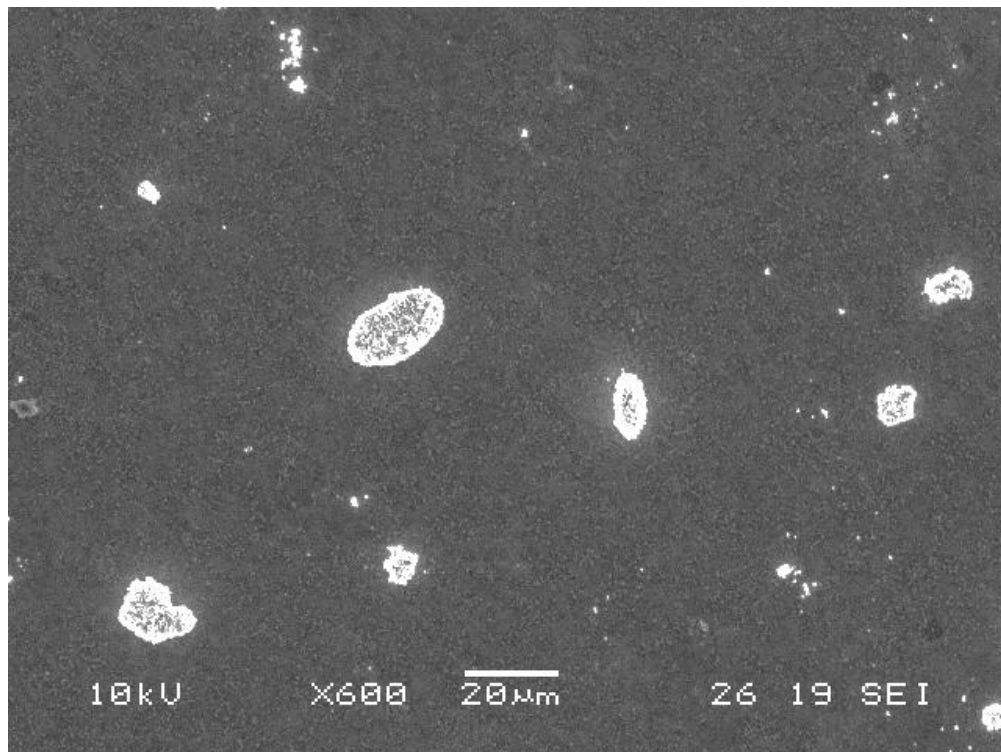


**Figure 5.36:** SEM of the iron coated SAM sample treated in hydrogen plasma at 1.5 kW for 1 hour reveals metallic globules on the surface of the sample. These metallic globules are also covered with diamond particles, whilst the most of the diamond layer appears to have been removed during the treatment due to insufficient annealing, as seen for the silver coated sample.

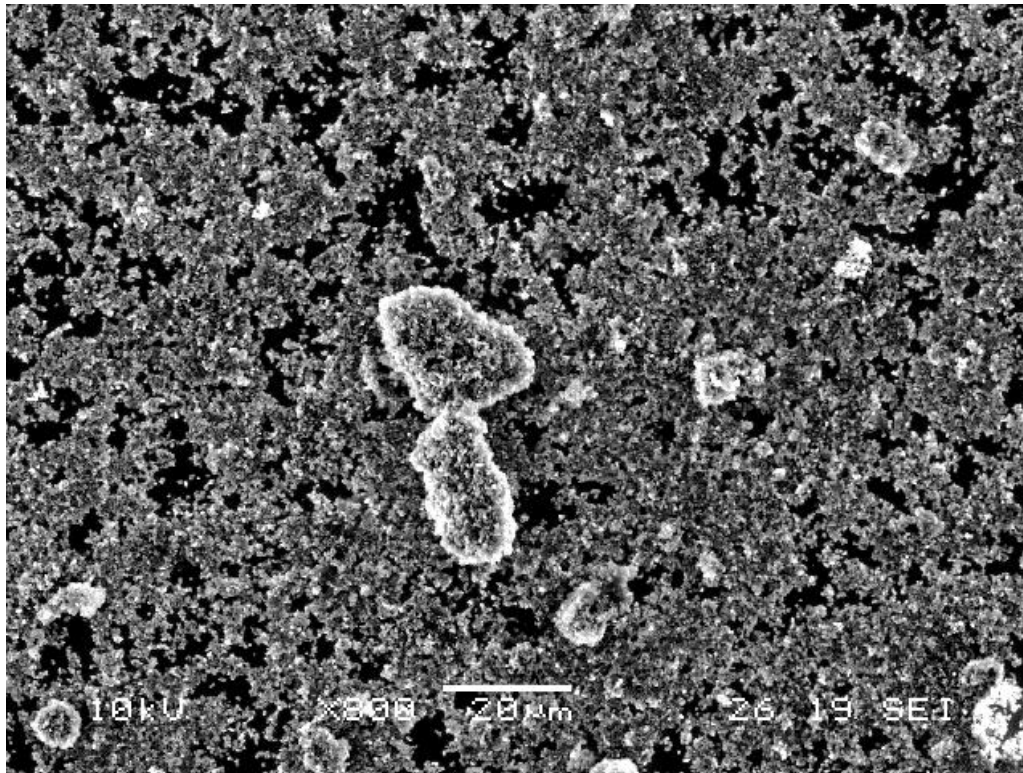


**Figure 5.37:** SEM of the titanium coated SAM sample treated in hydrogen plasma at 1.5 kW for 1 hour showing the layer of diamond nanoparticles remained adhered to the surface during the treatment. Large metallic globules coated with diamond particles can also be seen.

The production of metallic globules from the metal coatings under the influence of hydrogen plasma in these experiments correlates well with the observations of metallic globules associated with the diamond in the LPSSS process [55]. It can also be noted that the globule size is proportional to the melting points of the metals used in the investigation, increasing in the order Cu-Fe-Ti. Furthermore, it should be noticed that the globules produced by the treatment have dimensions larger than 50 nm, which was the original thickness of the metal coating.

To form globules such as this, smaller globules produced by the action of the hydrogen plasma on the metal film must be undergoing coalescence. This is where two bodies of the same phase come together to form a single phase [56]. The non spherical shape of the globules produced by the treatments provides support for this idea of coalescence.

The density of diamond nanoparticles adsorbed onto the surfaces of the metallic globules observed seems to give an indication of each metals affinity for carbon, increasing in the order Cu-Fe-Ti. The relative affinity for carbon of silver could not be commented on, since the majority of the silver was removed from the surface of the sample. However, since the trend shown by the other metals seems to correlate well with the experimental observations on the affinity of the metals for carbon, it can be predicted that silver globules would have the least diamond crystals adsorbed on the surface.

From these studies it was clear that the metal was being removed far too quickly from the surface for its effect to be observed. This can be deduced by the fact that all of the diamond crystals observed appear to be very bright under SEM, indicating that they have been hydrogen

terminated and possess NEA as would be expected following standard hydrogen plasma treatment.

Repeating the treatment of a silver coated SAM sample at the lowest possible microwave power which could sustain a plasma under the experimental conditions (0.6 kW) for 15 minutes was shown to produce globules on the surface of the sample. This is shown in **Figure 5.38** and as predicted there are very few crystals adsorbed onto the surface of the globules.

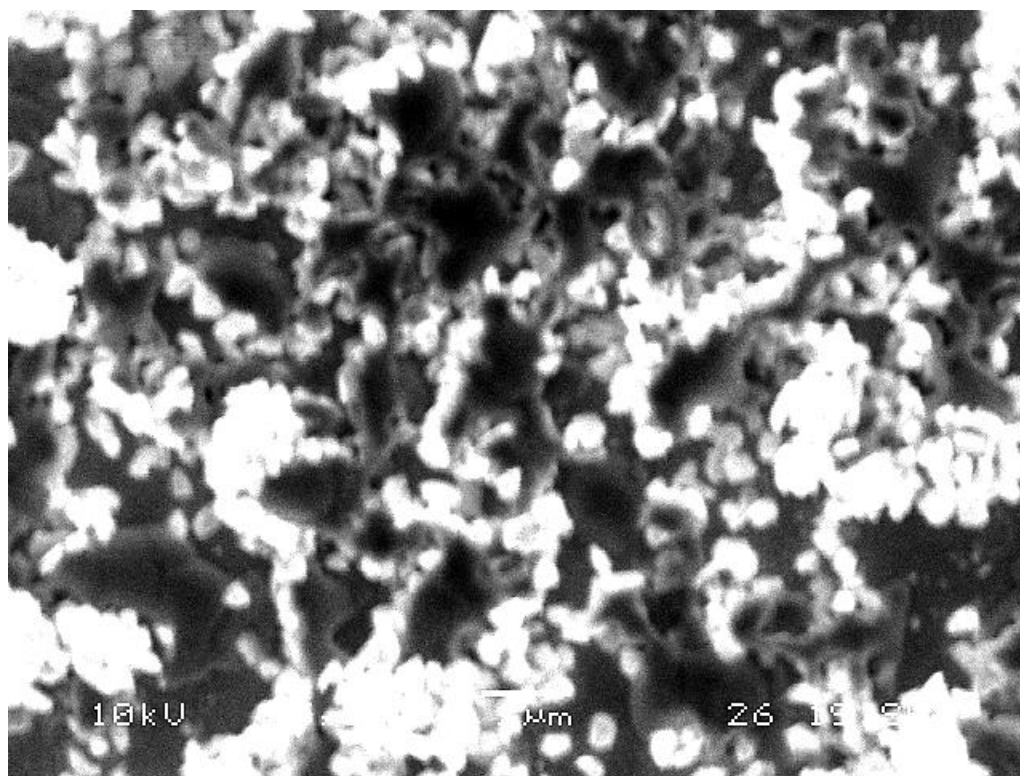


**Figure 5.38:** An SEM image of a silver coated SAM sample following hydrogen plasma treatment.

Similar experiments were repeated for the other metals and it was noted that the proportion of metal remaining on the surface after the 15 minute treatments increased in the order Ag-Cu-Fe-Ti, in the same way as the globule sizes in the first set of experiments. This is illustrated by a copper coated sample treated at 0.6 kW for 15 minutes which was found to have formed snakelike metallic globules on the surface (**Figure 5.39**).

Now that the proportion of metal left on the surfaces of the samples was substantial, it would have been interesting to observe the surfaces of the diamond crystals in the SAM. Unfortunately, the morphology of these surfaces could not be observed at high enough resolution using the microscope used for this investigation. Logically AFM would be the next best technique to use, but, since the metallic globules were rather large AFM could not be used. As already mentioned many of the diamond crystals appear to be very bright under SEM due to the termination of the surface with hydrogen atoms.

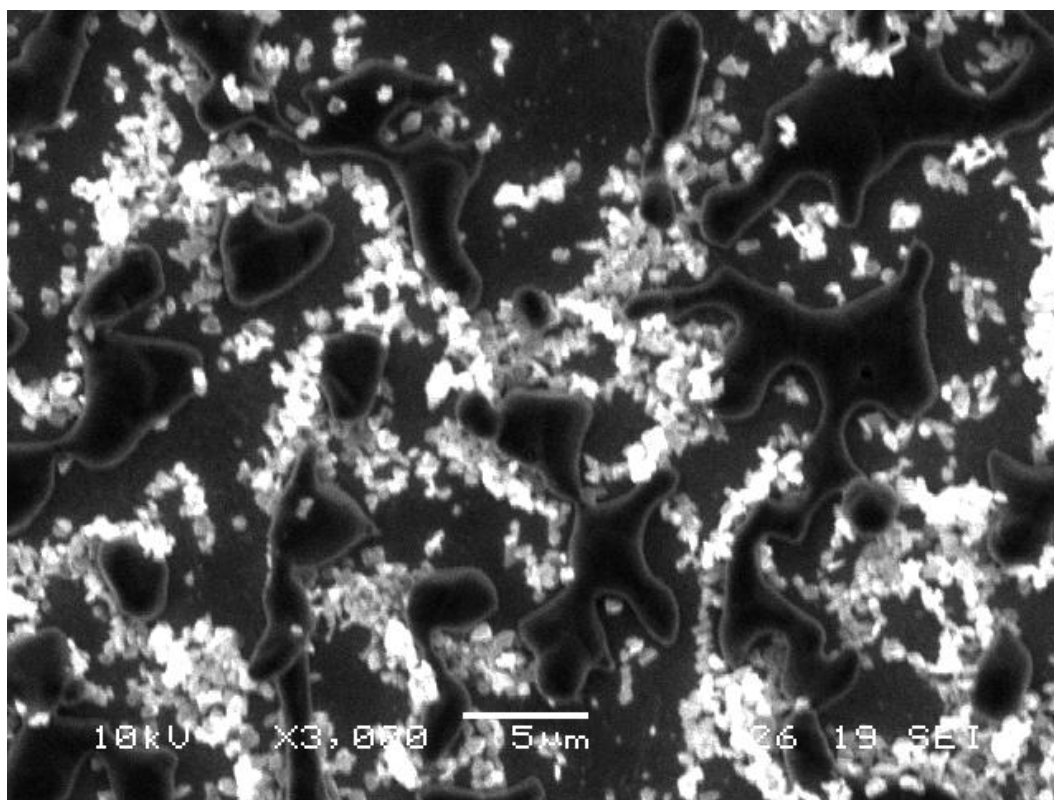


**Figure 5.39:** An SEM image of a copper coated SAM sample following hydrogen plasma treatment.

Since the state of the diamond surfaces could not be investigated for the small diamond crystals of the SAM samples, the removal of the metal from the surface of the samples was investigated. For this investigation, a Ti coated SAM sample was used. The reason for this is that Titanium appears to be removed most slowly of the metals used in this investigation. In this part of the investigation, OES was used to see if any emissions from metallic species could be observed in the plasma during the treatment and also indicate the point at which the highest removal rate of metal atoms from the surface occurs.

When using a MW CVD reactor, the plasma needs to be formed before the experimental parameters can be set to the desired conditions [34]. The general procedure for striking a plasma using this reactor is to increase the microwave power rapidly when the chamber is filled with hydrogen at a pressure of ~20 Torr [34]. Once the plasma has been struck, it has a large diameter such that the plasma contacts the fused-silica window and side walls of the chamber. At this point the pressure needs to be increased quickly to control the plasma and prevent it from etching material from the divider window or walls of the reactor.

Optical emission spectra taken when the plasma has just lit indicate the presence of species other than atomic hydrogen in the plasma (**Figure 5.40**). The intensity of emission from this non-hydrogen species decreased in subsequent spectra as the treatment parameters were being set, leading to an emission spectrum of pure hydrogen plasma, with a large  $H_{\alpha}$  peak and no other obvious features.

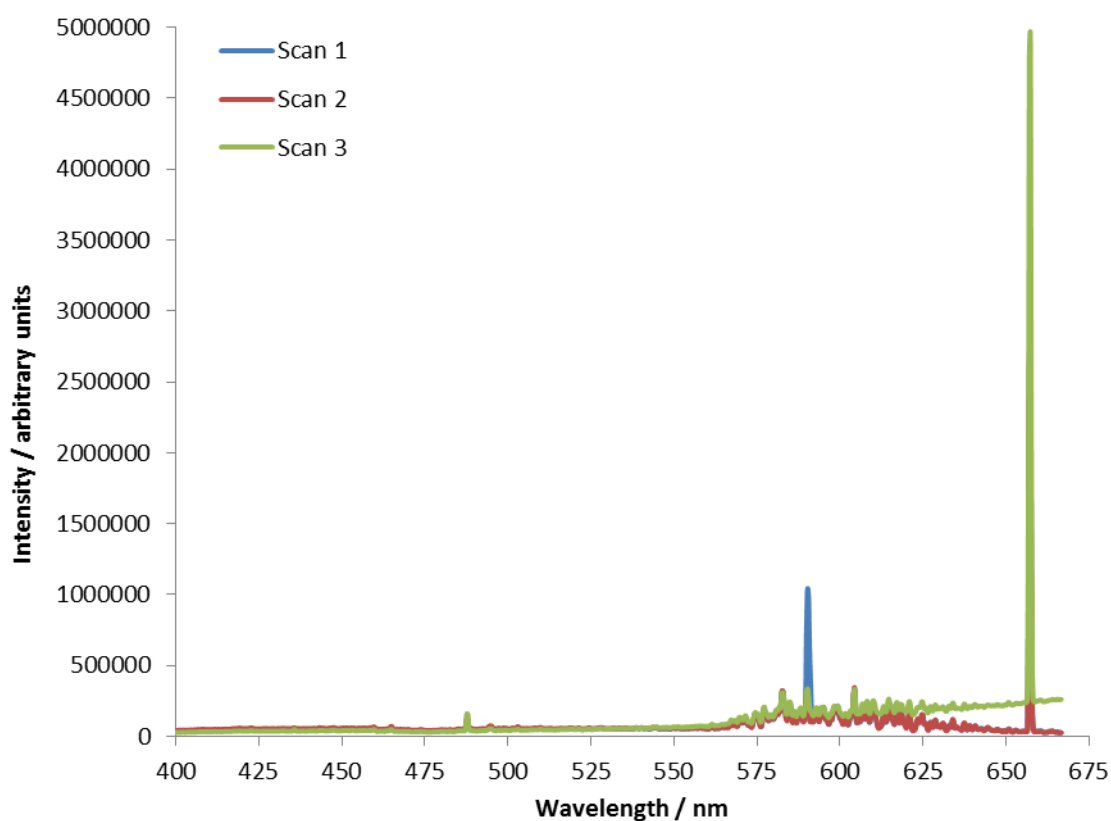


**Figure 5.40:** OES of the hydrogen plasma used to treat a titanium coated SAM sample at ignition of the plasma (scan 1), after the first scan had finished (scan 2) and once experimental conditions had been reached (scan 3).

Attempts were made to find the cause of this foreign peak in the OES spectrum but it was not possible to find a transition related to Ti which could account for the transition. At present the  $3^3D \rightarrow 2^3P$  transition of He seems to be the most likely candidate for the foreign emission since it matches the wavelength of the emission at 587 nm [57]. However, the source of this He is not known.

This experiment was terminated once the experimental conditions had been reached and it was evident that there was still a great deal of metal on the surface of the sample, some of which had become tarnished. Looking at this sample using SEM reveals a significant result: some of the metal with the highest melting point of the metals used in the investigation has been removed from the surface of the sample in some locations. This can be seen in **Figure 5.41**.

In addition to some of the diamond being exposed by the hydrogen plasma, some regions of the metal coating appear to be much thinner (showing the shape of the diamond crystals more prominently) and very small cracks can also be seen to have formed in the metal coating during the exposure period. These thin cracks are characteristic of a metallurgical phenomenon known as hydrogen embrittlement [58], which has been shown to be the cause of metallic component failures in a number of different situations [59,60].

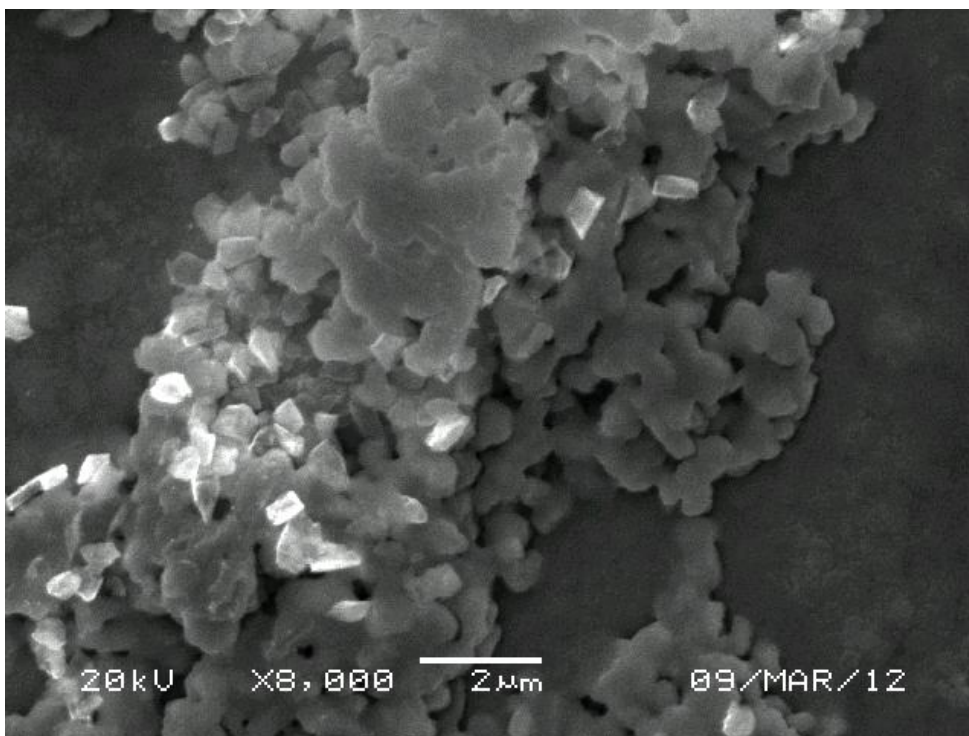


**Figure 5.41:** SEM of the titanium coated sample which was removed from the reactor shortly after the experimental conditions had been set reveals that some of the metal had been removed from the surface of the sample before the treatment had been properly started.

Hydrogen embrittlement is known to occur in environments where there is a high abundance of hydrogen and is thought to occur when hydrogen molecules adsorb onto the surface of a metal resulting in the formation of surface hydride species [58]. Adsorption of hydrogen onto a metal surface in this way forms the basis of the reduction of alkynes to cis-alkenes using Lindlar's catalyst in organic chemistry [61]. The atomic hydrogen associated with the surface can then diffuse into and migrate through the metal via the vacancies in the material [58]. If two hydrogen atoms collide in an interstitial site in the metallic structure the molecule formed will exert pressure on the metal atoms. As progressively more and more hydrogen builds up at such sites, defects such as cracks begin to form [58].

In the case of the hydrogen plasmas used in these experiments, the hydrogen is already in an atomic form when it reaches the surface. This means that the adsorption of the hydrogen molecule and subsequent breaking of the bond do not need to occur and atomic hydrogen can diffuse into the metal much more rapidly. Furthermore, the amount of atomic hydrogen in the plasma is extremely high and so a significant amount of atomic hydrogen can be incorporated into the metal very quickly. Under the reduced pressure used for these LPSSS-style treatments, the packing of the metal will be slightly less dense than it normally would be under standard conditions and so, the interstitial spaces through which the atomic hydrogen can diffuse in a Brownian motion will be larger. This leads to less frequent collisions between the metal atoms and hydrogen atoms, ultimately leading to an increase in the rate of atomic hydrogen diffusion through the material. This increases the likelihood of hydrogen molecules forming in interstitial sites within the metal to cause cracking.

Despite hydrogen embrittlement being evident on the surface of the sample in the form of small cracks, the phenomenon does not explain some regions on the surface became completely free of metal during a very short treatment. This must be due to the way in which the film is deposited onto the surface of the sample. The metal coatings are polycrystalline and inevitably there will be some regions which are coated slightly more thickly than others. Since the metal film is polycrystalline, the coating will have a significant number of grain boundaries. As shown for diamond, the edges of the metal crystals present at the grain boundaries will be etched by the atomic hydrogen. This seems reasonable since the metals used have much lower rankings on the Moh scale of hardness than diamond [62].

These processes of cracking and etching of the metal coating could quickly lead to isolated metal particles being produced on the surface of the sample. Since the film is only tens of nanometres thick, these metal particles will be nanoparticles. This is a significant realisation since it is well known that materials behave differently on the nanoscale to how they do in the bulk material [63].

The coalescence of the metallic globules on the surfaces of the samples observed in this investigation can only occur if molten globules are able to migrate across the surface [64]. The process of forming a larger globule reduces the surface energy of the particles [64]. Furthermore, these molten metal phases in this project have been shown to be forming hundreds of degrees below the standard melting point of the metal. This supports the idea that exotic nanoscale phenomena may be at work.

Previous work in the literature supports the results of this investigation and has shown that a film of nickel can be converted into nanoparticles which coalesce together to form larger particles under the influence of hydrogen plasma and thermal treatment [65]. Metal nanoparticles are currently widely used in the field of carbon nanotube growth [66,67] and their production by hydrogen plasmas has not yet been associated with the LPSSS process.

The mechanism of nanoparticle formation and globule coalescence from thin metal films has been described previously in reference [65] where the etching of the metal forms particles which decrease in size with further etching to form nanoparticles. Nanoparticles are known to experience melting point depression and there are a number of models for the process [68,69]. Despite being slightly different, these models are all based on the same principle that as the dimensions of the material are reduced the melting point decreases due to a reduction in the cohesive energy of atoms at the surface of the particle [70]. Once molten, these globules can move across the surface under the influence of thermal energy from the plasma and coalesce to form the large globules [65], as observed in this project. This effect of melting point depression due to the small size of the metal particles may be enhanced further by the interaction of metal atoms at the surface with hydrogen species. Electron donation from the metal atoms to hydrogen atoms to form hydrides will decrease the electron density contributing to the metal-metal bonding and so the bonding will be weaker. This may lead to further reductions in the melting point.

Now that the globule formation and removal of the metal films from the surface of the samples had been explained, the investigation was extended to using metal coated MCD samples. Due to the larger crystal size in these samples, it was expected that the effects of the metal on the

surface would be more easily observed by SEM. Furthermore, since the aim was to investigate the effect of the metal and the samples only 2 x2 mm<sup>2</sup>, thicker metal coatings were used to prevent rapid etching from the surface. Copper, iron and titanium coated MCD samples were treated in hydrogen plasma at 0.6 kW for 15 minutes and revealed that the different metals do in fact behave quite differently to one another.

In the Cu coated sample it was noted that the majority of the metal seemed to have been removed following the exposure to the hydrogen plasma, and the surface of the sample appeared to have a slight reddish tint. Analysis of this sample using SEM reveals that there is still copper on the surface of the diamond crystals, in the form of spherical particles. This can be seen in **Figure 5.42**.

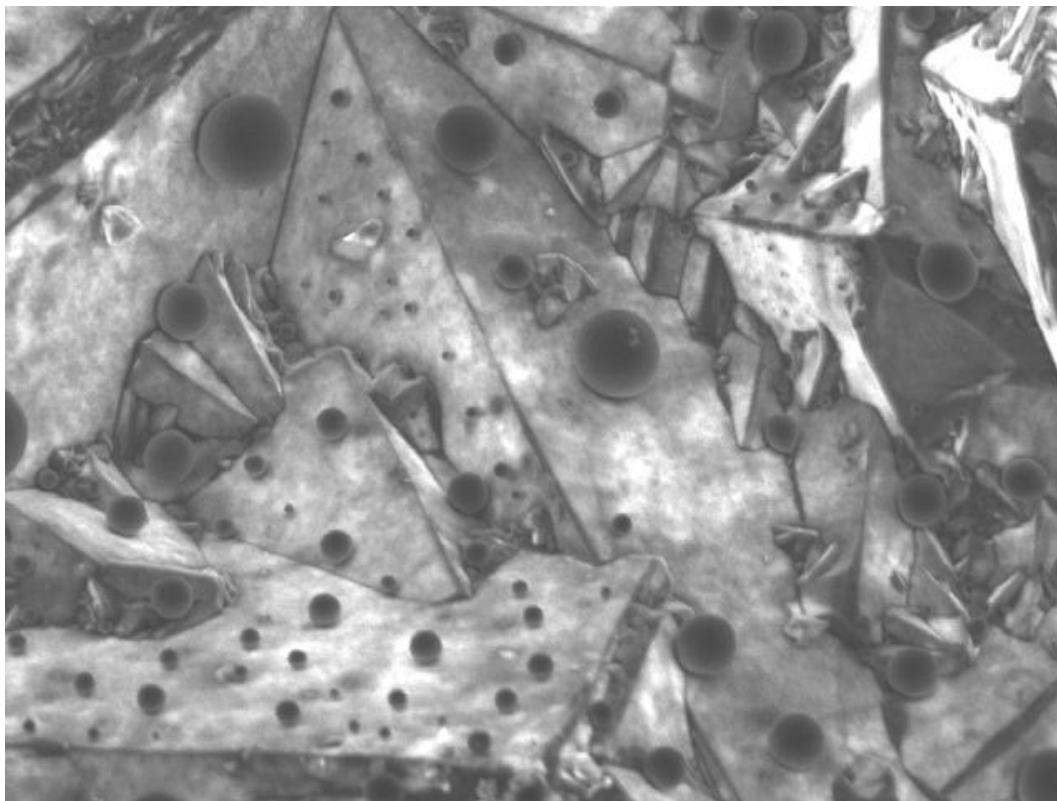


**Figure 5.42:** SEM image of a copper coated MCD sample treated in hydrogen plasma for 15 minutes at 0.6 kW, 100 Torr and 100 sccm.

From **Figure 5.42**, it is clear that there is a wide range of differently sized metal particles on the surface of the sample following hydrogen plasma treatment. This image suggests that the particle size may be dependent on the crystal orientation, since different facets seem to only be able to hold particles up to a certain sizes. This is rather odd since the surface is mainly {111} faceted, so the affinity for the metal should be the same on all faces. This suggests that the same may not have been completely flat on the substrate holder during treatment. However, this may warrant further investigation.

Perhaps the most logical explanation of the size distribution of the particles is related to the composition of the film prior to treatment. As already described, the metal coating is not a continuous single crystal and is polycrystalline. Within this polycrystalline film there are grains of

different sizes, with the largest grains being present at sites where the metal first deposited onto the surface. Since the coating is copper only, the etching by the hydrogen plasma at the grain boundaries will have occurred at the same rate over the sample surface. Therefore, larger grains will result in larger particles being formed whilst areas composed of many very small crystals will have been etched away to leave the diamond surface exposed.

In **Figure 5.42**, it is also clear that the metal particles did not melt leading coalescence. This is due to the metal particles being up to 5  $\mu\text{m}$  in size, rather than nanoscale as observed for the thinly coated diamond SAM samples. This can be largely attributed to the use of a thicker metal coating for this investigation.

In contrast to the copper coated sample, the iron coated sample did not show any obvious signs of the metal being present on the surface following treatment. As can be seen in **Figure 5.43**, no obvious metal particles could be seen on the surface of the diamond and it is very clear that the surface has been etched considerably by the metal, with small islands of the original diamond surface being left on the surface of the sample. These regions are very bright due to hydrogen termination. This etching of the diamond surface by metals has been reported previously [26] and is thought to be due to unpaired d-electrons in the metal [71]. This explains why iron with 4 unpaired d-electrons etched the diamond surface whilst copper, with 0 unpaired d-electrons did not.

In **Figure 5.43**, it is also clear to see that the iron has significantly etched the grain boundaries in the diamond material. This can be attributed to the fact that non-diamond carbon found at such sites is much less chemically inert than diamond and so will dissolve readily into the iron. In addition to the non-diamond carbon present at the grain boundaries, it is also possible that regions of diamond may transform to graphite under the influence of the metal [72]. Again, this non-diamond material is more soluble in the metal than diamond and so will dissolve readily. Due to these reactions described, it is clear that reactive metals will quickly become saturated with carbon. These carbon atoms occupy vacancies in the metal structure and weaken the metal-metal interactions. This makes the metal considerably softer and lowers the melting point (iron carbide melts at 1227°C [73]). In the presence of atomic hydrogen, this 'soft' metal-carbon mixture will be etched more quickly than the metal if it was pure, resulting in the rapid removal of iron from the surface of the sample. This explains why no metal can be seen in the SEM images of this sample.

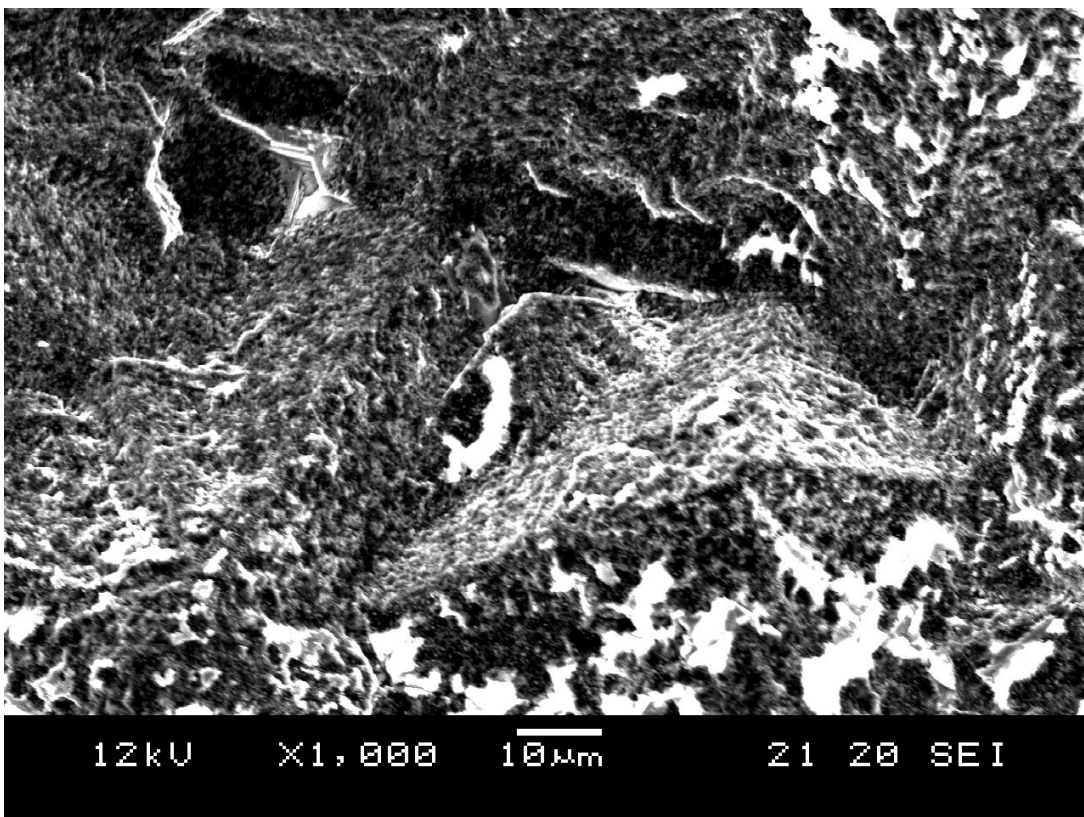
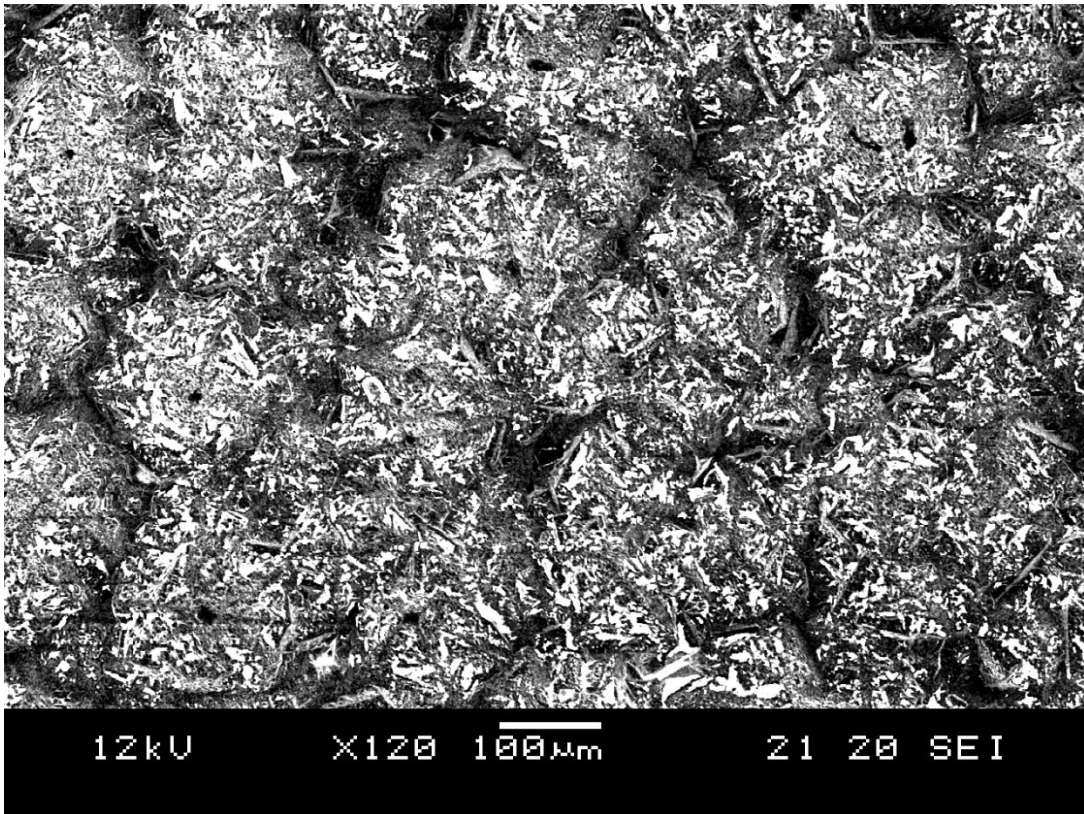


**Figure 5.43:** SEM images of the iron coated MCD sample following exposure to hydrogen plasma for 15 minutes at 0.6 kW, 100 Torr and 100 sccm.

In the case of the titanium coated sample, the hydrogen plasma treatment seemed to have very little effect on the coating, as shown in **Figure 5.44**. However, it should be noted that some regions of the coating have been removed by the plasma. These regions were most likely thinner or had smaller metal crystal sizes than other parts of the coating. In the case of the exposed regions of the surface, it should be noted that some crystal facets appear to have been etched slightly by the metal. This can be attributed to the fact that titanium has 2 unpaired d-electrons, so produces more of an etching effect than copper but less than iron. However, unlike the iron coated sample, there is no evidence of etching at the grain boundaries. The reason for this is not clear.

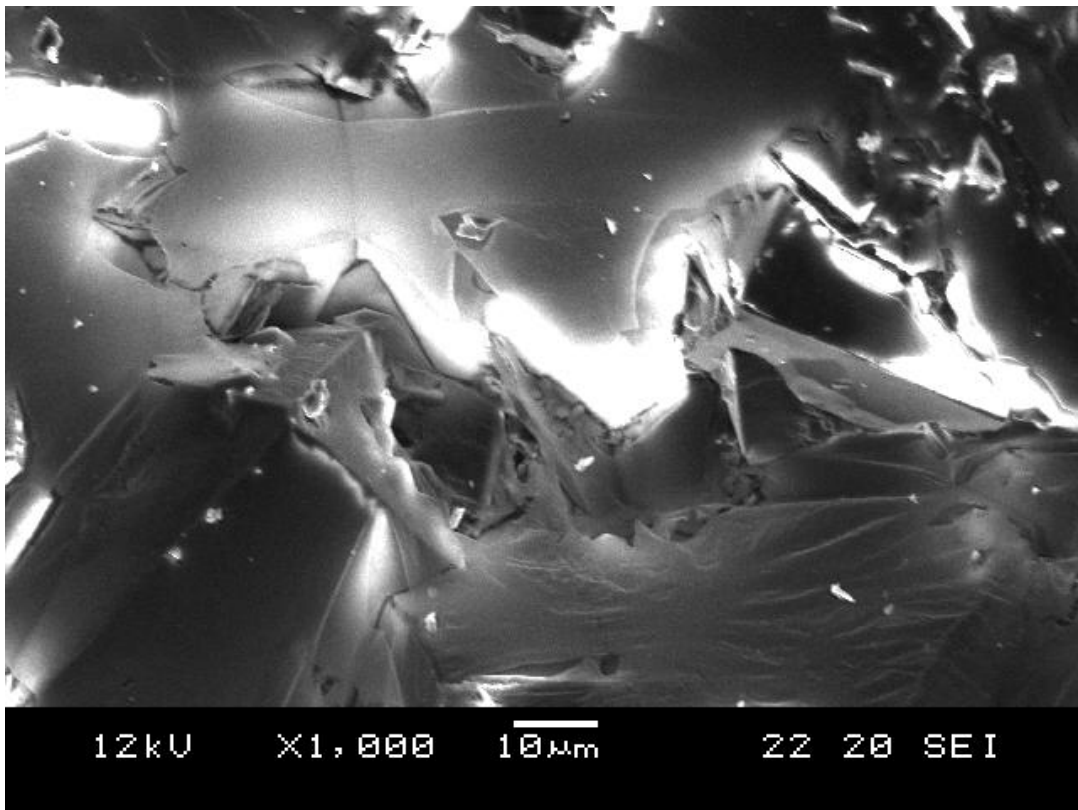
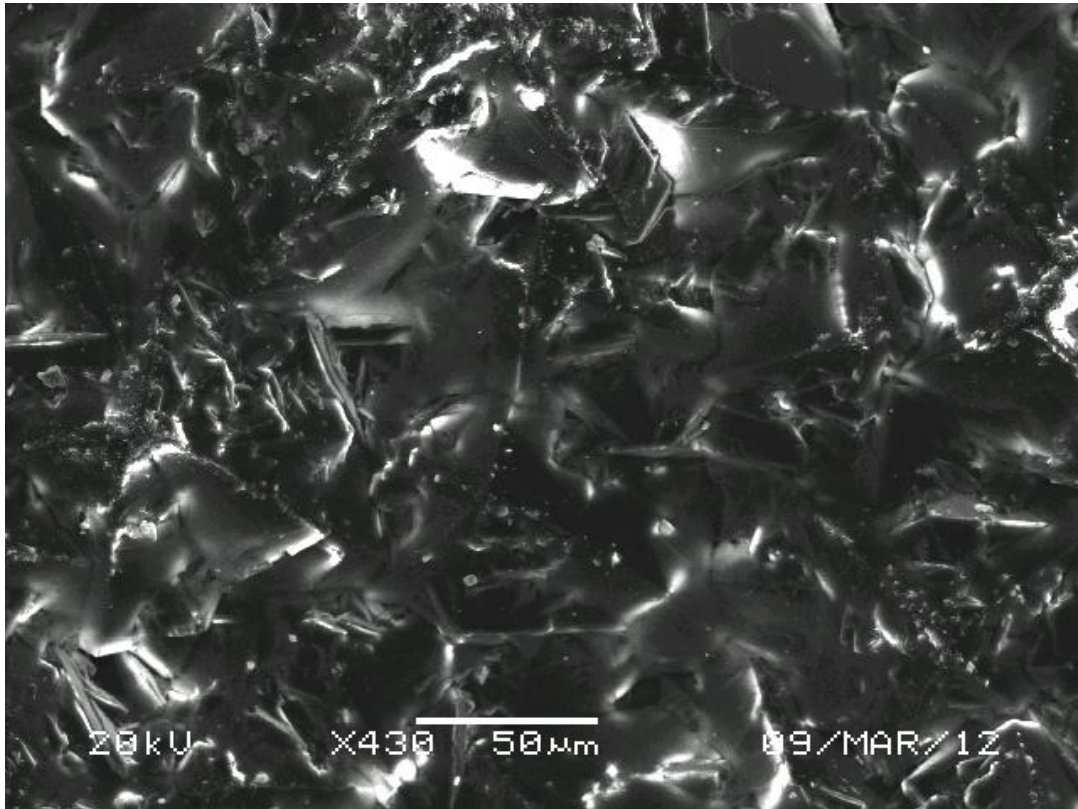


**Figure 5.44:** SEM images of titanium coated MCD samples treated in hydrogen plasma for 15 minutes at 0.6 kW, 100 Torr and 100 sccm.

## References

- [1] P. W. May (2000), Diamond thin films: a 21<sup>st</sup> century material, *Philosophical Transactions of the Royal Society of London A* **358**(1766), 473.
- [2] <http://gwyddion.net/>
- [3] P. Atkins, T. Overton, J. Rourke, M. Weller & F. Armstrong (2006), Shriver and Atkins Inorganic Chemistry, *Oxford University Press* (4<sup>th</sup> Ed.).
- [4] J. Filik (2005), Raman spectroscopy: a simple, non-destructive way to characterise diamond and diamond-like materials, *Spectroscopy Europe* **17**(5), 10-17.
- [5] M. N. R. Ashfold, P. W. May, C. Rego & N. M. Everitt (1994), Thin Film Diamond by Chemical Vapour Deposition Methods, *Chemical Society Reviews* **23**, 21-30.
- [6] Y. Yamazaki, K. Ishikawa, S. Samukawa & S. Yamasaki (2006), Defect creation in diamond by hydrogen plasma treatment at room temperature, *Physica B: Condensed Matter* **376-377**, 327-330.
- [7] M. Frenklach & H. Wang (1991), Detailed surface and gas-phase chemical kinetics of diamond deposition, *Physical Reviews B* **43**(2), 1520-1545.
- [8] J. C-M. Sung & J. Lin (2009), *Diamond nanotechnology: Synthesis and Applications*, *Pan Stanford Publishing Pte. Ltd.*
- [9] <http://examhelpersite.blogspot.co.uk/2011/06/p1-mayjune-2003.html>
- [10] J. C. Angus, H. A. Will & W. S. Stanko (1968), Growth of diamond seed crystals by vapour deposition, *Journal of Applied Physics* **39**(6), 2915.
- [11] J. Michler, J. Stiegler, Y. von Kaenel, P. Moeckli, W. Dorsch, D. Stenkamp & E. Blank (1997), Microstructure evolution and non-diamond carbon incorporation in CVD diamond thin films grown at low substrate temperatures, *Journal of Crystal Growth* **172**(3-4), 401-415.
- [12] A. Crisci, Francis Baillet, M. Mermoux, G. Bogdan, M. Nesládek & K. Haenen (2011), Residual strain around grown-in defects in CVD diamond single crystals: A 2D and 3D Raman imaging study, *Physica Status Solidi A* **208**(9), 2038-2044.
- [13] R. E. Rawles, R. Gat, W. G. Morris & M. P. D'Evelyn (1995), Hydrogen Plasma Treatment of Natural and Homoepitaxial Diamond, *Materials Research Society Proceedings* **416**, 299.
- [14] <http://physics.about.com/od/glossary/g/power.htm>
- [15] I. Villalpando, P. John, S. Porro & J. I. B. Wilson (2011), Hydrogen plasma etching of diamond films deposited on graphite, *Diamond and Related Materials* **20**(5-6), 711-716.
- [16] H. O. Pierson (1993), Handbook of Carbon, Graphite, Diamond and Fullerenes: Properties, Processing and Applications, *Noyes Publications*.
- [17] P. J. W. Vankan (2005), Molecules and Atoms in a Hydrogen Plasma Expansion, *verrijging van de graad van doctor aan de Technische Universiteit Eindhoven*.
- [18] W. J. Zhang, X. Jiang & Y. B. Xia (1997), The selective etching with H<sup>+</sup> ions and its effect on the oriented growth of diamond films, *Journal of Applied Physics* **82**(4), 1896-1899.
- [19] Z. Shpilman, I. Gouzman, E. Grossman, R. Akhvediani & A. Hoffman (2008), Hydrogen plasma and atomic oxygen treatments of diamond: chemical versus morphological effects, *Applied Physics Letters* **92**(23), 234103.
- [20] H. Kwarada (1996), Hydrogen-terminated diamond surfaces and interfaces, *Surface Science Reports* **26**(7), 206-259.

- [21] W. Zhang & X. Jiang (1998), The Contribution of H Ion Etching Under Different Substrate Bias to the Orientation Degree of Diamond Films, *Materials Research Society Proceedings* **513**, 421.
- [23] L. Wang, G. C. Yan, Y. Li, L. Cui & X. D. Zhu (2006), Bias-induced structural evolution of diamond films in plasma enhanced hot filament chemical vapour deposition with a two-step process, *Journal of Physics D: Applied Physics* **39**, 3350-3355.
- [24] C. J. Tang, A. J. Neves, A. J. S. Fernandes, J. Gracion & N. Ali (2003), A new elegant technique for polishing CVD diamond films, *Diamond and Related Materials* **12**, 1411-1416.
- [25] D. G. Lee, S. D. Harkness & R. K. Singh (1994), Excimer Laser Planarization of Diamond Films, *Materials Research Society Proceedings* **339**, 127.
- [26] W. Man, J. Wang, C. Wang, S. Wang & L. Xiong (2007) Planarising CVD diamond films by using hydrogen plasma etching enhanced carbon diffusion process, *Diamond and Related Materials* **16**(8), 1455-1458.
- [27] S. Ilias, G. Sené, P. Möller, V. Stambouli, J. Pascallon, D. Bouchier, A. Gicquel, A. Tardieu, E. Anger & M. F. Ravet (1996), Planarization of diamond thin films surfaces by ion beam etching at grazing incidence angle, *Diamond and Related Materials* **5**(6-8), 835-839.
- [28] D. T. Tran, C. Fansler, T. A. Grotjohn, D. K. Reinhard & J. Asmussen (2010), Investigation of mask selectivities and diamond etching using microwave plasma-assisted etching, *Diamond and Related Materials* **19**(7-9), 778-782.
- [29] G. M. R. Sirineni, H. A. Naseem, A. P. Malshe & W. D Brown (1997), Reactive ion etching of diamond as a means of enhancing chemically-assisted mechanical polishing efficiency, *Diamond and Related Materials* **6**(8), 952-958.
- [30] R. S. Sussman (2009), *CVD Diamond for Electronic Devices and Sensors*, John Wiley & Sons.
- [31] B. D. Thoms, M. S. Owens, J. E. Butler & C. Spiro (1994), Production and characterisation of smooth hydrogen terminated diamond C(100), *Applied Physics Letters* **65**(23), 2957-2959.
- [32] R. E. Rawles, S. F. Komarov, J. B. Hudson, M.P. D'Evelyn, R. Gat & W. G. Morris (1997), Mechanism of surface smoothing by a hydrogen plasma, *Diamond and Related Materials* **6**(5), 791-795.
- [33] R. E. Rawles (1996), Kinetics and Morphology of Homoepitaxial Diamond Growth by Chemical Vapour Deposition, PhD thesis, Rice University.
- [34] O. J. L. Fox (2011), Deposition of nanocrystalline diamond films by MW plasma CVD & Gas-Phase diagnostics using *in-situ* molecular-beam mass spectrometry and emission spectroscopy, PhD Thesis, Department of Chemistry, University of Bristol.
- [35] J. C. Richley (2011), Fundamental Studies of Diamond Chemical Vapour Deposition: Plasma Diagnostics and Computer Modelling, PhD thesis, Department of Chemistry, University of Bristol.
- [36] M. Frenklach, S. Skokov & B. Weiner (1994), An atomistic model for stepped diamond growth, *Nature* **372**, 535-537.
- [37] A. Cheesman (2006), Investigations into the fundamentals of gas-phase and gas-surface chemistry prevalent in the growth of chemical vapour deposited diamond, PhD Thesis, Department of Chemistry, University of Bristol.

- [38] O. M. Küttel, L. Diederich, E. Schaller, O. Carnal & L. Schlapbach (1995), The preparation and characterisation of low surface roughness (111) and (100) natural diamonds by hydrogen plasma, *Surface Science* **337**(1-2), L812-818.
- [39] C-L. Cheng, H-C. Chang, J-C. Lin & K-J. Song (1997), Direct observation of hydrogen etching anisotropy on diamond single crystal surfaces, *Physical Review Letters* **78**(19), 3713-3716.
- [40] S-G. Ri , H. Wanatabe, M. Ogura, D. Takeuchi, S. Yamasaki & H. Okushi (2006), Hydrogen plasma etching mechanism on (001) diamond, *Journal of Crystal Growth* **293**(2), 311-317.
- [41] N. Lee & A Badzian (1995), Effect of misorientation angles on the surface morphologies of (001) homoepitaxial diamond thin films, *Applied Physics Letters* **66**(17), 2203-2205.
- [42] N. Lee & A. Badzian (1997), A study on surface morphologies of (001) homoepitaxial diamond films, *Diamond and Related Materials* **6**(1), 130-145.
- [43] R. E. Stallcup & J. M. Perez (2001), Scanning tunnelling microscopy studies of temperature-dependent etching of diamond (100) by atomic hydrogen, *Physical Review Letters* **86**(15), 3368-3371.
- [44] R. E. Stallcup II, Y. Mo, T. W. Scharf & J. M. Perez (2007), Formation of nanometer-size high-density pits on epitaxial diamond (100) films, *Diamond and Related Materials* **16**(9), 1727- 1731.
- [45] C. C. Battaile, D. J. Srolovitz, I. I. Olenik, D. G. Pettifor, A. P. Sutton, S. J. Harris & J. E. Butler (1999), Etching effects during the chemical vapour deposition of (100) diamond, *Journal of Chemical Physics* **111**(9), 4291-4300.
- [46] K. Bobrov, A. J. Mayne, A. Hoffman & G. Dujardin (2003), Atomic-scale desorption of hydrogen from hydrogenated surfaces using STM, *Surface Science* **528**(1-3), 138-143.
- [47] B. Koslowski, S. Strobel, M. J. Wenig, R. Martschat & P. Ziemann (1998), On the roughness of hydrogen-plasma treated diamond (100) surfaces, *Diamond and Related Materials* **7**(2-5), 322-326.
- [48] T. I. Hukka, T. A. Pakkanen & M. P. D'Evelyn (1994), Chemisorption of Hydrogen on the Diamond (100)2x1 Surface: An *ab Initio* Study, *Journal of Physical Chemistry* **98**(47), 12420- 12430.
- [49] I. I. Oleinik, D. G. Pettifor, A. P. Sutton & J. E. Butler (2000), Theoretical study of chemical reactions on CVD diamond surfaces, *Diamond and Related Materials* **9**(3-6), 241-245.
- [50] R. Roy, K. A. Cherian, J. P. Cheng, A. Badzian, C. Langlade, H. Dewan & W. Drawl (1997), Precipitation of diamond from  $Me_xC_yH_z$  solutions at 1 ATM, *Materials Research Innovations* **1**, 117-129.
- [51] W. D. Callister & D. G. Rethwisch (2010) *Materials Science and Engineering*, John Wiley & Sons.
- [52] [http://en.wikipedia.org/wiki/File:Pure\\_iron\\_phase\\_diagram\\_\(EN\).svg](http://en.wikipedia.org/wiki/File:Pure_iron_phase_diagram_(EN).svg)
- [53] [http://www.engineeringtoolbox.com/melting-temperature-metals-d\\_860.html](http://www.engineeringtoolbox.com/melting-temperature-metals-d_860.html)
- [54] K. K. Chan, G. A. J. Amaratuga & T. K. S. Wong (1992), Defined etching of carbon-diamond films on silicon using an oxygen plasma with titanium masking, *Diamond and Related Materials* **1**(2-4), 281-284.
- [55] R. Roy, H. S. Dewan, K. A. Cherian, J. P. Cheng, A. Badzian, W. Drawl & C. Langlade (1995), Precipitation of diamond from metallic liquids below 1 atm, *Materials Letters* **25**(5-6), 191-193.

- [56] L. Chen, Y. Li & R. Manasseh (1998), The coalescence of bubbles – a numerical study, *Third International Conference on Multiphase Flow*, 1-8.
- [57] H-M. Katsch, E. Quandt & T. Schneider (1996), The influence of metastables on the plasma-induced emission in a helium RF discharge, *Plasma Physics and Controlled Fusion* **38**, 183-192.
- [58] I. A. Barnoush (2011), Hydrogen embrittlement. <http://www.uni-saarland.de/fak8/wwm/research/phd-barnoush/hydrogen.pdf>
- [59] R. P. Jewett, R. J. Walter, W. T. Chandler & R. P. Frohberg (1973), Hydrogen environment embrittlement of metals, *NASA CR-2163*.
- [60] J. L. Gillete & R. L. Kolpa (2007), Overview of Interstate Hydrogen Pipeline Systems, *Argonne National Laboratory, ANL/EVS/TM/08-2*.
- [61] H. Lindlar (1952), Ein neuer Katalysator für Selective Hydrierungen, *Helvetica Chimica Acta* **35**(2), 446-450.
- [62] [http://en.wikipedia.org/wiki/Mohs\\_scale\\_of\\_mineral\\_hardness](http://en.wikipedia.org/wiki/Mohs_scale_of_mineral_hardness)
- [63] H. Hann, A. Sidorenko & I. Tiginyanu (2009), *Nanoscale Phenomena: Fundamentals and Applications*, Springer.
- [64] B. Ingham, T. H. Lim, C. J. Dotzler, A. Henning, M. F. Toney & R. D. Tilley (2011) *Chemistry of Materials* **23**(14), 3312-3317.
- [65] S-C. Chang, T-C. Lin & J-H. Lee, Converting nickel film to nano particles using hydrogen plasma treatment, *Solid State Technology* **50**(11). Article can be found at <http://www.electroiq.com>
- [66] H. Li, J. K. Jo, L. Zhang, C-S. Ha, H. Suh & I. Kim (2010), A General and Efficient Route to Fabricate Carbon Nanotube-Metal Nanoparticles and Carbon Nanotube-Inorganic Oxides Hybrids, *Advanced Functional Materials* **20**(22), 3864-3873.
- [67] D. Takagi, Y. Homma, H. Hibino, S. Suzuki & Y. Kobayashi (2006), Single-Walled Carbon Nanotube Growth from Highly Activated Metal Nanoparticles, *Nano Letters* **6**(12), 2642-2645.
- [68] K. K. Nanda, S. N. Sahu & S. N. Behera (2002), Liquid-drop model for the size-dependent melting of low-dimensional systems, *Physical Reviews A* **66**(1), 013208.
- [69] C. Q. Sun, Y. Wang, B. K. Tay, S. Li, H. Huang & Y. B. Zhang (2002), Correlation between the Melting Point of a Nanosolid and the Cohesive Energy of a Surface Atom, *Journal of Physical Chemistry B*, **106**(41), 10701-10705.
- [70] C. Q. Sun (2007), Size dependence of nanostructures: impact or bond order deficient, *Progress in Solid State Chemistry* **35**(1), 1-159.
- [71] E. Paul, C. J. Evans, A. Mangamelli, M. L. McGlaufflin & R. S. Polvani (1996), Chemical aspects of tool wear in single point diamond turning, *Precision Engineering* **18**(1), 4-19.
- [72] Y. Chen, L. C. Zhang & J. A. Arsecularatne (2007), Polishing of polycrystalline diamond by the technique of dynamic friction. Part 2: Material removal mechanism, *International Journal of Machine Tools & Manufacture* **47**(10), 1615-1624.
- [73] <http://www.americanelements.com/fec.html>

# CHAPTER 6

## Conclusions

---

In this project, the effects of a range of hydrogen plasma treatments on PCD surfaces have been investigated using SEM and AFM. From this work, it is clear that no matter how the treatment parameters are controlled, hydrogen plasma treatments will always cause significant etching of the non-diamond material located between the grains in MCD films. During rapid etching of this non-diamond material it has been shown that dislocations can be released from the surface, as well as reducing strain in the material produced by the manner in which diamond grows under standard CVD conditions.

High temperature plasma treatments at 1000°C have been shown to cause drastic graphitisation of the diamond surface. This was attributed to the high flux of atomic hydrogen producing large areas of high energy radical sites on the diamond surface which revert to the more thermodynamically stable  $sp^2$  hybridisation at high temperatures. This effect is not caused by high energy atomic species since OES confirmed a decline in high energy species with increasing pressure.

This investigation has also confirmed that the flow rate of  $H_2$  into the reactor has no effect on the result of the hydrogen plasma treatment. This indicates that low flow rates of hydrogen can be used for such treatments and from a commercial point of view, this would lead to lower treatment costs. All treatments at different flow rates produced very similar results, despite a higher proportion of atomic hydrogen being detected in the centre of the plasma by OES for a lower flow rate. This was attributed to a dilution effect within the plasma from new  $H_2$  introduced to the reactor. Since no effect was observed on the surface roughness, it has been suggested that the proportion of atomic hydrogen produced by any plasma discharge is more than sufficient to saturate the surface and allow the surface reactions to occur at the maximum possible rate, depending on the temperature.

Experiments using different microwave powers have shown that the roughness of the surface increases with power, despite the temperature being the same in all treatments. OES confirmed that the proportion of atomic hydrogen in the plasma increases with the power and this can be attributed to more energy being transferred to the gaseous reagents. At the highest microwave power, thin peaks could be observed in the surface. It has been suggested that these peaks are formed due to etching by high energy hydrogen species. In the literature significant etching of this type has been attributed to ionic species, but these species could not be observed in this experiment due to the limitations of OES.

In addition to the roughening effects described, it has also been noted that hydrogen plasma treatments reduce the sharpness of crystal edges and can produce improved faceting on some larger crystallographic planes. The surfaces are assumed to be {100} surfaces. Other crystal morphologies have been shown to be significantly etched by hydrogen plasma treatments leading to small grain sizes with a more 'ballas' morphology.

In a study of the effect of prolonged exposure to hydrogen plasma, the results of a series of 10 minute treatments produced different results to a single 1 hour treatment. Following the hour of exposure to hydrogen plasma, both samples showed increased surface roughness. However, the sample treated for 1 hour showed significantly more graphitisation of the surface. This was explained by simple probabilistic arguments where over a long period of time, the likelihood of a localised region of diamond surface becoming activated by hydrogen abstraction is higher.

A further experiment was also performed using as grown SCD from a HPHT source. In its original state the surface of this material was shown to have a number of defects and following treatment a high density of pyramidal pits were observed in the surface. The discussion of these results provided substantial evidence that the mechanism of surface smoothing by hydrogen plasmas is etching at step edges. This was rationalised using a 'number of nearest neighbours' argument. This conclusion could provide an insight into the homoepitaxial growth of diamond layers on SCD surfaces which are known to possess atomically smooth surfaces.

Overall, this study has shown diamond surfaces exposed to hydrogen plasma treatments at low temperatures and low microwave powers will experience the lowest possible magnitude of roughening effects. Furthermore, through the use of short exposures to the plasma, these effects can be further reduced and would so allow the smoothing of the diamond surface to be the dominant effect.

A further study was also undertaken into the effects of metals on diamond surfaces under hydrogen plasma conditions. In this work, diamond SAMs on W were used as substrates and coated in thin metal films of Ag, Cu, Fe or Ti. Treatments of these samples in hydrogen plasma showed that such thin films were easily removed from the surface of the sample. However, examination of the samples using SEM has shown that metallic globules can be found on the surface of the samples. The metallic globules are thought to be formed due to hydrogen embrittlement processes producing cracks in the metal film. Plasma etching at these cracks and grain boundaries in the metal layer produces small metal nanoparticles which have depressed melting points compared to the standard melting point of the bulk metal. These molten particles then move across the surface under the influence of high thermal energy from the plasma and can sometimes encounter another molten globule. At this point, the globules coalesce. The coalescence of a number of molten metallic globules in this way produces the snake-like and irregularly shaped globules observed in this investigation.

Since these globules were forming and the metal no longer wetting the surface of the diamond crystals, the diamonds became exposed to the hydrogen plasma. This resulted in standard hydrogen plasma treatment, as determined by the high brightness of the crystals under SEM. It is expected that similar effects to those seen following standard hydrogen plasma treatments of PCD would be observed, such as the smoothing of sharp crystal edges.

In a study using the larger crystals in a MCD film, short treatments showed that metal films can produce thermochemical etching of the diamond surfaces. Iron was particularly effective, leaving a very rough surface. Ti was found to only slightly etch the diamond surface whilst Cu did not have any effect, only forming spherical globules on the surface of the material. The thicker film used for these investigations meant that the metal particles formed were several microns in

size. This meant that they did not suffer from melting point depression like the metal nanoparticles previously described and so remained as solid spheres on the surface.

# CHAPTER 7

## Suggestions for future work

---

To provide more grounds for the conclusion that hydrogen plasmas cause smoothing of diamond surfaces mainly by etching, a number of additional experiments should be performed. As-grown SCD and SCD which has been polished using a lapping technique should be exposed to hydrogen plasma. These SCD samples should be from natural, HPHT and CVD sources to enable the differences between the materials from various sources to also be investigated.

In the case of the natural and HPHT as-grown surfaces, the formation of etch pits due to etching at the edges of defects would be expected. This 'etched' surface should then be exposed to hydrogen plasma for more time to confirm whether etching at step edges will eventually cause the pits to merge as expected. In theory, this process should eventually produce large, smooth areas on the diamond surface. However, these experiments could take a significant amount of time to achieve an atomically smooth surface on the samples. The reason for this is that the depth of the deepest defect will determine the amount of material needs to be removed from the surface before a smooth surface is obtained.

This progression would not be expected for diamond produced by homoepitaxial CVD, which already possesses an atomically smooth surface. In this case, it would be interesting to see if the hydrogen plasma causes defects to form in the surface during long periods of exposure to hydrogen plasma. If defects do not form in the atomically smooth surface, then it would be possible to batch-treat many diamond samples in the presence of atomic hydrogen and simply leave the reactor running until an atomically smooth surface is formed on all of the diamonds.

Being able to treat many samples at once would have a number of benefits, not only in terms of the production time of device grade diamond, but in reducing the overall energy requirements of the production process, since the plasma does not need to be lit many times over.

In parallel with these studies on as-grown SCD, polished diamond surfaces should also be investigated. In this project, it has been shown that a brief period of hydrogen plasma treatment at a high temperature at the end of diamond growth can induce graphitisation and drastically increase the time required for removing material from the surface by lapping. This process would allow the defects in the diamond surface to be removed quite rapidly, making the diamond surfaces more uniform. However, the lapping procedure produces scratch marks on the surface. As already mentioned in a previous chapter, these scratched surfaces have been the subject of much of the hydrogen plasma treatments reported in the literature. Analysing these samples before and after 'post-polishing hydrogen plasma treatment' should show that the samples become considerably smoother. However, at first glance it will be difficult to determine whether the treatment causes the polish marks to become less prominent due to etching or surface migration.

The most simple way in which it may be possible to determine the mechanism of smoothing could be weighing the samples as previously done in the literature. Obviously, if the mechanism is hydrogen atom assisted surface migration, the mass of the sample should remain the same.

However, in the case of etching, it is possible that the amount of diamond material removed from the surface by the treatment will be very small and so the mass of the sample may not decrease to a level to be considered as significant. This is the major problem with using the mass of the samples as a means of determining the mechanism since using a number of samples with different masses will expand the error margins and so may mask some of the small changes in mass.

A way to deal with this problem would be to etch a deep gulley across the centre of a sample using a laser, as shown in **Figure 7.1**. By noting the thickness of the sample at the bottom of the gulley and the top surface of the sample, it will be possible to observe changes to the sample following treatment much more obviously. This measuring would be performed using SEM, where the scale bar can be used to determine the thickness of the sample at the points of interest.

Following hydrogen plasma treatment, it would be expected that the walls of the gulley would be completely etched to leave a thinner sample with an atomically smooth surface. On the other hand, if the thickness of the film following treatment is between the measurements of the bottom of the gulley and the top of the surface, then surface migration is playing a significant role in the smoothing process. The combination of these measurements of the sample dimensions and masses should give a clearer picture as to the processes occurring at the diamond surface during hydrogen plasma treatment.

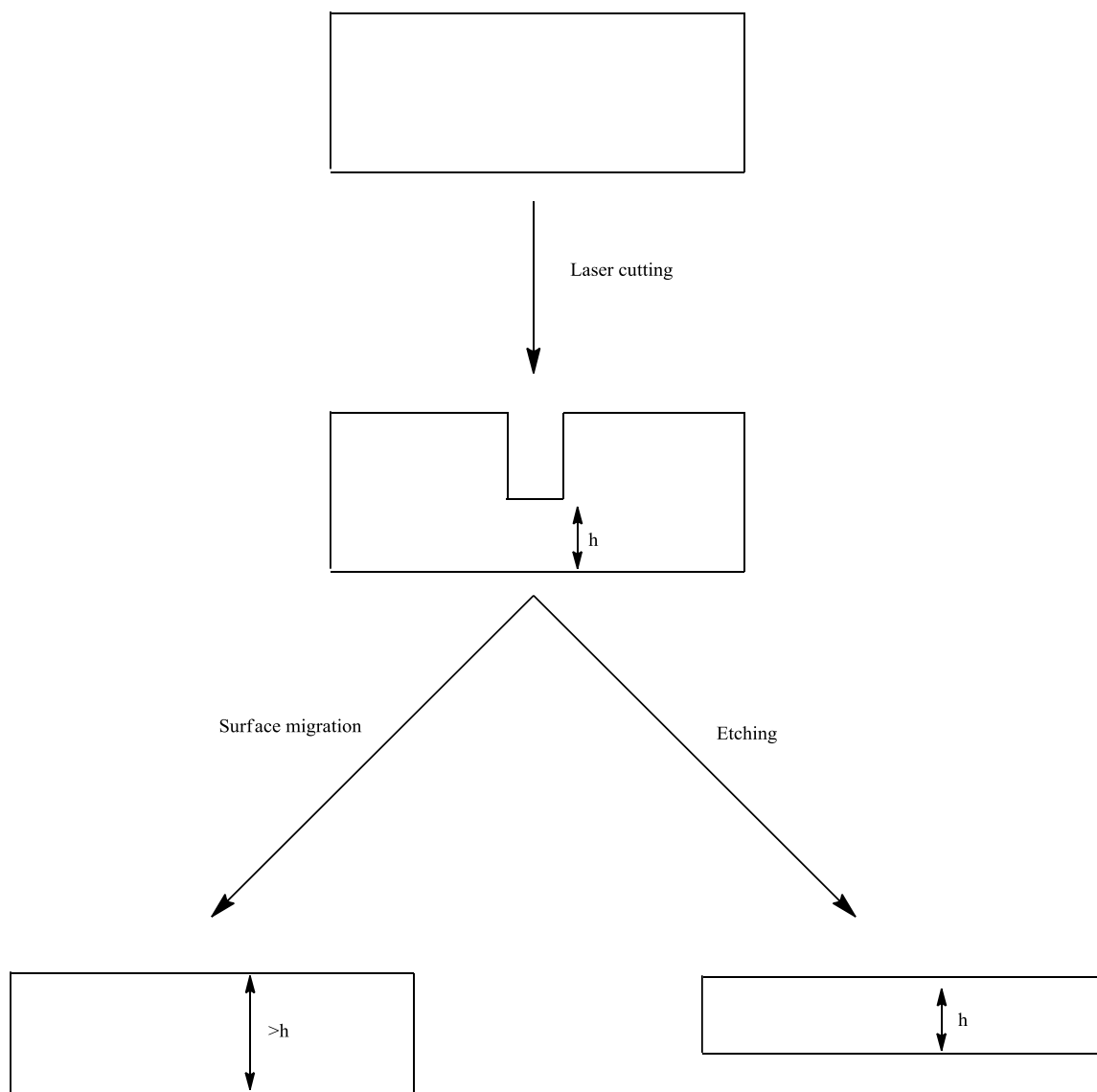


**Figure 7.1:** An illustration of the proposed experiment using a deep gully etched into an SCD sample by a laser as a means of determining the mechanism of surface smoothing by hydrogen plasma treatment.  $h$  is the height from the bottom of the sample to the bottom of the trench. *Figure designed by author.*

Despite one mechanism appearing to be dominant, there is also a high probability that the other process will play a role in the surface smoothing. For this reason computational studies will need to be performed to demonstrate how the growth, migrations and etching reactions work in together to produce homoepitaxial diamond with atomically smooth surfaces. It would be hoped that these computational models would provide the closest fit to the experimental growth rates simulated so far. Furthermore, this computational work could then be compared with previous work in the field.

In addition to the investigation into the main mechanism of smoothing by hydrogen plasma treatments, it would also be possible to show that graphitising the surface of the diamond using high temperature hydrogen plasma conditions could enhance other methods of polishing such as thermochemical etching and  $O_2$  plasma treatments. By investigating a range of other polishing

methods it may be possible to identify the fastest and most reproducible way of fabricating device grade diamond surfaces. It may also be possible to refine the chosen technique further leading to improved performance and reductions in cost. These would be beneficial developments from a commercial point of view.

With regards to the investigations into LPSSS-style treatments, it is clear that the thermochemical reaction between some metals and the diamond surface makes the use of thin metal films as a means of enhancing hydrogen plasma etching unsuitable. Some metals etch the diamond significantly as well as etching grain boundaries. Due to this etching, the integrity of PCD samples can be reduced to the extent where the sample disintegrates and it is also possible that in the presence of more metal and also longer treatments, nanodiamond particles may be removed from the substrate completely.

These factors indicate that PCD materials may not be suitable as substrates for LPSSS-style treatments. However, as of yet it has not been determined whether the thermochemical reaction of the metal with the diamond surface enhances the hydrogen plasma treatment. This possibility could be investigated using a large SCD sample coated with a thin layer of Fe and treated under hydrogen plasma conditions. If a large sample is used, it will not be completely etched away by the metal during the treatment and furthermore, SCD has not grain boundaries, leading to no risk of the sample disintegrating. If the time required to produce a smooth surface is reduced significantly by the presence of the metal (i.e. the increase in the rate of hydrogen plasma smoothing outweighs the time required for coating) then the technique may have potential for use in commercial settings.

If the technique is shown to be useful in a commercial setting, the issue of recovering as much of the metal as possible during the treatment will need to be addressed. The optimal situation would be to catch the 'hot' metal atoms which are etched from the surface of the sample by using a form of 'cold-finger' as used in sublimations in synthetic chemistry. By positioning this water-cooled finger near chamber outlet, it may be possible to recover a significant proportion of the metal which has been etched from the surface of the sample. This cooling would also cause atomic hydrogen species to recombine to form molecular hydrogen and so the metal deposited onto the cold finger will not be etched further. Since material is being recovered using the 'cold-finger' it can be reused in subsequent treatments. Recycling the metal in this way has potential to significantly reduce the cost of the procedure.

In the majority of the future work on LPSSS, it is expected that the technique will be investigated as a method of diamond formation distinct from CVD and HPHT. In these investigations the diamond growth will need to be studied using a number of different carbon sources both gaseous (e.g. 1% CH<sub>4</sub> in H<sub>2</sub>) and solid (eg. graphite and amorphous carbon) in combination with different metals. In these investigations it will be the diamond growth in the bulk of the metal which will be of most interest.

In the case of investigations using a methane precursor, enhanced diamond nucleation at the surface of a carbon rich metal is expected. This effect has been mentioned in a previous chapter of this project and so is not of great interest for the LPSSS process. In these treatments, it is expected that the molten metal will need to be saturated with carbon before diamond will form in the bulk. This was reported in the original work on LPSSS diamond growth.

To achieve the desired saturation from the solid carbon sources, the ratio of metal to carbon needs to be optimised. As a starting point, a 1:1 metal atom to carbon atom mixture should be used. For most metals, this will be more than enough carbon to saturate the metal beyond the point where carbide compounds are formed (carbides are commonly found in the form of  $M_3C$ ), reminiscent of the original LPSSS experiments. The samples should be treated for 12 hours in these investigations to allow sufficient time for diamond crystals to nucleate within the molten metal.

The next task will be finding the diamond crystals forms in the bulk of the metal, which will solidify as a block when the treatment is finished. The easiest solution to this would be to cut the treated metal-carbon block into slices and analyse each slice using ultra-high resolution SEM. In order to make the diamond crystals even more prominent it may be necessary to treat the treated metal-carbon slice for a short time in acid to dissolve any graphite which may be preventing small diamond crystals from being viewed.

One major problem with these treatments is that a large amount of metal will be required. Due to the risk of contamination, these treatments cannot be performed in the MWCVD system at the University of Bristol. A HFCVD system could be more useful. Due to the  $H_2$  dissociating due to the transfer of thermal energy from the filament to the gas, HFCVD systems provide a lower flux of atomic hydrogen and so the etch rate of the metal would be lower. This also means that less hydrogen embrittlement will occur due to less atomic hydrogen permeating the metal, and so the metal will melt closer to its standard melting point. This, coupled with the fact that nanoscale processes are no longer relevant to a large block of metal, makes the melting points of the metals in the treatments much more predictable and controllable. However, the treatments may require an additional heat source to be added to the set-up to produce a molten metal phase for the treatment.

Once a 'bulk' molten metal phase has been formed, it will need to be contained within the reactor to prevent it from flowing into the reactor and causing contamination. A solution for this would be to make a 'sand-pit'-like container from a material with a high melting point such as W. An illustration of such a container is shown in **figure 7.2**.

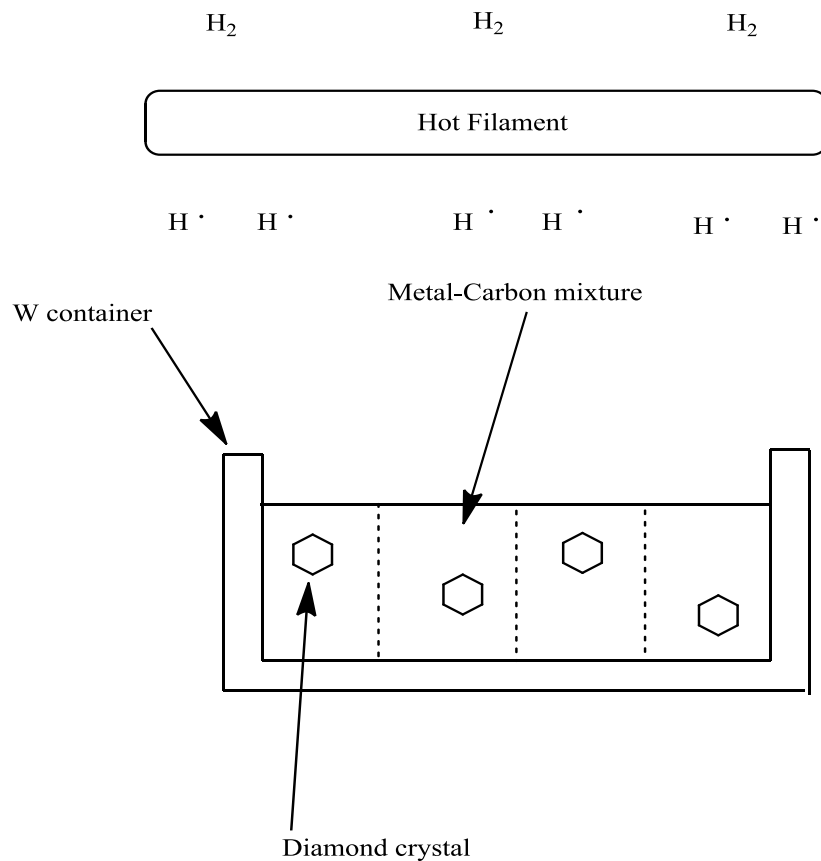


**Figure 7.2:** An illustration of the experiment set-up for investigating LPSS diamond growth using large amounts of metal. The dotted lines indicate cutting the solidified block which has trapped the newly formed diamond crystals into sections for analysis. *Figure designed by author.*

When the treatment is over, the molten metal in the container will cool to form a solid block. At this point it will not be possible to see any of the diamonds which have hopefully formed inside the metal. To analyse the contents of the metallic solid phase, the block should be cut into sections using a laser cutter and analysed under high resolution SEM to try and identify diamond crystals. It is possible that some small diamond crystals may be destroyed by the laser cutting process, but by using a long treatment, it would be hoped that large crystals would be formed which could surface the cutting process. Using plasma etching or acid treatment could prove to be useful for making the diamond crystals more prominent under SEM, since the inert diamond crystals will react much more slowly with the etchant species than the metals causing the diamonds to protrude from the surface being analysed.

It is clear that the future investigations into LPSS may be quite complicated and require a great deal of work. However, if LPSS is shown to form diamond in the bulk of the metal, the technique could have a dramatic impact on the way in which diamond-based devices are produced. If the growth of diamond in the bulk of the molten metal phase is confirmed, an investigation into SCD growth using LPSS should be performed. LPSS may present a way of producing SCD at much faster rates than is possible with current CVD techniques and would allow a wide variety of cheap carbon containing materials to be used. If this were to come to fruition, LPSS could lead to substantial developments in diamond based technologies.